THE UNIVERSITY OF CHICAGO

NOVEL CELLULAR MODELS OF HUMAN MYOPATHIES

A DISSERTATION SUBMITTED TO

THE FACULTY OF THE DIVISION OF THE BIOLOGICAL SCIENCES

AND THE PRITZKER SCHOOL OF MEDICINE

IN CANDIDACY FOR THE DEGREE OF

DOCTOR OF PHILOSOPHY

DEPARTMENT OF PATHOLOGY

BY

ELLIS YOUNG-EUN KIM

CHICAGO, ILLINOIS

JUNE 2018

TABLE OF CONTENTS

LIST OF FIGURES

LIST OF TABLES

LIST OF COMMON ABBREVIATIONS

CNBP: CCHC-type zinc finger nucleic acid binding protein

DM: Myotonic dystrophy

DM1: Myotonic dystrophy type 1

DM2: Myotonic dystroph type 2

DMD: Duchenne muscular dystrophy

DMPK: Dystrophia myotonia protein kinase

iMyoD: inducible MyoD

iPSC-CMs: induced pluripotent stem cell-derived cardiomyocytes

iPSCs: induced pluripotent stem cells;

LGMD2C: limb girdle muscular dystrophy

MBNL1: Muscleblind-1

SGCG: γ-sarcoglycan

UDCs: urine-derived cells

ZNF9: Zinc finger 9

ACKNOWLEDGEMENTS

First and foremost, I would like to thank Dr. Elizabeth McNally for being my thesis advisor and allowing me to pursue this research in her laboratory. She is always open to new ideas, including setting up a cell culture system that was new to the lab, and has been a wonderful mentor for the last few years. She will continue to be an inspiration for me, and I am very grateful for having had an opportunity to work in her lab. My committee members, Drs. Ivan Moskowitz, Marcelo Nobrega, Nancy Schwartz, and Chris Weber have offered valuable insights and guidance throughout my project. They are truly a dream team of advisors a graduate student could ask for, and I am very fortunate to have had them encourage and challenge me throughout this journey.

The McNally lab has been my home for the last few years and the people in the lab make it such a fun and stimulating place to work. I am so happy to have had the chance to work with many past and current members of the lab. Before I joined the lab, I had a wonderful time working with Kayleigh Swaggart, who carved out time from her busy thesis writing schedule and made sure I had a good experience during my rotation. Meg Puckelwartz helped me set up the necessary equipment when I first joined the lab. Eugene Wyatt worked closely with me to not only teach me valuable skills, but also to offer advice throughout my years in the lab. Dave Barefield taught me cardiac physiology and always had witty comments to make me laugh. Pat Page worked closely with me to become a tissue culture expert and was always willing to help me. Andy Vo, a fellow graduate student, bounced ideas around with me about my project, offered experiments I could pursue, and always lent a helping hand or an ear to listen to me and to ground me. Tharrie Daniels was always there to celebrate small successes along the way and

to help me through a rough patch when there was one. So many other members of the lab, Kate Fallon, Greg Aubert, Bella Salamone, Anthony Gacita, Chi-Chi Ohiri, Michele Hadhazy, Mattia Quattrocelli, Kay-Marie Lamar, Quan Gao, Brandon Gardner, Bridget Biersmith , and James Warner have made the last few years fly by. All of the members of the lab have made this journey special by teaching me techniques, helping me analyze data, offering advice, and holding fun conversations at lunch. They are not just valuable colleagues, but wonderful friends that I have had the absolute fortune to have made along the way.

While the people in the lab have pulled and pushed me through my time in lab, there are many friends from outside the lab who have walked beside me to support me through this journey. Amulya Lingaraju and Jacquie Handley both started in the Pathology program with me and have not only been invaluable classmates, but also some of the best friends I have. Kristian Coerper, Mary Frances Picone, and Elizabeth Lee never let me forget that I am continuing to make progress, however slow it may seem at the time. Cathy Chen went on many adventures with me in and out of Chicago, and Serena Chao was always a call away even though she does not live in Chicago. I am so fortunate to be surrounded by such extraordinary group of friends.

Finally, I am infinitely grateful to my parents for everything they have done to support me. They are my biggest fans and have given me the opportunity to pursue whatever I wanted to, and encouraged me throughout all these years. They always inspire me to do my best, but have also taught me to let things unfold. They are always there to listen to me, offer the best pieces of advice, and lift me up. I am incredibly lucky to have such supportive, loving parents.

ABSTRACT

The muscular dystrophies are a group of genetically and clinically heterogenous disorders characterized by progressive muscle weakness and wasting. Animal models provide valuable insights into disease mechanisms. However, in light of the growing list of variants associated with human myopathies, patient-specific cell-based models could serve as complementary tools in disease modeling and therapy testing.

Generation of cell-based models requires a cell source. Ideally, the cells would be easy to isolate and can be collected through a non-invasive method. We demonstrate that cells derived from urine samples can serve as source cells to be either directly reprogrammed into myotubes or reprogrammed first into induced pluripotent stem cells and then differentiated to cardiomyocytes. Generation of myotubes from patients with Duchenne muscular dystrophy and limb girdle muscular dystrophy 2C captured the patient-specific genetic alterations and recapitulated disease phenotypes, demonstrating the utility of urine cell-derived myotubes in disease modeling.

One of the muscular dystrophies that has been challenging to model in mice is myotonic dystrophy (DM), as it arises from unstable repeat expansions in *DMPK* (DM1) or *CNBP* (DM2) gene. Transcription of these repeat expansions leads to formation of RNA foci that can sequester splicing regulators such as muscleblind-1 (MBNL1). This functional depletion of MBNL1 leads to missplicing of its target genes, shifting the splicing profile from adult to embryonic transcripts. We created cell-based skeletal and cardiac models from DM1 and DM2 patients in order to investigate the disease mechanisms in each tissue. DM1 myotubes and iPSC-derived cardiomyocytes displayed MBNL1 clusters and missplicing profiles, whereas DM2 cells exhibited MBNL1 distribution and missplicing patterns resembling those of control cells. In

addition, iPSC-derived cardiomyocytes revealed calcium mishandling in DM1 and DM2. Combined, these findings suggest that DM2 may have additional mechanisms that lead to calcium mishandling in the absence of splicing aberrations. Transcriptional analysis of iPSC-derived cardiomyocytes implicated alterations in potassium channel expression as a potential mediator behind cardiac dysfunction in DM.

These studies demonstrate that cell-based skeletal and cardiac muscle models can serve as a platform upon which disease mechanisms can be investigated. Additionally, the ability to generate patient-specific models could open up avenues for their use in testing gene-specific therapies.

CHAPTER 1

CELL-BASED MODELS FOR DISEASE MODELING OF THE MUSCULAR DYSTROPHIES

OVERVIEW

The muscular dystrophies are a heterogeneous group of diseases that present with highly variable clinical presentations that arise from multiple mutations in a number of different genes. While mouse models serve as a valuable tool in elucidating disease mechanisms, inherent differences in mice and humans could limit their utility. Cell-based systems developed from each patient can provide a complementary approach in disease modeling as well as therapy testing, especially as more gene-specific treatments become available. In this introduction, I will focus on currently available cell-based models of skeletal and cardiac muscle to study the muscular dystrophies. As generation of these models are based on previous findings from developmental processes of the skeletal muscle and the heart, I will provide overviews on myogenesis and cardiogenesis. These models were applied to study one type of muscular dystrophy, the myotonic dystrophies, in depth. As such, overviews on clinical phenotypes, current understanding of pathogenic mechanism, as well as mouse models of myotonic dystrophies will be covered.

INTRODUCTION

Animal models have been a mainstay for studying disease mechanisms and testing potential therapies for various human diseases. Mouse models are the most commonly used model system, and these models have, and continue to, serve as valuable resources in providing *in vivo* insights. However, while a disease may be linked to one causal gene, allelic heterogeneity could lead to

different pathogenic mechanisms in the same disease as the location of the variant can result in a range of consequences. In addition, as sequencing technologies become more widely available due to decrease in cost, more and more genes associated with inherited diseases are being identified, and the list of genes associated with myopathies, both skeletal and cardiac, continues to grow. Although variants in the same gene could have different effects on the disease course, it is impractical to generate and maintain mouse models representing each pathogenic variant, given cost, time, and space constraints. Therefore, cell-based models created from patient cells can serve as a valuable complementary tool to study specific variants. Cells isolated from patients capture their genetic alterations of interest, and they also allow researchers to study the variants within the genetic landscape of the specific patient. Below, I will discuss currently available cell-based models of skeletal muscle as well as induced pluripotent stem cell-derived cardiomyocytes and their use in disease modeling. In this thesis, I describe cellular models of limb girdle muscular dystrophy (LGMD), Duchenne muscular dystrophy (DMD), and myotonic dystrophy (DM). Mouse models are available for both LGMD and DMD, and the goal of having specific models for these disorders was to provide a platform for testing mutation-specific therapies. Myotonic dystrophy, the most common autosomal dominant neuromuscular disorder, has been more challenging to model in mice due to its genetic nature as a nucleotide repeat expansion disorder.

Human skeletal muscle models in muscular dystrophy

Muscular dystrophies are a group of heterogeneous disorders that share common characteristics of progressive muscle weakness and wasting (Mercuri & Muntoni, 2013). As muscular dystrophy subtypes may target distinct muscle groups, the muscular dystrophies are classified by

the patterns of genetic inheritance, their causative genes, and the groups of muscles affected. It is possible to isolate myoblasts, the regenerative cells of muscle, directly from human muscle biopsies, and this method has been widely employed (Malatesta, Giagnacovo, Cardani, Meola, & Pellicciari, 2013; Spinazzola & Gussoni, 2017). However, generating myoblast cultures requires invasive, open muscle biopsies which are problematic for those with muscle wasting disorders, especially from pediatric population.

The most common inherited muscular dystrophy of the childhood is Duchenne muscular dystrophy (DMD), which is an X-linked recessive disorder that affects about 1 in 5,000 boys (Guiraud et al., 2015; Mercuri & Muntoni, 2013). Usually diagnosed before age 5, DMD is a severe disease that results in muscle wasting and weakness, which lead to loss of ambulation around age 10 (Guiraud et al., 2015). Genetically, DMD arises from a loss-of-function mutation in the *DMD* gene that encodes for dystrophin (Aartsma-Rus, Ginjaar, & Bushby, 2016). Dystrophin normally localizes to the inner surface of the sarcolemma where it interacts with other membrane-associated proteins, such as dystroglycans and sarcoglycans (Guiraud et al., 2015). Together, these proteins form dystrophin associated protein complex (DAPC) that stabilizes the muscle membrane and also serves as an important link between the intracellular and the extracellular environments of the muscle (Guiraud et al., 2015). In DMD, mutations in *DMD* gene results in a loss of protein expression and destabilizes the muscle membrane (Gao & McNally, 2015). Majority of the DMD patients (60-70%) have deletions of one or more exons while others have point mutations or exon duplications (Aartsma-Rus et al., 2016; Gao & McNally, 2015). These mutations lead to a disruption in the reading frame of *DMD* and formation of premature stop codon that result in loss of protein (Gao & McNally, 2015).

Other proteins in the DAPC are also linked to muscular dystrophies, one of which is limb girdle muscular dystrophy 2C (LGMD2C). LGMD2C is an autosomal recessive disorder that arises from loss-of-function mutations in *SGCG* gene, which encode γ-sarcoglycan protein (Mercuri & Muntoni, 2013). γ-sarcoglycan is a transmembrane protein that associates with dystrophin in the DAPC to help stabilize the muscle membrane (Guiraud et al., 2015). Similar to DMD, deletions in *SGCG* gene causes a shift in reading frame that leads to premature stop codon and subsequent loss of protein (Gao et al., 2015).

Overview of myogenesis

Skeletal muscle is formed by an intricate developmental process regulated by both extrinsic signals from nearby cells and intrinsic signals within the tissue. During embryonic myogenesis, a transcriptional cascade orchestrates the formation of muscle (Bentzinger, Wang, & Rudnicki, 2012; Chal & Pourquie, 2017). The expression of sine oculis-related homeobox 1 and 4 (Six1 and Six4, respectively) transcription regulators first specify progenitors to myogenic lineage (Bentzinger et al., 2012; Grifone et al., 2005). These proteins act as cofactors in the nucleus of muscle progenitor cells and upregulate Pax3, as well as MyoD, MRF4, and myogenin (Grifone et al., 2005). Expression of paired-homeobox transcription factors Pax3 and Pax7 commits these cells into the muscle lineage, where $Pax3^+$ cells contribute to fiber formation during early stages of embryonic development and $Pax7^+$ cells build muscle later in development (Chal & Pourquie, 2017). MyoD and Myf5 expression follows Pax3/7, further committing the progenitors to the myoblast stage (Bentzinger et al., 2012). Expression of MyoD and Myf5 in turn induces upregulation of myogenin and MRF4, which promote myocytes to fuse and form myotubes (Figure 1.1) (Bentzinger et al., 2012). Myf5, MyoD, MRF4, and myogenin are collectively

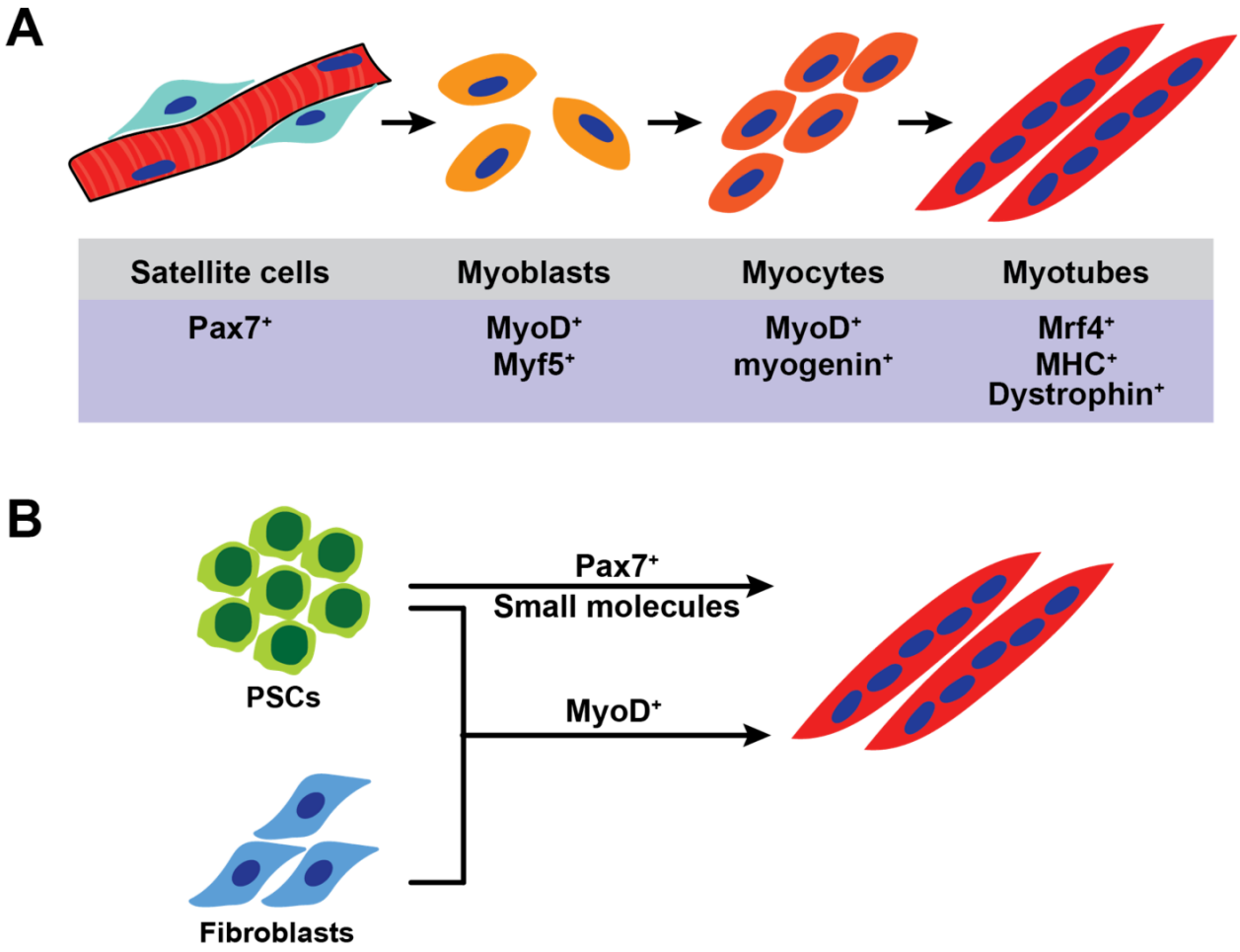

Figure 1.1 Myogenesis and cell-based skeletal muscle generation

(A) Adult myogenesis initiates with activation of $Pax7^+$ satellite cells. After committing to muscle lineage, satellite cells become myoblasts and upregulate myogenic regulatory factors, MyoD and Myf5. With myogenesis, myoblasts withdraw from cell cycle and begin to terminally differentiate. This is accompanied by elongation and alignment and upregulation of myogenin. Myoblasts then fuse to form multinucleated myotubes that express Mrf4, as well structural proteins including myosin heavy chain (MHC) and dystrophin. **(B)** Currently available methods to generate cell-based skeletal muscle models include direct differentiation of pluripotent stem cells (PSCs) and direct reprogramming of fibroblasts. PSCs engineered to express Pax7 or MyoD have been generated and differentiated to muscle lineages. Treatment of PSCs with a combination of small molecules to induce mesoderm formation followed by growth factors has been reported to promote myogenic differentiation. Direct reprogramming of fibroblasts with MyoD is sufficient to promote differentiation into myotubes-like structures.

termed myogenic regulatory factors (MRFs) for their role in myogenesis (Chal & Pourquie, 2017). Notably, a seminal study showed that expression of MyoD alone was sufficient to drive non-myogenic cells, such as fibroblasts, into myogenic lineage (R. L. Davis, Weintraub, & Lassar, 1987; Tapscott et al., 1988).

Currently available animal skeletal muscle models

There are two main cell models of skeletal myogenesis, both established from rodents. The C2C12 line represents mouse myoblasts (Blau et al., 1985; Yaffe, 1968) and L6 line is derived from rats (Yaffe, 1968). C2C12 myoblasts were originally isolated by Yaffe *et al* from 2-month old normal mice after crush injury and then subcloned by Blau *et al* (Blau et al., 1985; Yaffe, 1968). While C2C12 is considered an immortalized line, the process by which this was achieved is not well documented and has potentially occurred spontaneously during the culture process (Nowak et al., 2004). C2C12 was originally diploid at the time of subclone selection (Blau et al., 1985), but has since been reported to be near tetraploids (Casas-Delucchi et al., 2011). Other than myogenic lineage, C2C12 lines can be differentiated to osteoblastic lineage with bone morphogenic protein 2 (BMP2) stimulation (Katagiri et al., 1994). L6 myoblasts were established from thigh muscles of a newborn rat and were treated to methylcholanthrene, a carcinogen, for immortalization (Yaffe, 1968). Both C2C12 and L6 myoblasts differentiate and fuse into myotubes under low serum conditions (McMahon et al., 1994; Portier, Benders, Oosterhof, Veerkamp, & van Kuppevelt, 1999). Other available, but less widely used, cell models include MM14 (Linkhart, Clegg, & Hauschika, 1981) and BC3H1 cells (Schubert, Harris, Devine, & Heinemann, 1974). Originally isolated from mouse brain neoplasm, BC3H1 cells were later suggested to be of ectodermal origin and defective in terminal differentiation

(Taubman et al., 1989). These models serve as valuable tools in skeletal muscle research, but there are concerns regarding how faithfully they recapitulate human muscle physiology, as they originate from mice and rats and are transformed lineages. These cells also represent non-disease conditions, so disease-specific mutations need to be created in order to study them. Also, as some of these cell lines have gone through immortalization processes that can add additional stress to the cells, human cell-based systems may provide more power in muscular dystrophy studies.

Current human cell-based skeletal muscle models

In order to establish human skeletal muscle models, many of the currently available models employ myogenic regulatory factors in order to drive myogenesis. Primary normal human myoblasts are commercially available, (Owens, Moreira, & Bain, 2013), and recently, there have been immortalized myoblast lines derived from a number of distinct neuromuscular diseases (Mamchaoui et al., 2011). Other than human myoblasts, there are broadly two methods to generate human skeletal muscle models: directed differentiation of pluripotent stem cells (PSCs), and directed reprogramming of somatic cells (Chal & Pourquie, 2017).

Pluripotent stem cells (PSCs) can be manipulated into muscle lineages using the myogenic regulatory factors, notably Pax7 and MyoD (Figure 1.1). Darabi *et al* showed that expression of Pax7 in human embryonic stem cells (ESCs) and induced pluripotent stem cells (iPSCs) can generate myogenic precursors that can then be transplanted into mice to improve dystrophin expression in the context of the *mdx* mouse, a model for DMD (Darabi et al., 2012). Multiple groups have shown that overexpression of MyoD in PSCs promotes myogenesis and, in some cases, these cells integrated into the mice muscle upon transplantation (Abujarour et al., 2014; Goudenege et al., 2012; Tanaka et al., 2013; Young et al., 2016). Small molecule-based

approaches have also been used to differentiate PSCs into myogenesis. Shelton *et al* showed that Pax7-positive myogenic cells can be generated by GSK3 inhibition to promote mesodermal specification followed by growth factor treatments (Shelton et al., 2014). Using small molecules and growth factors, Chal *et al* generated myotubes from human iPSCs that exhibit spontaneous twitching (Chal et al., 2015). However, as derivation of skeletal muscle from iPSCs is a relatively recent development, these methods can be less reliable and also result in lower than desirable efficiency (Chal et al., 2015; Shelton et al., 2014).

Direct reprogramming of somatic cells by MyoD has remained a mainstay method due to its ease and general reliability. MyoD expression vectors have been developed to generate skeletal muscle models from mice and humans (Kimura et al., 2008; Lattanzi et al., 1998). After the transduction with MyoD constructs, fibroblasts fuse and form multinucleated myotubes (Kimura et al., 2008). While this method generates myotubes more efficiently, constitutive overexpression of MyoD is not a physiologically relevant and the model lacks features of mature muscle, such as transverse tubules.

Development of induced pluripotent stem cells

Induced pluripotent stem cells (iPSCs) are created by reprogramming somatic cells into an embryonic stem cell (ESC)-like state, where they resemble ESC colony morphology, display upregulation of endogenous pluripotency factors, and differentiate to three germ layers (Shi, Inoue, Wu, & Yamanaka, 2017; Takahashi et al., 2007). The first iPSCs were described a little over a decade ago and were generated by reprogramming mouse fibroblasts into cells that resemble embryonic stem cells (Takahashi & Yamanaka, 2006). A year later, iPSCs reprogrammed from human fibroblasts were reported (Takahashi et al., 2007; J. Yu et al., 2007)

and have served as an important platform for human disease modeling. Unlike embryonic stem cells that require human embryos, human iPSCs are not as ethically controversial since they are generated from non-embryonic sources. Further, they can be generated from cells that can be obtained with minimal risk, such as those isolated from peripheral blood or urine samples. Compared to primary cells that have limited cell division capacities, iPSCs can be maintained in culture for many passages, making them an attractive source for modeling specific mutations, for drug screens, or for mechanistic studies. Recent discovery and developments in CRISPR/Cas9 genome editing techniques now allow for modification of iPSCs to create isogenic controls, although these technologies may require extensive selection steps that impose stress on the cells.

Cell sources for iPSC generation

The initial generation of iPSCs were done using dermal fibroblasts (Takahashi et al., 2007; J. Yu et al., 2007). Since then, other sources of somatic cells have been identified in addition to fibroblasts, including blood and urine (Figure 1.2) (Raab, Klingenstein, Liebau, & Linta, 2014). For reprogramming into iPSCs, peripheral blood samples can be used either directly after isolation of mononuclear cells (Quintana-Bustamante & Segovia, 2016), or after transformation of isolated B lymphocytes into lymphoblastoid cell lines (LCLs) using Epstein-Barr virus (Choi et al., 2011; Rajesh et al., 2011).

Recently, cells isolated from urine samples have been used as a source for iPSC reprogramming (Afzal & Strande, 2015; Xue et al., 2013; T. Zhou et al., 2011). Urine cells first gained interest due to their potential use in genitourinary tissue repair (Bodin et al., 2010; Wu, Liu, Bharadwaj, Atala, & Zhang, 2011). Urine-derived cells (UDCs) are thought to be of renal epithelial origin, potentially from the upper urinary tract based on morphology, growth potential,

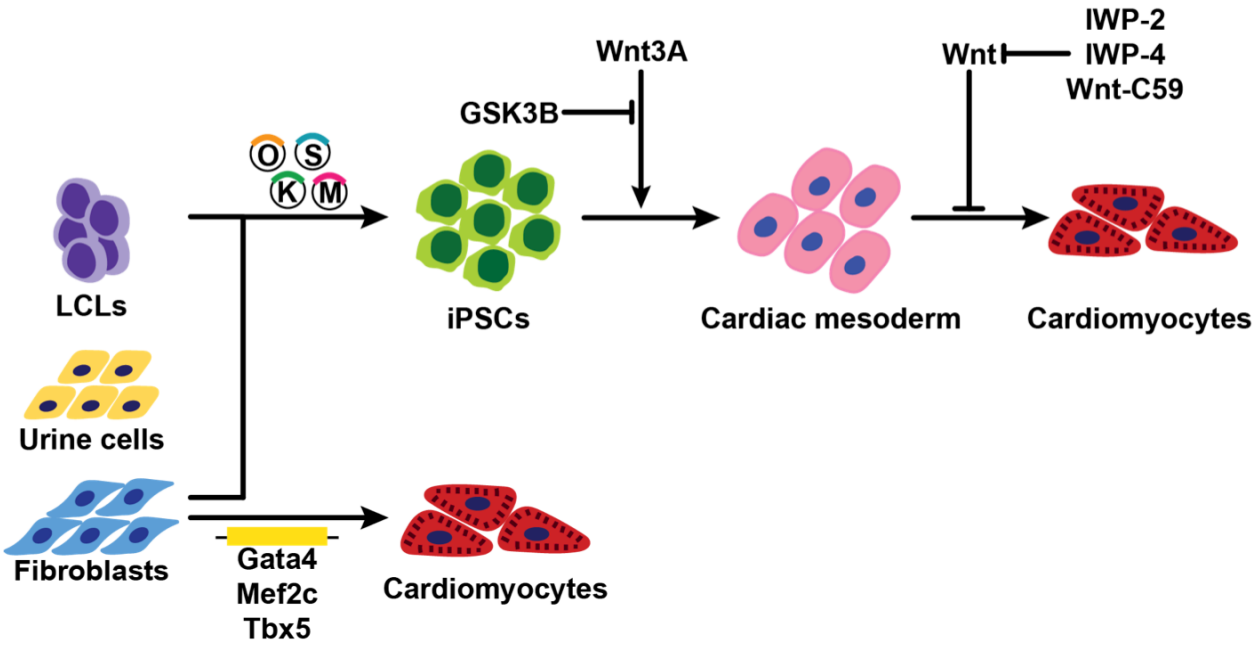

Figure 1.2 Methods to generate human cardiomyocyte models

Somatic cells, including peripheral blood mononuclear cells, lymphoblastoid cell lines (LCLs, lymphoblasts transformed with Epstein-Barr virus), urine-derived cells, and fibroblasts can each be reprogrammed into induced pluripotent stem cells (iPSCs) using Yamanaka factors (OSKM: Oct3/4, Sox2, Klf4, Myc). Once reprogrammed, iPSCs differentiate into cardiomyocyte lineages by modulating the Wnt signaling pathway. Wnt3A activation is achieved using inhibitors of GSK3B. Following this, Wnt signaling is inhibited to allow the cells to differentiate into cardiomyocyte-like cells. Like skeletal myotubes, iPSC-CMs are not a fully differentiated cell and lack transverse tubules and other features found in mature myocytes. Direct reprogramming of fibroblasts using a combination of Gata4, Mef2c, and Tbx5 has also been developed to generate cardiomyocytes (Ieda et al., 2010).

and the multipotent nature of the cells (Bharadwaj et al., 2011; Chun et al., 2012). UDCs display mesenchymal stem cell surface markers (Guan et al., 2014), and can be differentiated into multiple lineages, including urothelial, osteogenic, adipogenic, neurogenic, and myogenic (Bharadwaj et al., 2013; W. Chen et al., 2014).

Delivery methods of pluripotency factors

In order to induce pluripotency, somatic cells are treated to exogenously express the four factors, Oct4, Sox2, Klf4, and c-Myc, collectively termed Yamanaka factors (Takahashi & Yamanaka, 2006). Since the discovery of these pluripotency factors, blocking p53 expression was shown to increase reprogramming efficiency (Kawamura et al., 2009) and are now used in some reprogramming strategies (Okita et al., 2011). These factors were initially delivered by retroviral vectors, but concerns regarding integration and constitutive activation of the construct, as well as formation of teratomas in mouse models following transplantation of iPSC-derived cells have been raised (Duinsbergen, Salvatori, Eriksson, & Mikkers, 2009; Shao & Wu, 2010). In order to reduce genomic integration of these constructs, both viral and non-viral integration-free methods of factor delivery have been described. For viral delivery, adenovirus and Sendai virus have been used, but a low reprogramming efficiency of 0.0002% in human fibroblasts was reported for adenovirus (Malik & Rao, 2013; W. Zhou & Freed, 2009). Sendai virus exhibits higher reprogramming efficiency reported to be around 0.07% in fibroblasts (Schlaeger et al., 2015). Episomal vectors can be used as a non-viral factor delivery method, where the vectors are electroporated (Okita et al., 2011). Reprogramming with episomal vectors have reported efficiency of 0.01% (Schlaeger et al., 2015). Other non-viral methods include mRNA transfection, which exhibits reprogramming efficiency as high as 2%, but also carries low

success rate of 60% on a survey conducted on 55 laboratories from 12 countries (Schlaeger et al., 2015). This comparatively low success rate for mRNA-mediated reprogramming may limit its use.

IPSC-derived cardiomyocytes as human disease models

Overview of cardiogenesis

Cardiomyocyte lineage cells mostly arise from the mesoderm. During gastrulation, epiblasts ingress at the primitive streak and undergo epithelial-mesenchymal transition (EMT) to form mesoderm (Arnold & Robertson, 2009). This process of mesoderm formation occurs through signaling from components of bone morphogenic protein (BMP), nodal, and Wnt pathways (Arnold & Robertson, 2009). Primitive streak formation is induced by expression of nodal produced by the epiblasts, which in turn activates BMP4 expression in the extraembryonic ectoderm (Arnold & Robertson, 2009). BMP4 upregulation then signals to epiblasts and activates Wnt3, which maintains nodal expression (Arnold & Robertson, 2009). Wnt also upregulates transcription factor brachyury/T, which in turn upregulates another transcription factor eomesodermin (Eomes) (Brade, Pane, Moretti, Chien, & Laugwitz, 2013). T and Eomes then promote expression of mesoderm posterior 1 (Mesp1), which marks the cardiogenic mesoderm (Brade et al., 2013). This commitment towards cardiogenic mesoderm is aided by inhibition of Wnt signaling through expression of Dkk1 and Frzb2 (Brade et al., 2013; Spater, Hansson, Zangi, & Chien, 2014). Mesp1+ cardiogenic progenitor cells then migrate anteriorly to form the cardiac crescent, or the first heart field (FHF), which later fuses at the midline to form the primitive heart tube (Brade et al., 2013; Spater et al., 2014). The second heart field (SHF) progenitors are positioned posteriorly and medially to the FHF and allow the heart tube to grow

as development continues (Brade et al., 2013; Spater et al., 2014). FHF cells are committed to cardiomyocyte lineage earlier than SHF cells, and give rise to mostly left ventricular and atrial cardiomyocytes (Spater et al., 2014). SHF cells contribute mostly to the formation of the right ventricle and the atria (Spater et al., 2014).

Differentiation of iPSCs into cardiomyocytes

Cardiac differentiation of iPSCs is modeled after previous knowledge of the intricate signaling pathways during cardiac development in the mouse. Broadly, two major methods of cardiomyocyte differentiation exist in the field: embryoid body (EB) formation and monolayer culture. Both methods use modulation of signaling pathways elucidated from studies of cardiogenesis *in vivo*. First, activation of Wnt3A specifies iPSCs to mesodermal lineage (Burridge, Keller, Gold, & Wu, 2012). This is achieved by either treating iPSCs with a combination of Activin A and BMP4 that lead to direct activation of Wnt3A (Hudson, Titmarsh, Hidalgo, Wolvetang, & Cooper-White, 2012; Laflamme et al., 2007), or by inhibiting GSK3β, which is an inhibitor of Wnt3A (Burridge, Holmstrom, & Wu, 2015; Lian et al., 2013). After mesoderm specification, cells are then committed to cardiac lineage through inhibition of Wnt pathway (Burridge et al., 2012). This inhibition can be achieved using Wnt inhibitors, such as IWP-2, IWP4, and Wnt-C59 (Burridge et al., 2015; Hudson et al., 2012; Lian et al., 2013). Spontaneous beating is usually observed as early as day 7 after the start of differentiation (Burridge et al., 2015). Cardiomyocytes differentiated from iPSCs express major types of ion channels expressed in adult cardiomyocytes and develop contractile calcium cycling machineries (Del Alamo et al., 2016). However, iPSC-CMs have been shown to have transcriptional profiles

resembling those of fetal cardiomyocytes (van den Berg et al., 2015) and lack transverse tubules (Gherghiceanu et al., 2011; Robertson, Tran, & George, 2013).

IPSC-CMs as disease models

Mouse models of cardiac diseases provide valuable insights into disease mechanisms and are platforms for testing therapeutic interventions. However, the list of genetic variants associated with human cardiac conditions like cardiomyopathies expands daily, and it is not possible to model every variant or possibly even every gene in mice. Additionally, the physiological and structural differences between mouse and human hearts can render some modeling of human variants in mice ineffective. Physiologically, mice have a heart rate that is about 10 times higher than that of humans, which results in shorter action potentials (Salama & London, 2007). This difference in heart rate also leads to a need for faster repolarization in mice and the consequent use of repolarizing channels that are different from humans (Nerbonne, Nichols, Schwarz, & Escande, 2001; Salama & London, 2007). Moreover, the primary myosin heavy chain isoform expressed in the mouse heart differs from that in the human heart, where *Myh6* is the dominant form in mice and *MYH7* is the major form in human hearts (England & Loughna, 2013). These interspecies differences warrant a need for human-based systems to complement animal studies.

For some inherited cardiovascular disorders, iPSC-CMs have been shown to recapitulate key disease phenotypes. For example, arrhythmogenic phenotypes including long QT syndromes due to mutations in *KCNH2* (Itzhaki et al., 2011) and *KCNQ1* (Moretti et al., 2010) and Timothy syndrome (Yazawa et al., 2011) arising from a mutation in *CACNA1C* have been modeled and recapitulate pathologic features. Cardiomyopathic disorders like hypertrophic cardiomyopathy (HCM) (Lan et al., 2013) and dilated cardiomyopathy (DCM) (Sun et al., 2012) arising from

mutations in *MYH7* and *TNNT2*, respectively, also display pathogenic features in cells that are similar to what is seen in intact hearts. IPSC-CMs have also been used in drug toxicity studies (Burridge et al., 2016; Sharma et al., 2017), highlighting their potential as a tool in high-throughput drug screenings.

Myotonic dystrophy is a repeat expansion disorder

Myotonic Dystrophy (DM) is the most common adult onset muscular dystrophy, and arises from nucleotide repeat expansions. Nucleotide tandem repeats, also referred to as microsatellite DNA, consist of one- to six-nucleotide long motifs that repeat themselves (Hannan, 2018). It has been estimated that about 3% of genomic DNA consists of tandem repeats (Subramanian, Mishra, & Singh, 2003). While tandem repeats are found in coding and non-coding regions of the genome, it is thought that many tandem repeats located in the non-coding regions act as transcriptional modulators by serving as binding sites for transcription factors (Bagshaw, 2017). Tandem repeats are also implicated in alternative splicing and mRNA stability, depending on the position of the repeats within a given gene structure (Bagshaw, 2017). Tandem repeats can be transcribed and form complexes with the DNA, termed R loops, where they may affect RNA structure and function (Santos-Pereira & Aguilera, 2015).

In repeat expansion disorders, tandem repeats expand beyond what is considered the normal length and, these expansions disrupt many biological processes, especially when transcribed into RNA. Two of the earliest diseases to be associated with repeat expansion are fragile X syndrome (Verkerk et al., 1991) and spinal and bulbar muscular atrophy (La Spada, Wilson, Lubahn, Harding, & Fischbeck, 1991). More than 20 repeat expansions disorders have been described with many causing neurological conditions (La Spada & Taylor, 2010). It is

important to recognize that next generation, massively parallel sequencing does not readily detect repeat expansions; thus, the number of repeat expansion disorders may be underestimated and underdiagnosed (Treangen & Salzberg, 2011). The short read nature of next generation sequencing does not align repeats accurately (Treangen & Salzberg, 2011). Longer read sequencing methods may also fail to detect repeat expansions since the polymerases necessary for sequence determination may be unable to synthesize through the long repetitive sequences (Ashley, 2016).

Myotonic dystrophy (DM) is a repeat expansion disorder inherited in an autosomal dominant fashion and is the most common adult-onset muscular dystrophy with an estimated frequency of 1 in 8,000 (Lau, Sy, Corbett, & Kritharides, 2015). There are two types of DM, each associated with repeat expansions in two different genes (Meola & Cardani, 2015). Myotonic dystrophy type 1 (DM1) is associated with CTG trinucleotide expansion in 3' untranslated region of dystrophia myotonica protein kinase (*DMPK*) gene on chromosome 19q13.3 (Brook et al., 1992; Fu et al., 1992; M. Mahadevan et al., 1992). Myotonic dystrophy type 2 (DM2) is associated with CCTG tetranucleotide expansion in intron 1 of nucleic acid-binding protein (*CNBP/ZNF9*) gene on chromosome 3q21 (Liquori et al., 2001; Meola & Cardani, 2015; Ranum, Rasmussen, Benzow, Koob, & Day, 1998). DM1 is generally thought to be more common form of the two subtypes, with prevalence ranging from 1 in 8,300 to 1 in 10,700 in European populations (Thornton, 2014). However, the milder nature of DM2 may lead to its underdiagnosis. A genetic screen for DM2 in the Finnish population, estimated the frequency of DM2 as 1 in 1,830, which is more than 10 times the clinical estimates of frequency (Suominen et al., 2011). Since DM2 presents later in life with weakness and heart failure, it is possible that this constellation of symptoms is simply not diagnosed.

DM1 has a good correlation between the number of repeats and disease age of onset. Current guidelines consider repeat lengths between 5 and 35 as normal, and 38 to 50 repeats as asymptomatic, or a “pre-mutation” state (Ashizawa & Baiget, 2000; Turner & Hilton-Jones, 2014). There are four general categories of DM1 classified by repeat length (or repeat number) and age of onset. For those having between 50 and 150 repeats, the presentation is generally a later-onset DM1. Repeat lengths of 50-1000 are associated with adult-onset DM1, which is termed classical DM1. Repeat lengths of >800 can present as childhood-onset DM1, and for those with >1,000 repeats, congenital DM1 may occur (Turner & Hilton-Jones, 2014). Although there is clear overlap of these categories, these general classifications are helpful in clinical diagnoses.

These tandem repeat regions show genetic instability where the repeat numbers may differ within or between tissues, leading to somatic mosaicism (Higham, Morales, Cobbold, Haydon, & Monckton, 2012; Morales et al., 2012). The repeat expansions also show a bias towards expansion when transmitted to the next generation, exhibiting genetic anticipation where disease severity increases in the next generation (Ashizawa et al., 1994). Not all repeat expansion disorders show genetic anticipation, but it is well described for DM1 (Meola & Cardani, 2015), where the classical congenital onset DM1 is linked to cognitive impairment and respiratory failure, which can lead to death in early life (Echenne & Bassez, 2013).

Compared to DM1, DM2 is characterized by having a greatly expanded repeat length, usually greater than 5,000 (Liquori et al., 2001). Moreover, unlike DM1, DM2 does not show a correlation between the number of repeats and the age of onset (Meola & Cardani, 2015). In DM1, the CTG repeat expansions are generally uninterrupted (Kamsteeg et al., 2012). In contrast, in DM2 the disease locus in healthy individuals can exhibit CCTG repeats that are

interrupted as a complex motif $(TG)_n(TCTG)_n(CCTG)_n$ (Liquori et al., 2003). In disease, uninterrupted CCTG sequence expands beyond 30 repeats, and reported number of repeats varies from 55 to 11,000 with a mean of about 5,000 repeats (Bachinski et al., 2009; Liquori et al., 2001). It should be emphasized that accurate detection of repeat length and determination of its interrupted or uninterrupted status is technically challenging. Thus, the accuracy of repeat length in DM2, or even the larger repeat numbers of DM1, may be only estimated. That said, DM2 is characterized by later age of onset, and genetic anticipation is not generally a feature of DM2, nor has a congenital form of DM2 been convincingly described (Udd & Krahe, 2012).

Clinical presentations of DM1 and DM2

DM1, especially with earlier age of onset, is a more systemic disorder compared to DM2. For adult-onset DM1, which is the most prevalent form of the disease (Udd & Krahe, 2012), patients usually present between ages of 10 and 30 with myotonia, which is defined as hypercontraction and usually affects the hands (Thornton, 2014). Myotonia can also involve tongue or other facial muscles, which could lead to dysarthria and dysphagia as the disease progresses (Meola & Cardani, 2015; Udd & Krahe, 2012). Over time weakness ensues, with wasting of cranial, trunk, and distal limb muscles (Thornton, 2014). Ptosis of the eye muscles and wasting of temporalis and masseter muscles, contribute to the characteristic myopathic appearance in DM1 (Thornton, 2014; Turner & Hilton-Jones, 2010).

DM1 also targets the heart, where the most common manifestations are arrhythmias. On electrocardiography (ECG), DM1 patients show PR interval and QRS complex prolongation (Thornton, 2014). A meta-analysis of DM1 cardiac studies conducted between 1980 and 2010 (n = 1,828) found atrioventricular block in 28.2% of DM1, followed by bundle branch blocks

(LBBB 5.7%, RBBB 4.4%) (Petri, Vissing, Witting, Bundgaard, & Kober, 2012). Premature ventricular contractions were the most common form of arrhythmia (14.6%), followed by atrial fibrillation (5.0%) (Petri et al., 2012). Left ventricular systolic dysfunction may also develop and was seen in 7.2% of the patients (Petri et al., 2012). DM1 patients are also at a risk for sudden death. One of the studies included in the meta-analysis followed 406 patients over 10 years and identified that 20% (81 patients) of the patients died, where about 30% of the deaths were attributed to sudden death (Groh et al., 2008). The most common cause of nonsudden death was respiratory failure (39.5%) (Groh et al., 2008). These data are representative of the cardiopulmonary defects in DM1.

Clinically, DM2 is considered a milder form of the two DM subtypes, and clinical features can be highly variable between patients (Udd & Krahe, 2012). Unlike DM1 where myotonia is seen in the majority of adult-onset cases, DM2 patients may not show any signs of myotonia, clinically or on electromyography (Udd & Krahe, 2012). The absence of myotonia features on electromyography may contribute to the underdiagnosis of DM2. DM2 patients usually present with prominent myalgia or proximal lower limb muscle weakness (Meola & Cardani, 2017; Udd & Krahe, 2012). One study of 38 DM2 patients found the most common cardiac manifestations to be conduction defects (35.9%), left ventricular systolic dysfunction (15.7%), and supraventricular arrhythmias (15.8%) (Wahbi et al., 2009). A recent study of 32 DM2 patients found that subclinical myocardial injury, detected by MRI, was already present in patients with preserved ejection fraction (Schmacht et al., 2016). Together, these studies identify key differences between DM1 and DM2, specifically with regard to the degree of myotonia in DM1 and the absence of certain systemic features in DM2. Skeletal muscle weakness and cardiac rhythm disturbances are in common to both DM1 and DM2. Other clinical features in

DM include cataracts, which are shared by DM1 and DM2, and central nervous system symptoms, such as sleep disorders and cognitive alterations, which are generally observed in DM1 (Meola & Cardani, 2015). A comparison of DM1 and DM2 clinical features can be found in Table 1.1.

Table 1.1 Comparison of clinical features between subtypes of myotonic dystrophy

	DM1	DM2
Skeletal muscle		
Myotonia	High prevalence	Not common
Myalgia	None/mild	Common
Facial muscle involvement	Usually	Minimal
Neck muscle involvement	Common	Common
Limb muscles affected	Finger flexor Ankle flexor	Finger flexor Hip flexors Thigh flexors
Respiratory muscle weakness	Common	Common in later life
Cardiac		
Conduction block	Common	Potentially as common as DM1
Arrhythmia	Atrial > ventricular	Atrial > ventricular
ECG findings	Increased PR, QRS intervals	Increased PR, QRS interval
LV systolic dysfunction	10-20%	Similar to DM1
Central nervous system		
Cognitive changes	Anxiety, memory impairment, etc	Uncommon
Sleep disturbance	Daytime hypersomnolence	Uncommon
Eye		
Cataracts	Occurs at <55 years of age	Occurs at <55 years of age
Metabolic/endocrine		
Glucose intolerance	Present	Milder than DM1
Hypogonadism	Present	Milder than DM1
Gastrointestinal		
Dysmotility	Present	Unknown

Toxic RNA gain-of-function as a pathogenic mechanism in DM

The main mechanism that has been proposed for DM is toxic RNA gain-of-function leading to alternative splicing of genes linked to key aspects of the myotonic phenotype (Figure 1.3) (Meola & Cardani, 2015). The expanded nucleotide repeats in DM, when transcribed into CUG RNA, are retained in the nucleus forming secondary hairpin structures of double stranded RNA (B. M. Davis, McCurrach, Taneja, Singer, & Housman, 1997; Napierala & Krzyzosiak, 1997). RNA aggregates are readily detectable in the nuclei of DM cells (Mankodi, Lin, Blaxall, Swanson, & Thornton, 2005; Mankodi et al., 2001). How these RNA aggregates contribute to disease is likely multifactorial. Sequestration of RNA binding proteins is one key mechanism. Specifically, sequestration of the muscleblind (MBNL) family of RNA proteins and CUG-binding protein 1 (CUGBP1) have each been implicated in myotonic pathogenesis. Notably, most of these studies have been carried out in the setting of DM1, and fewer studies have focused on DM2.

The MBNL family include 3 isoforms, MBNL1, MBNL2, and MBNL3. MBNL1 shows ubiquitous expression pattern and serve as the primary isoform in most tissues, while MBNL2 is predominantly expressed in the brain and has been implicated in the brain pathology of DM1 (Charizanis et al., 2012; Konieczny et al., 2014). MBNL3 is minimally expressed in skeletal muscle, and has been suggested to act as an antagonist of myogenesis (Lee, Smith, Amieux, & Wang, 2008; Lee, Squillace, & Wang, 2007). All three MBNL proteins have been shown to be sequestered by CUG repeats (Fardaei et al., 2002; Miller et al., 2000). Specifically, MBNL1 was shown to interact with double strand CUG repeat structures in a screen where it was crosslinked to CUG repeat region and then identified through mass spectrometry (Miller et al., 2000). MBNL1 expression level normally rises during development, and this rise accompanies the shift

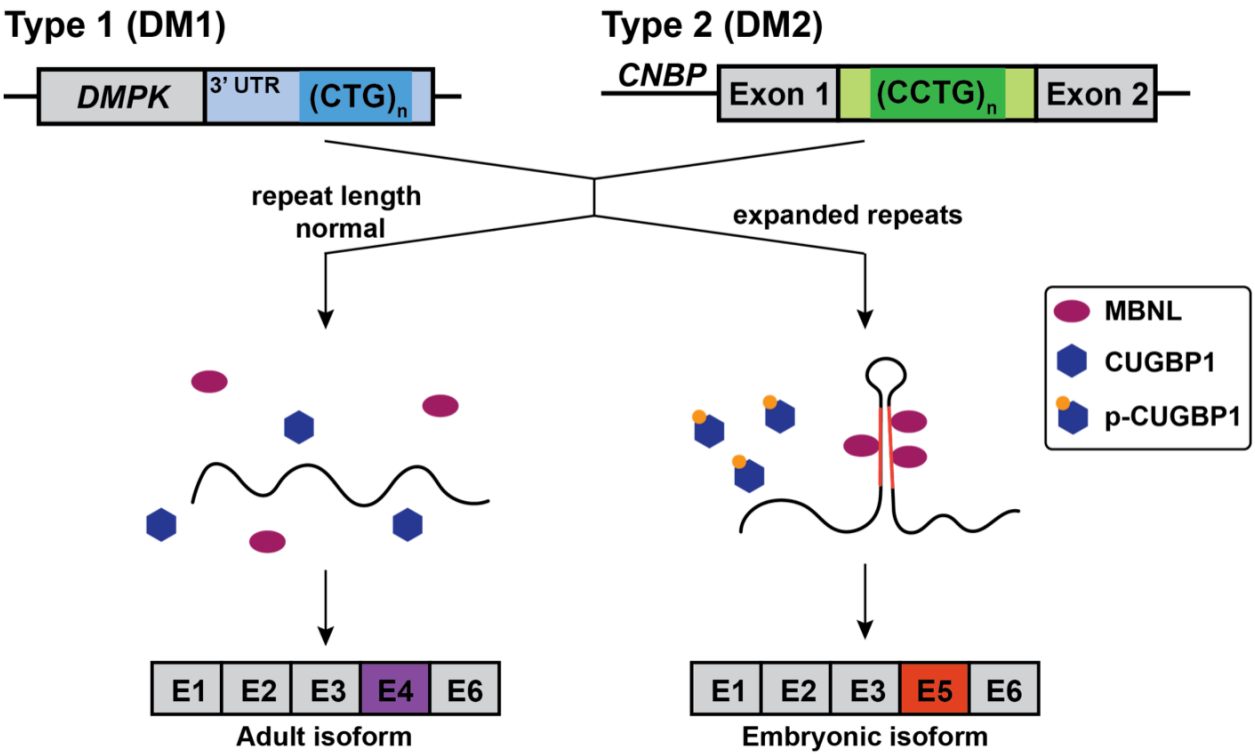

Figure 1.3 Pathogenic mechanism in myotonic dystrophy

In myotonic dystrophy, CTG and CCTG nucleotide tandem repeats are expanded and lead to clinical phenotypes that primarily effect skeletal muscle and the heart. Transcription of these expanded nucleotide repeats produces double stranded RNA aggregates, which can be detected within nuclei. These RNA aggregates bind RNA binding proteins, the most well-studied of which is muscleblind (MBNL). MBNL normally functions as a splicing regulator and aids in expression of adult transcript isoforms (Konieczny, Stepniak-Konieczna, & Sobczak, 2014). When RNA aggregates bind MBNL, MBNL is functionally depleted and its downstream genes are misspliced, most commonly as embryonic transcript splice forms. Another RNA binding protein implicated in DM pathogenesis is CUG binding protein 1 (CUGBP1). In DM1, CUGBP1 is upregulated and hyperphosphorylated. This activates CUGBP1, which also acts as a splicing regulator. CUGBP1 is thought to have an opposing role to MBNL where it aids in splicing of embryonic transcript isoforms. Therefore, the functional loss of MBNL and activation of CUGBP1 together lead to a shift in splicing from adult to embryonic isoforms. Notably, these RNA binding protein changes have been best described in DM1, especially in DM1 skeletal muscle.

of splicing pattern from embryonic to adult isoforms (Konieczny et al., 2014). In DM1, MBNL1 is sequestered by CUG repeat regions and becomes functionally depleted from the nucleus (X. Lin et al., 2006). This leads to missplicing of downstream effector genes, including chloride channel (*CLCN1*), which has been associated with myotonia (Mankodi et al., 2002). This missplicing, as well as myotonic discharges on electromyography, was subsequently rescued by exogenous delivery of *Mbnl1* to the leg muscle in a mouse model that carries skeletal muscle-specific 250 CTG repeats (HSA^{LR}, model is discussed in the section below) (Kanadia et al., 2006). Missplicing of another gene that encodes insulin receptor, *INSR*, has been linked to insulin resistance in DM (Savkur, Philips, & Cooper, 2001; Savkur et al., 2004). Glucose uptake assay in DM1 myotubes generated by MyoD conversion of fibroblasts demonstrated decreased insulin responsiveness compared to control myotubes (Savkur et al., 2001).

CUGBP1 is a distinct RNA binding protein also misregulated in DM1. Unlike MBNL1 that binds double strand CUG repeat structures, CUGBP1 binds single strand CUG repeats *in vitro* (Lambert et al., 2014; Timchenko, Cai, et al., 2001). CUGBP1 has not been observed in RNA foci, and therefore is not thought to share the same mechanism as MBNL (Mankodi et al., 2003; Miller et al., 2000). However, like MBNL, CUGBP1 does contribute to the regulation of alternative splicing (Barreau, Paillard, Mereau, & Osborne, 2006). CUGBP1 is increased in human DM1 skeletal muscle and heart (X. Lin et al., 2006; Mankodi et al., 2005; Philips, Timchenko, & Cooper, 1998). In addition, CUG repeat RNA promotes hyperphosphorylation and stabilization of CUGBP1, which in turn leads to an increase in steady state levels of the protein (Kuyumcu-Martinez, Wang, & Cooper, 2007). This hyperphosphorylation is mediated through protein C kinase (PKC), although the exact mechanism underlying the activation of PKC through repeat expansion is still unknown (Kuyumcu-Martinez et al., 2007). Increased CUGBP1

has been linked to missplicing of *INSR* (Savkur et al., 2001) and *CLCN1* (Mankodi et al., 2002), as well as cardiac troponin (*TNNT2*) in the heart (Philips et al., 1998). While increased CUGBP1 has been shown consistently in DM1, in DM2, there have been conflicting results on CUGBP1 where an increase (Jones et al., 2015), decrease (Cardani et al., 2014), and no change (Cardani et al., 2013) have all been reported. Thus, it is possible that CUGBP1 contributes to distinct pathogenic mechanisms in DM subtypes.

Other proteins involved in messenger ribonucleoprotein (mRNP) complexes have also been implicated in DM pathogenesis. One such family is DEAD-box helicases, specifically DDX5, DDX17, and DDX6. DDX5 and DDX17 were shown to co-localize with CUG repeat constructs in HeLa cells (Laurent et al., 2012). The same study also showed that DDX5 disrupted the CUG secondary structures and stabilized MBNL1 binding to CUG repeats (Laurent et al., 2012). This binding enhancement by DDX5 was not as pronounced with CCUG repeats of DM2 (Laurent et al., 2012). DDX5 also regulates alternative splicing of *TNNT2* (Laurent et al., 2012). These findings suggest that DDX5 serve as a modulator of MBNL1 in DM1, while its effect may not be as apparent in DM2. Pettersson *et al* showed that overexpression of another DEAD-box helicase, DDX6, alters MBNL1 localization in DM1 fibroblasts to be a more diffuse pattern (Pettersson et al., 2014). DDX6 overexpression also reduced ribonuclear foci formation in DM1 fibroblasts, as well as promoting a slight correction in missplicing of *INSR* (Pettersson et al., 2014). On the other hand, reduction of DDX6 increased ribonuclear foci formation (Pettersson et al., 2014). Together with DDX5 results, these findings suggest that DDX5 and DDX6 potentially have opposing roles with respect to their interaction with MBNL1, where DDX5 enhances MBNL1 binding to CUG repeats and DDX6 inhibits it.

Staufen1, another RNA binding protein normally associated with mRNA transport (Kiebler et al., 1999), decay (Y. K. Kim, Furic, Desgroseillers, & Maquat, 2005), as well as translational efficiency (Dugre-Brisson et al., 2005), has also been implicated in alternative splicing in DM1 (Ravel-Chapuis et al., 2012). Staufen1 expression is increased in skeletal muscle of DM1 patients (Ravel-Chapuis et al., 2012). In C2C12 cells expressing 200 CUG repeats, Staufen1 did not alter ribonuclear foci or MBNL1 cluster formation (Ravel-Chapuis et al., 2012). Interestingly, expression of Staufen1 was observed to change *INSR* alternative splicing to the same degree as expression of MBNL1 in DM1 human fibroblasts that have been converted with MyoD, suggesting Staufen1 as an alternative splicing regulator (Ravel-Chapuis et al., 2012).

Rbfox1 (also known as A2BP1), a member of Rbfox family of RNA-binding proteins, is specifically expressed in the neurons (Underwood, Boutz, Dougherty, Stoilov, & Black, 2005), skeletal muscle, and heart (Kiehl, Shibata, Vo, Huynh, & Pulst, 2001) and functions as an alternative splicing regulator (C. Zhang et al., 2008). RNA-seq analysis of skeletal muscle isolated from mice deleted for Rbfox1 displayed alternative splicing in various genes important in the formation of the cytoskeletal and the sarcomeres, as well as those important in calcium signaling, suggesting that Rbfox1-dependent genes are important in adult muscle function (Pedrotti et al., 2015). In DM1 embryonic and adult cells, expression of Rbfox1-dependent splice isoforms was also detected (Klinck et al., 2014). Further, this study found alternative splicing events shared by both Rbfox1 and MBNL1, suggesting that their function as co-regulators of splicing in DM1 (Klinck et al., 2014).

Mouse models of myotonic dystrophy

Mouse models of myotonic dystrophy, especially DM1, have been developed and provided valuable insight into DM pathogenesis (Gomes-Pereira, Cooper, & Gourdon, 2011). These models (summarized in Table 1.2-1.4) can be broadly classified into three categories: models that modulate gene expression at or around DM loci, models that express repeat expansions, and models that recapitulate the misregulation of splicing factors.

For DM1, two separate *Dmpk* knockout mice, a *Six5* knockout mouse, and an *DMPK* overexpression mouse have each been reported. One $Dmpk^{-/-}$ model was found to have grossly normal phenotype (Jansen et al., 1996), while a second $Dmpk^{-/-}$ model exhibited skeletal muscle phenotype resembling DM1, including progressive skeletal myopathy and weakness (Reddy et al., 1996). Structural abnormalities of skeletal muscle sections were also noted, but myotonic discharges were not observed by electromyography (EMG) (Reddy et al., 1996). *SIX5* is a neighboring gene positioned 3' to *DMPK* in humans, and the level of *SIX5* expression has been reported to be decreased in DM1 due to suppression through repeat expansion in *DMPK* (Klesert, Otten, Bird, & Tapscott, 1997; Thornton, Wymer, Simmons, McClain, & Moxley, 1997). The $Six5^{-/-}$ mouse model was created to evaluate the role of reduced *Six5* expression in disease. These mice developed cataracts, but no skeletal or cardiac muscle phenotypes, suggesting that downregulation of *SIX5* contributes to cataract development in DM1 (Klesert et al., 2000; Sarkar et al., 2000). The effects of *DMPK* overexpression have also been studied in a mouse model that carry 25 copies of human *DMPK* (Jansen et al., 1996; O'Cochlain et al., 2004). This model developed myotonic discharges on EMG, displayed skeletal myopathy on histological studies, as well as walking impairment and reduced exercise tolerance (O'Cochlain et al., 2004). In the heart, *DMPK* overexpression led to hypertrophic cardiomyopathy and altered

Table 1.2 Mouse models of DM that display skeletal muscle phenotypes

Model	Effect	Skeletal muscle phenotype					
		Histo-path	EMG	Weakness	RNA foci	MBNL1 foci	Splicing shift
Gene expression modulation							
Dmpk$^{-/-}$		X	X				
Dmpk$^{-/-}$		O	X	O			
Six5$^{-/-}$							
Tg26	*Dmpk* O/E	O	O	O			
Znf9$^{+/-}$		O	O	O			
Repeat expression							
HSA^{LR}	$(CUG)_{250}$	O	O			O	O
DM300	$(CTG)_{300}$	O	O	O	O		O
DMSXL	$(CTG)_{1000-1800}$		O	O	O	X	
EpA960	HSA promoter, $(CTG)_{960}$	O	O	O	O	O	O
GFP-*DMPK*-$(CTG)_5$	$(CTG)_5$ in 3' UTR	O	O		X	X	
GFP-*DMPK*-$(CTG)_{200}$	$(CTG)_{200}$ in 3' UTR				O	O	
DM2-HSAtg	$(CCTG)_{121}$ expansion in intron under HSA promoter		O		O	O	X
Misregulation of splicing factor							
Mbnl1$^{\Delta 3/\Delta 3}$		O	O				O
Mbnl2$^{GT4/GT4}$		X	X				X
Mbnl2$^{-/-}$		O	O				O
CUGBP1-TR	*CUGBP1* O/E	O					
MCKCUGBP1	*CUGBP1* O/E	O					O
TRECUGBP1	*CUGBP1* O/E in muscle	O		O			X

O/E = overexpression; histopath = histopathological changes; EMG = myotonia detected on electromyography

Under phenotypes: O = phenotype present; X = phenotype absent; blank = not determined

Rows that are shaded in green model DM2. All others are DM1 models.

Table 1.3 Mouse models of DM that display cardiac phenotypes

Model	Effect	Cardiac phenotype					
		Histopath	CM?	Conduction defect	RNA foci	MBNL1 foci	Splicing shift
Gene expression modulation							
Tg26	*Dmpk* O/E		HCM	O			
Znf9$^{+/-}$		O		O			
Repeat expression							
DMSXL	$(CTG)_{1000-1800}$				O	X	O
EpA960	α-MHC promoter, $(CTG)_{960}$	O	DCM	O	O	O	O
GFP-*DMPK*-$(CTG)_5$	5 CTG repeats in 3' UTR			O			
Misregulation of splicing factors							
Mbnl1$^{\Delta 3/\Delta 3}$							O
TRECUGBP1	*CUGBP1* O/E in heart	O		O			O

O/E = overexpression; histopath = histopathological changes
Under phenotypes: O = phenotype present; X = phenotype absent; blank = not determined
Rows that are shaded in green model DM2. All others are DM1 models.

Table 1.4 Mouse models of DM that display non-myopathic phenotypes

DM subtype	Model	Other phenotypes	Reference
Gene expression modulation			
DM1	*Dmpk*$^{-/-}$		(Jansen et al., 1996)
	Dmpk$^{-/-}$		(Reddy et al., 1996)
	Six5$^{-/-}$	Cataracts	(Sarkar et al., 2000)
	Tg26	Smooth muscle tone deficits	(Jansen et al., 1996) (O'Cochlain et al., 2004)
DM2	*Znf9*$^{+/-}$	Cataracts	(W. Chen et al., 2007)
Repeat expression			
DM1	HSA^{LR}		(Mankodi et al., 2000)
	DM300	Age-dependent defects in glucose metabolism Growth retardation High mortality	(Seznec et al., 2000) (Guiraud-Dogan et al., 2007) (Vignaud et al., 2010)
	DMSXL	Growth retardation	(Huguet et al., 2012)
	EpA960 (heart)	Death within 2 weeks	(Wang, Kearney, De Biasi, Taffet, & Cooper, 2007)
	EpA960 (muscle)		(Orengo et al., 2008)
	GFP-DMPK-$(CTG)_{5 \text{ or } 200}$		(M. S. Mahadevan et al., 2006)
	DMPK-GFP-$(CTG)_n$	Defective muscle differentiation	(Storbeck et al., 2004)
DM2	DM2-HSAtg	CUGBP1 upregulation in liver	(Salisbury et al., 2009) (Udd et al., 2011)
Misregulation of splicing factors			
	Mbnl1$^{\Delta 3/\Delta 3}$	Cataracts	(Kanadia et al., 2003)
	Mbnl2$^{GT4/GT4}$		(X. Lin et al., 2006)
	Mbnl2$^{-/-}$		(Hao et al., 2008)
	CUGBP1-TR	Delayed myogenesis Growth retardation	(Timchenko et al., 2004)
	MCKCUGBP1	Neonatal lethality	(Ho, Bundman, Armstrong, & Cooper, 2005)
	TRECUGBP1 (muscle)		(Ward, Rimer, Killian, Dowling, & Cooper, 2010)
	TRECUGBP1 (heart)	Death within two weeks	(Koshelev, Sarma, Price, Wehrens, & Cooper, 2010)

rhythm, such as ventricular tachyarrhythmia (O'Cochlain et al., 2004). However, as DMPK overexpression is not what occurs in DM, the value of this model is limited.

Expression of the repeat expansions itself has also been used to model DM1. HSA^{LR} mice were engineered as a transgene to express 250 CUG repeats under a human skeletal actin promoter in order to target expression of the repeats to skeletal muscle (Kanadia et al., 2003). This model recapitulated skeletal muscle features of DM1 including myotonic discharges detected as early as 4 weeks of age, myopathic histology in older mice, MBNL1 sequestration, and associated missplicing (Kanadia et al., 2003). However, these mice did not show muscle weakness or wasting (Kanadia et al., 2003). The DM300 mouse model was engineered to have a randomly inserted CTG repeat sequence with more than 300 copies, and these mice developed skeletal muscle phenotypes including ribonuclear foci formation in myoblasts, myotonia, myopathic changes, and progressive muscle weakness (Seznec et al., 2000; Vignaud et al., 2010). These mice also displayed systemic features including defects in glucose metabolism and growth retardation (Guiraud-Dogan et al., 2007). A related mouse model, DMSXL, was developed when DM300 mice were found to develop a further repeat expansion after breeding and transmission of the mutant allele (Huguet et al., 2012). DMSXL mice had histopathological findings in skeletal muscle, weakness, and mild myotonia (Huguet et al., 2012). These mice showed ribonuclear foci, but no MBNL1 sequestration, in both skeletal muscle and the heart (Huguet et al., 2012). The tissue-specific effects of repeat expansion could be evaluated with EpA960 mice that express repeats in either skeletal (Orengo et al., 2008) or cardiac muscle (Wang et al., 2007). These mice carry the last exon of *DMPK* with 960 interrupted CTG repeats under CMV promoter and a floxed SV40 polyadenylation site is placed upstream to prevent expression of *DMPK* transgene (Wang et al., 2007). Crossing of these mice with mice expressing

tamoxifen-inducible Cre under α-myosin heavy chain or human α-skeletal actin allows for generation of heart- (Wang et al., 2007) or skeletal muscle-specific model (Orengo et al., 2008). EpA960 mice showed DM1-like changes in the skeletal muscle, such as ribonuclear foci formation, MBNL1 sequestration and missplicing event, as well as histopathological changes (Orengo et al., 2008). The hearts of EpA960 mice exhibited dilated cardiomyopathy characterized by dilated left ventricle with thin wall and systolic and diastolic dysfunctions detected on echocardiography, as well as arrhythmia characterized by longer PR interval and QRS widening on electrocardiography (ECG) (Wang et al., 2007). These mice also showed ribonuclear foci and MBNL1 sequestration, embryonic splice isoform expressions, and CUGBP1 upregulation (Wang et al., 2007). However, the nucleotide repeats expressed in these mice were interrupted repeats, whereas less than 5% of DM1 patients are thought to carry interrupted repeats (Kamsteeg et al., 2012). Other CTG expansion models include a model in which a GFP-tagged *DMPK* carrying 91 repeats was overexpressed (Storbeck et al., 2004). This model showed defects in muscle differentiation only(Storbeck et al., 2004). Interestingly, one model with five CTG repeats that was initially developed as a control mouse to $(CTG)_{200}$ mouse displayed myotonia and missplicing of *Clcn1* and *Tnnt3* in the skeletal muscle, as well as heart block (M. S. Mahadevan et al., 2006). Notably, the transgene expression in this model was inducible with tetracycline, and withdrawal of tetracycline after the onset of the symptoms reverted both skeletal muscle and cardiac phenotypes in 11 out of 14 and 7 out of 14 mice, respectively (M. S. Mahadevan et al., 2006).

To assess the degree to which individual splicing factors contribute to DM1 pathogenesis, MBNL1, MBNL2, and CUGBP1 have each been manipulated in the mouse. An *Mbnl1* knockout mouse model, $Mbnl1^{\Delta 3/\Delta 3}$, exhibited myotonic discharges and myopathy, as well as missplicing

of *Clcn1* in the skeletal muscle and *Tnnt2* in the heart (Kanadia et al., 2003). Two separate mouse models of *Mbnl2* knockout have been generated. One model was found to have normal phenotype (X. Lin et al., 2006), while the other model developed myopathy on histology, myotonia, and *Clcn1* missplicing (Hao et al., 2008). Overexpression of CUGBP1 has also been tested in mice. One model of CUBGP1 overexpression showed delayed myogenesis (Timchenko et al., 2004), while another model of CUGBP1 overexpression specifically in skeletal muscles and heart was shown to have neonatal lethality (Ho et al., 2005). Neonatal mice from this model showed missplicing in both skeletal muscle and the heart, as well as histological abnormalities in the skeletal muscle (Ho et al., 2005). Overexpression of CUGBP1 specifically in skeletal muscle showed functional impairment, central nuclei on histology, and embryonic splicing profiles (Ward et al., 2010), while overexpression specifically in the heart showed cardiac conduction defects manifested as increased PR interval and QRS complex, histological changes, and embryonic splicing profiles (Koshelev et al., 2010).

DM2 has been less modeled in the mouse, likely due to the large number of CCTG repeats seen in human DM2. Two models have been reported so far, where the first is a genetic deletion of *Znf9 (Cnbp)* and the second is a CCUG expansion model. Homozygous deletion of *Znf9* was embryonically lethal (W. Chen et al., 2007). Heterozygous deletion of $Znf9^{+/-}$ recapitulated many of DM2 phenotypes (W. Chen et al., 2007) including myotonia, muscle wasting, increased central nuclei and variability in fiber size, and walking defects in skeletal muscle, and a prolonged PR interval and cardiac hypertrophy in the heart (W. Chen et al., 2007). These mice also developed cataracts, recapitulating an additional finding seen in DM2 (W. Chen et al., 2007). However, conflicting results regarding whether there is a decrease in ZNF9/CNBP level in DM2 exist, as studies showing both a decrease (Huichalaf et al., 2009; Pelletier et al.,

2009) and no change (Margolis, Schoser, Moseley, Day, & Ranum, 2006; Massa et al., 2010) in protein level of ZNF9 have been reported. This could potentially limit the relevance of *Znf9*$^{+/-}$ model. Also, as DM2 patients display either no or mild myotonia clinically or on EMG, the observation of myotonia in *Znf9*$^{+/-}$ mice may suggest that the expression level of ZNF9/CNBP in DM2 patients is not as low as in the mouse model. DM2-HSAtg is third DM2 model that expresses 121 CCUG repeats under HSA promoter (Salisbury et al., 2009; Udd et al., 2011). These mice showed ribonuclear foci with MBNL1 co-localization in the skeletal muscle displayed myotonia on EMG without aberrant splicing of *Clcn1* (Udd et al., 2011). These mice also showed ribonuclear foci in other organs, including brain and smooth muscle, and no abnormal splicing was observed (Udd et al., 2011).

While these animal models have been useful for highlighting aspects of the myotonic phenotype, no model genetically and pathologically reflects the DM, especially DM2 where the models have been limited in scope. Therefore, to expand what is known about DM pathogenetic mechanisms, I describe in this dissertation novel cellular models of human myopathic phenotypes. The purpose of this work was to create platforms that provide insightful complements to the existing animal models and that ultimately may prove useful as a format in which to test potential therapies.

Outline of dissertation

In this dissertation, I describe the development of cell-based disease models to study multiple forms of muscular dystrophies and their associated cardiomyopathies. Chapter 2 details the development of a noninvasive skeletal muscle model that can be applied in a patient-specific manner. Overexpression of the myogenic regulator, MyoD, has been shown to induce skeletal

muscle differentiation in human fibroblasts (Kimura et al., 2008). Based on this knowledge, we sought to develop a skeletal muscle model that can be obtained from a noninvasive source. I isolated cells from urine samples, induced MyoD expression, and differentiated urine-derived cells into myotubes in culture. These myotubes displayed expression of skeletal muscle proteins, such as dystrophin and fast myosin heavy chain. When urine cells were isolated from patients with muscular dystrophies, the myotubes carried the genotypic defects and recapitulated disease phenotypes. These models have now been used to test exon skipping to correct the underlying genetic defect (Wyatt et al., 2018).

In Chapter 3, this myotube model was used to generate models of myotonic dystrophy type 1 and 2. Here we demonstrated that myotubes differentiated from DM1 patients recapitulated disease phenotypes and showed intranuclear MBNL1 cluster as well as missplicing events. Furthermore, DM1 myotubes had a decrease in dystrophin expression when compared to DM2 and control myotubes, which may reflect a myogenic defect in DM1 that has been suggested by at least one study (Timchenko, Iakova, Cai, Smith, & Timchenko, 2001). DM2 myotubes, in contrast to DM1, resembled myotubes generated from healthy controls, suggesting a distinct pathogenic profile from DM1 and that MBNL1 may only minimally contribute to DM2 pathogenesis.

Chapter 4 describes experiments in which I generated iPSCs from both DM1 and DM2 patients. These iPSCs were differentiated into cardiomyocytes in order to better understand cardiac pathogenesis in DM. Using iPSCs and iPSC-CMs, I found that ribonuclear foci were readily detected with RNA fluorescence *in situ* hybridization in both DM1 and DM2 cells. Furthermore, RNA foci increased with cellular differentiation in both DM1 and DM2 cells. Similar to myotubes, DM1 iPSC-CMs displayed frequent intranuclear MBNL1 clusters, as well

as alternatively spliced transcripts. In contrast, DM2 iPSC-CMs displayed an MBNL1 pattern similar to healthy control iPSC-CMs as well as splicing profiles that resembled healthy control cells. Calcium handling in iPSC-CMs was different in DM1 and DM2, compared to iPSC-CMs from healthy controls, but DM1 and DM2 iPSC-CMs each had unique features of aberrant calcium handling. RNA sequencing performed on healthy control, DM1, and DM2 iPSC-CMs identified misregulated potassium channels as potentially contributing to ion imbalance in the DM1 and DM2.

In Chapter 5, I summarize findings from this dissertation and provide interpretation of the results. I also discuss potential mechanisms behind the difference between DM1 and DM2 pathogenesis, as well as future directions with these cell-based systems. These systems add to the existing model systems by providing a noninvasive, patient-specific disease models that can serve as platforms upon which mechanistic studies and therapeutic screens can be conducted.

CHAPTER 2

DIRECT REPROGRAMMING OF URINE-DERIVED CELLS WITH INDUCIBLE MYOD FOR MODELING HUMAN MUSCLE DISEASE

(modified from Kim et al., Skeletal Muscle, 2010)

OVERVIEW

Cellular models of muscle disease are taking on increasing importance with the large number of genes and mutations implicated in causing myopathies and the concomitant need to test personalized therapies. Developing cell models relies on having an easily obtained source of cells and, if the cells are not derived from muscle itself, a robust reprogramming process is needed. Fibroblasts are a human cell source that works well for the generation of induced pluripotent stem cells, which can then be differentiated into cardiomyocyte lineages and, with less efficiency, skeletal muscle-like lineages. Alternatively, direct reprogramming with the transcription factor MyoD has been used to generate myotubes from cultured human fibroblasts. Although useful, fibroblasts require a skin biopsy to obtain and this can limit their access, especially from pediatric populations. We now demonstrate that direct reprogramming of urine-derived cells is a highly efficient and reproducible process that can be used to establish human myogenic cells. We show that this method can be applied to urine cells derived from normal individuals as well as those with muscle diseases. Furthermore, we show that urine-derived cells can be edited using CRISPR/Cas9 technology. With progress in understanding the molecular etiology of human muscle diseases, having a readily available, non-invasive source of cells from which to generate muscle-like cells is highly useful.

This chapter was previously published under the same title and was a collaborative work with Eugene Wyatt (E. Y. Kim, Page, Dellefave-Castillo, McNally, & Wyatt, 2016). Eugene Wyatt and I developed the model, performed and imaged immunofluorescence, ran RT-PCR and qRT-PCR analyses, and analyzed the data. Eugene Wyatt performed CRISPR/Cas9 mediated genome editing and validation. Eugene Wyatt and I wrote and edited the manuscript. Patrick Page assisted with maintenance of tissue culture. Lisa Dellefave-Castillo recruited and consented patients. Elizabeth McNally recruited patients, helped analyze the data, and edited the manuscript.

INTRODUCTION

The genetic diversity of muscle diseases, including the muscular dystrophies, is extensive (Mercuri & Muntoni, 2013; Rahimov & Kunkel, 2013). Defining underlying mechanisms and developing therapies to correct these defects require appropriate models of disease. Animal models offer *in vivo* insight and have proved highly useful, but animal models are time consuming and costly to develop and cannot represent the large number of alleles responsible for muscle diseases. Cellular models of disease have expanded in recent years with significant advances in reprogramming and the creation of induced pluripotent stem cells (iPSCs) for many disorders. For muscle diseases, the comparative ease of generating cardiomyocytes, rather than skeletal myocytes, from iPSCs has led to this cell type being used as a surrogate for skeletal muscle (Dick et al., 2013; Guan et al., 2014; B. Lin et al., 2015). Although progress has been made in generating muscle-like lineages from iPSCs, this process is still time consuming and has variable outcomes within and across culture systems (Chal et al., 2015; R. Darabi & R. C. Perlingeiro, 2016). Other commonly used cell models of skeletal muscles include the mouse C2C12, rat L6, and human myoblast cell lines, which undergo differentiation into multinucleate myotubes under appropriate conditions (Owens et al., 2013; Portier et al., 1999). These myoblast models have been highly useful for the field but represent normal skeletal muscle and not disease-specific conditions. While myoblasts can be cultured from human muscle, biopsies from patients are invasive and at times problematic for those with muscle mass-limiting conditions. A non-invasive patient-specific *in vitro* skeletal muscle model is desirable for studying pathogenesis and testing potential drugs.

Direct reprogramming of fibroblasts with MyoD into myotubes was a central experiment used to demonstrate the role of transcription factors (R. L. Davis et al., 1987; Tapscott et al.,

1988). Since that original observation, MyoD delivery into fibroblasts has been optimized using viral vectors and this method can be applied to make directly reprogrammed myogenic cells from humans and mice (Cooper et al., 2007; Lattanzi et al., 1998). A fusion between MyoD and the estrogen receptor was generated to create a tamoxifen-inducible MyoD, and this construct has been used in mouse and human fibroblasts to induce myogenesis (Hollenberg, Cheng, & Weintraub, 1993; Kendall et al., 2012; Kimura et al., 2008). Thus, direct reprogramming of fibroblasts remains a highly useful method for modeling human muscle diseases. However, dermal fibroblasts are obtained through skin biopsy, and the invasive nature of skin biopsy, while considerably less than muscle biopsy, can be particularly problematic in children.

One potential non-invasive source of patient-specific cells is cells isolated from urine. It has been estimated that about 2,000 to 7,000 renal tubular epithelial cells are shed in urine everyday (Ingelfinger, 2002; Rahmoune et al., 2005). Obtaining a urine sample is non-invasive, making urine a good source of cells, especially from children. Urine cells have been isolated from both healthy volunteers and patients of a wide age range (Bharadwaj et al., 2013; Dorrenhaus et al., 2000; Rahmoune et al., 2005; Y. Zhang et al., 2008). Urine-derived cells (UDCs) are thought to be of a mixed population that originates from either the renal epithelium or the uroepithelium (Rahmoune et al., 2005; Y. Zhang et al., 2008). Interestingly, a subset of UDCs have been observed to carry mesenchymal stem cell markers as well as low endogenous expression of Oct3/4, a pluripotency marker (Afzal & Strande, 2015; Bharadwaj et al., 2013; Guan et al., 2014). As such, UDCs demonstrate propensity for differentiation into several lineages, one of which is muscle-like (Bharadwaj et al., 2013; W. Chen et al., 2014).

We show here that UDCs serve as a non-invasive source for MyoD-induced myogenesis. UDCs transduced with a tamoxifen-inducible MyoD lentiviral vector (iMyoD) formed

multinucleate myotubes following induction with tamoxifen and culture in differentiation media for up to 38 days. Urine cell-derived myotubes expressed muscle marker transcripts, formed sarcomeres, and displayed contractile properties. Further, UDCs isolated from individuals with muscular dystrophies were also able to form myotube-like structures and reflected the disease mutations. Thus, UDCs are a ready source for direct reprogramming by MyoD and provide an easily obtainable, non-invasive source for modeling disease mechanisms.

MATERIALS AND METHODS

Urine collection and cell isolation

Written and informed consent was obtained from all human subjects. All work was approved by and conducted under the Institutional Review Boards of the University of Chicago (IRB8249) and Northwestern University (IRB STU00104548), which serve as the ethics boards for each institution, respectively. All studies were conducted in compliance with the Helsinki Declaration. Urine samples were collected using midstream clean catch kits according to the directions provided in the kits (Parter Medical Products Inc, Carson, CA; 273516). Cells were isolated within 1h of collection using a modified protocol previously published with minor modifications (T. Zhou et al., 2012). Briefly, the entire urine samples were equally distributed into 50 mL conical tubes and centrifuged at 400x*g* for 10 minutes at room temperature. The supernatant was aspirated leaving ~ 1 mL of urine into which pellets were resuspended and combined into a single tube, if necessary. Ten mL of wash buffer was added per 100 mL of initial urine sample. Samples were centrifuged at 200x*g* for 10 minutes at room temperature. The supernatant was aspirated leaving ~ 0.2 mL, and the cell pellet was resuspended in 1 mL of primary media. All media formulations were obtained from a previously published protocol and are detailed below

(T. Zhou et al., 2012). Cells were plated in 24-well plates pre-coated with 0.1% gelatin (Millipore, Billerica, MA; ES-006-B, Stemcell Technologies, Vancouver, Canada; 7903). Roughly 1/3 of the cell suspension was plated in the first well, with the remaining 2/3 equally divided into 4 additional wells. The final volume in each well was then brought to 500 μL with primary media. The plates were placed in a 37°C incubator with 5% CO_2.

For three days, 500 μL of primary media was added to each well every 24h. On day 4, 1.5 mL of primary media was removed and replaced with 500 μL of proliferation media. An aliquot of the primary media was added to separate dish containing Dulbecco's Modified Eagle Medium (DMEM) supplemented with 10% FBS without antibiotics or antimycotics to test for potential contamination. On day 5, all media was removed from each well and replaced with 500 μL of proliferation media, which was changed daily until the isolated cells expanded and were replated in larger dishes. Antibiotics and antimycotics were removed from media once uncontaminated cultures were confirmed. Isolated cells were observed as early as one day after the addition of proliferation media. When the cells became confluent or when cell foci began to outgrow the monolayer, cells were trypsinized using 0.25% trypsin-EDTA (Thermo Fisher Scientific, Waltham, MA; 25200-072), subcultured, and designated as passage 1 (p1). Modifications from (T. Zhou et al., 2012) include plating of cells in 5 wells of a 24-well gelatin coated plate (vs a single well of 12-well plate), increase of FBS content in the proliferation media to 15%, and the removal of the antimyoctics and antibiotics from the media after lack of contamination was observed.

Media composition

All media were made following a previously published protocol (T. Zhou et al., 2012). Wash buffer consisted of 1x phosphate-buffered saline (PBS) without Ca^{2+} and Mg^{2+} (Thermo Fisher Scientific, Waltham, MA; 14190-250) supplemented with 1% penicillin/streptomycin (Thermo Fisher Scientific, Waltham, MA; 15070-063) and 0.5 μg/mL amphotericin B (Sigma Aldrich, St. Louis, MO; A2942). Primary media was composed of 1:1 mix of high glucose DMEM without sodium pyruvate (GE Healthcare, Logan, UT; SH30022.FS) and Ham's F-12 Nutrient Mix (Thermo Fisher Scientific, Waltham MA; 11765-054) supplemented with Renal Epithelium Growth Medium SingleQuot Kit Supplements (Lonza, Basel, Switzerland; CC-4127), 10% fetal bovine serum (Thermo Fisher Scientific, Waltham, MA; 16000-044), 1% penicillin/streptomycin, and 0.5 μg/mL amphotericin B. Proliferation media was composed of 1:1 mix of Renal Epithelium Growth Medium Bullet Kit (Lonza, Basel, Switzerland; CC-3190) and high glucose DMEM supplemented with 15% FBS, 0.5% Glutamax (Thermo Fisher Scientific, Waltham, MA; 35050-061), 0.5% non-essential amino acids (Thermo Fisher Scientific, Waltham, MA; 11140-050), and 2.5 ng/mL of bFGF (Peprotech, Rocky Hill, NJ; 100-18B, Miltenyi Biotec Inc, San Diego, CA; 130-093-842), PDGF-AB (Peprotech, Rocky Hill, NJ; 100-00AB), and EGF (Peprotech, Rocky Hill, NJ; AF-100-15). The Renal Epithelium Growth Medium (REGM) Bullet Kit was made according to the manufacturer's instructions, with the omission of the amphotericin B/gentamycin supplement. Freeze media was composed of DMEM (Thermo Fisher Scientific, Waltham, MA; 11995-073) supplemented with 30% FBS, 1x pen/strep, and 10% DMSO (Sigma Aldrich, St. Louis, MO; D2650).

Lentiviral construct and transduction

The tamoxifen-inducible MyoD lentiviral construct (pLv-CMV-MyoD-ER(T)), referred to as iMyoD, was previously described (Kimura et al., 2008) and kindly provided by Dr. Jeffrey Chamberlain (University of Washington; Addgene plasmid # 26809). The construct was packaged by the Skin Disease Research Center DNA/RNA Delivery Core at Northwestern University (Chicago, IL). Urine cells from healthy volunteers or patients were plated in 12-well plates at 75,000 cells/well and transduced within 24-36h of plating with iMyoD at MOI = 50. Transductions were performed in proliferation media with reduced serum (5%) and 7.5 μg/mL polybrene (Millipore, Billerica, MA; TR-1003-G) for 6-16h in a 37°C incubator.

Evaluation of transduction efficiency

After transduction, an aliquot of cells were plated in two wells of a 24-well plate at 2000-10000 cells/cm^2. Cells were treated with 5 μM 4-hydroxytamoxifen (Sigma Aldrich, St. Louis, MO; H7904) for 24 to 48 hours and MyoD was detected using immunofluorescence. Methods and antibodies are as described below. A minimum of three fields and a minimum of 100 cells total were analyzed to determine transduction efficiency. MyoD-positive nuclei and total nuclei were counted per field and efficiency was calculated by dividing the number of MyoD-positive nuclei by the total number of nuclei per field. Efficiencies were graphed as mean ± standard error of the mean (SEM) using GraphPad Prism (GraphPad, La Jolla, CA). All images were taken using the Floid Cell Imaging Station (Thermo Fisher Scientific, Waltham, MA; 4471136). The cell counts for MyoD-positive nuclei were performed manually using ImageJ (NIH, Bethesda, MD), while the cell counts for total nuclei were performed using the Particle Analyzer function of ImageJ (NIH, Bethesda, MD).

Myogenic differentiation

Transduced cells were plated in 24-well plates coated with 8 μg/cm^2 collagen I (Sigma Aldrich, St. Louis, MO; C3867, Corning, Corning, NY; 354236) at a density of 37,500 to 50,000 cells/cm^2, and cultured until confluent. Cells were then overlaid with Growth Factor Reduced Matrigel (Corning, Corning, NY; 354230) diluted 1:4 in cold DMEM/F-12 50:50 mix (Corning, Corning, NY; 10-092-CV). Matrigel was allowed to gel for two to three hours at 37°C. The Matrigel-overlaid iMyoD-treated cells were induced with 4-hydroxytamoxifen (2.5 μM, 24-48h) diluted in high glucose DMEM (Thermo Fisher Scientific, Waltham, MA; 11995-073) supplemented with 10% FBS. Hydrocortisone dexamethasone (HD) differentiation media was based on previously published formulation (W. Chen et al., 2014; Zuk et al., 2002) and was composed of high glucose DMEM with sodium pyruvate supplemented with 10% FBS, 5% horse serum (Thermo Fisher Scientific, Waltham, MA; 16050-122), 50 μM hydrocortisone (Sigma Aldrich, St. Louis, MO; H0888), and 0.1 μM dexamethasone (Sigma Aldrich, St. Louis, MO; D4902). Two hundred and fifty μL of differentiation media was replaced every 72 hours. Additional coatings tested during plating optimization included: collagen IV (Sigma Aldrich, St. Louis, MO; C5533), fibronectin (Sigma Aldrich, St. Louis, MO; F1141), laminin (Sigma Aldrich, St. Louis, MO; L2020), Growth Factor Reduced Matrigel, poly-L-lysine (Sigma Aldrich, St. Louis, MO; P4832), poly-D-lysine (Sigma Aldrich, St. Louis, MO; P6407).

RNA analysis

Differentiated myotubes were collected at three different time points (7, 14, and 28 days). Cells were gently washed with cold 1x PBS. Washes were repeated until most of the Matrigel was removed. RNA was isolated in TRIzol (Thermo Fisher Scientific, Waltham, MA; 15596-018)

following the manufacturer's instructions. Glycogen (Thermo Fisher Scientific, Waltham, MA; AM9510) was added at 50-100 μg/mL to the isopropanol before RNA precipitation. RNA concentration was determined using NanoDrop 2000 (Thermo Fisher Scientific, Waltham, MA). RNA (1000-1500 ng) was reverse transcribed using qScript cDNA SuperMix (Quanta Biosciences, Gaithersburg, MD; 95048-025). cDNA (30-50 ng) was used per PCR reaction and the products were separated on 1.5% agarose gel with ethidium bromide. Gels were visualized and imaged on the UVP Transilluminator (UVP, Upland, CA). Quantitative PCR was performed with 30-50 ng of cDNA using iTaq Universal SYBR Green Supermix (Bio-Rad, Hercules, CA; 1725124) with biological triplicates when available and technical duplicates. Cq values were averaged for each pair of technical duplicates and normalized to GAPDH. ΔCq values were calculated as $Cq_{(gene\ of\ interest)} - Cq_{(GAPDH)}$, and ΔΔCq values were calculated as 2^(-ΔCq). ΔΔCq values were then multiplied by 1,000 as an arbitrary factor for graphing purposes. ΔΔCq values were graphed as mean ± SEM using GraphPad Prism (GraphPad, La Jolla, CA). Primers used for RT- and qRT-PCR are listed in Tables 2.1 and 2.2.

Table 2.1 Primers used for PCR analysis of myotubes

ACTA1	F: AGCCCTCCTTCATCGGTATGG
	R: TTCGTCGTCCTGAGAAGTCG
ACTN2	F: CTAAAATGTTGGATGCTGAAGACA
	R: CAGCAATATCCGACACCATCTTGC
DES	F: AAGGGCACTAACGATTCCCT
	R: CATCCCGTGTCTCGATGGTC
DMD (exons 1 to 3)	F: TCCTGGCATCAGTTACTGTGTT
	R: TATGCTGCTTCCCAAACTTAGAA
DMD (exons 42 to 50/51)	F: CAATGCTCCTGACCTCTGTG
	R: GAGTAGGAGAGGCTCCAATA
DMD (exons 44 to 48)	F: GAACAGTTTCTCAGAAAGAC
	R: GCAGCAGATGATTTAACTGC
GAPDH	F: ACCACAGTCCATGCCATCAC
	R: CCACCACCCTGTTGCTGTAG

Table 2.1 continued

MYH2	F: GAGGCTGACTCGTCCTGCTTTA
	R: GACTGATTCTCTCGGTCAGTCA
MYH3	F: CTTGTGGGCGGAGGTCTGG
	R: GCCACTTGTAGGGGTTGACA
MYOG	F: ACCCAGGGGATCATCTGCTCA
	R: CACTGGCATCGGGAAGAGAC
SGCG	F: TCTAAGATGGTGCGTGAGCAG
	R: GCCACAGACAGGTACAGCTT

Table 2.2 Primers used for qPCR analysis of myotubes

ACTN2	F: CTAAAATGTTGGATGCTGAAGACA
	R: CATTCCAAAAGCTCACTCGCTA
DES	F: GATCAATCTCCCCATCCAGA
	R: TGGCAGAGGGTCTCTGTCTT
GAPDH	F: GTGGACCTGACCTGCCGTCT
	R: GGAGGAGTGGGTGTCGCTGT
MYH2	F: TCTCCAAAGCCAAGGGAAAC
	R: TGCGCAGTCAGGTCATTGAT
MYH3	F: TTGATGCCAAGACGTATTGCT
	R: GGGGGTTCATGGCGTACAC
MYOG	F: GCTGTATGAGACATCCCCCTA
	R: CGACTTCCTCTTACACACCTTAC

Immunofluorescence microscopy

Differentiated myotubes were subject to immunofluorescence microscopy at four different time points (7, 14, 28, and 35 days). Myotubes were gently washed with 1x PBS (Thermo Fisher Scientific, Waltham, MA; 14200-166) three times, or until most of the Matrigel was removed, and then fixed in either 4% paraformaldehyde (15 minutes at RT) or ice cold 100% methanol (2 minutes on ice). Myotubes fixed in paraformaldehyde were subsequently permeabilized in 0.25% Triton-X (Sigma Aldrich, St. Louis, MO; T8787) for 20 minutes at RT. Cells were blocked in 10% horse serum for 30 minutes to 1 hour at 4°C. Primary antibody incubations were done overnight at 4°C. Cells were washed three times for 10 minutes each with PBS, where PBS was

supplemented with 0.1% Triton-X in the second wash. Cells were incubated with secondary antibodies (1 hour at RT), and then washed three times for 10 minutes each as described above. Nuclei were stained with Hoechst 33342 (1:10,000, Thermo Fisher Scientific, Waltham, MA; H3570). Plates were imaged on the Zeiss Axio Observer Z.1 inverted microscope (Carl Zeiss Microscopy, Jena, Germany) and/or Floid Cell Imaging Station. All antibodies were diluted in 0.1% Triton-X and 2% horse serum, and all solutions were made with 1x PBS.

Antibodies

Primary antibodies were as follows: rabbit polyclonal anti-MyoD (1:1,000, Santa Cruz, Dallas, TX; sc-304), mouse monoclonal anti-desmin (1:1,000, Sigma Aldrich, St. Louis, MO; D1033), mouse monoclonal anti-α-actinin (1:1,000, Sigma Aldrich, St. Louis, MO; A7811), rabbit polyclonal anti-dystrophin (1:1,000, Thermo Fisher Scientific, Waltham, MA; PA1-37587), mouse monoclonal anti-dystrophin (1:100, Leica Biosystems, Newcastle, UK; NCL-DYSB), mouse monoclonal anti-MYH1 (1:10 or 2 μg/mL, deposited to Developmental Studies Hybridoma Bank by Fischman, DA; MF 20), mouse monoclonal anti-fast myosin heavy chain (1:1,000, Sigma Aldrich, St. Louis, MO; M4276), mouse monoclonal anti-titin antibody (1:10 or 2 μg/mL, deposited to Developmental Studies Hybridoma Bank by Greaser, ML; 9 D10), rabbit polyclonal anti-γ-sarcoglycan (1:300 to 1: 500 (McNally, Passos-Bueno, et al., 1996)). DMD patient myotubes were single labeled with the mouse monoclonal dystrophin antibody. Secondary antibodies were as follows: Alexa Fluor 488 donkey anti-rabbit (1:1,1000; A21206), Alexa Fluor 488 donkey anti-mouse (1:1,000; A21202), Alexa Fluor 594 donkey anti-rabbit (1:1,000; A21207), Alexa Fluor 594 donkey anti-mouse (1:1,1000; A21203, all Thermo Fisher Scientific, Waltham, MA).

Sequencing

DMD exons 42 through the junction of exons 50 and 51 were amplified by PCR, gel purified using QIAEXII Gel Extraction Kit cat 20021 (Qiagen, Valencia,CA; 20021). The purified products were amplified by PCR using nested primers for *DMD* exons 44 through 48 and then sequenced at the NUSeq Core at Northwestern University (Chicago, IL). Chromatograms and sequences were analyzed on SeqMan Pro (DNASTAR, Madison, WI) and FinchTV (Geospiza, Seattle, WA).

CRISPR/Cas9 design

To generate a point mutation in control urine cells, we used the Cas9-GFP plasmid designed by the Zhang lab (Addgene plasmid #48138) (Ran et al., 2013). The CRISPR design tool (crispr.mit.edu) was used to identify and select guide RNA (gRNA) targets in human *SGCG* exon 6. The target on the anti-sense strand was gRNA 5' CTAAGGTCTTGAAACGGGT 3'. This guide permitted a synonymous mutation of the protospacer adjacent motif (PAM), and preserved the 5' *SGCG* exon 6 sequence. The gRNA was expressed from the U6 polymerase III promoter as previously described (Mali et al., 2013). The promoter, crRNA-tracrRNA and target were synthesized as a gBlock by Integrated DNA Technologies (IDT, Coralville, IA), then PCR amplified (F: TGTACAAAAAAGCAGGCTTTAAAG; R: TAATGCCAACTTTGTACAAGAAAG) and purified using the Qiagen PCR purification kit (Qiagen, Valencia, CA; 28106). The single-stranded oligodeoxynucleotide (ssODN) was designed according to published guidelines (F. Chen et al., 2011). The ssODN, based on the anti-sense strand template, was centered in between the nuclease site and the desired thymine deletion with 71 bp flanking arms on either side (142 bp total). It contained a downstream G>A

synonymous mutation that destroyed the PAM –NGG site (CGG > CAG). The ssODN ultramer ggagaggttgttaatatttgaacaaaaattcttacCTAAGGTCTTGAAACGGGTCaGCTCTGACAAGGGGT GTCTCCACTGAATGTTCAAAAGAGCCCCTTCAGGCCctaaacaaaaaacaaagatgtatcaggagcaga ag was synthesized and PAGE purified by IDT. Upper case letters indicate the *SGCG* exon 6 coding region, lower case letters indicate the flanking intronic regions. The single underlined region encodes the targeted mutation of the protospacer adjacent motif (PAM), and the double underlined sequence is the 4 adenine (A) sequence that encodes the single thymine (T) deletion in the exon 6 coding region.

Electroporation with CRISPR reagents

On the day of electroporation, urine cells were trypsinized, centrifuged at 400x*g* for 5 min (RT) and resuspended in PBS. An aliquot was removed for cell counting and cells were centrifuged at 400x*g* for 5 min (RT). Cells were resuspended in electroporation buffer 1 x 10^6 cells/mL (Bio-Rad, Hercules, CA; 165-2677) and 2 x 10^5 cells were added to the Cas9 GFP plasmid (1 μg), U6 gRNA (500 ng) and ssODN (0.5 nmol) reagents. After gentle mixing, the cells were placed in a sterile cuvette with a 0.4cm gap (Bio-Rad, Hercules, CA; 1652088) and electroporated using Gene Pulser Xcell Electroporation System (Bio-Rad, Hercules, CA; 1652660) with the following settings: 1) single square wave pulse, 200 V, 20 msec or 2) three square waves pulses, 150 V, 20 msec (0.1s between pulses). The electroporated cells were added to gelatin-coated 6-well plates and brought to a final volume of 2 mL with proliferation media. The media was replaced within 12h, and replaced every 24h for 3-5 days until fluorescence-activated cells sorting (FACS).

FACS sorting and clonal expansion

Prior to cell sorting, 96-well plates were pre-coated with 0.1% gelatin and placed in the incubator for 1h. Gelatin was removed and replaced with 100 μL of proliferation media that was supplemented with 0.5x pen/strep. The electroporated cells were trypsinized, centrifuged, and resuspended in 1 mL of proliferation media supplemented with 0.5x pen/strep. Single cell sorting of GFP positive cells into 96-well plates was conducted by the Northwestern Flow Cytometry Facility using the FACS AriaII (BD Biosciences, San Jose, CA). After sorting, 96-well plates were briefly centrifuged at 200x*g* for 1 min (RT) and placed in a 37°C incubator. After 48h, 100 μL of proliferation media without pen/strep was added to the 96-well plates. A complete media exchange was performed on days 4, 8, and 12 using proliferation media without pen/strep. Expansion of single cell clones was evident 7-10 days after FACS, with confluent wells observed about day 14. Confluent wells were subcultured onto gelatin-coated 24-well plates until confluent and then subcultured onto gelatin coated 6-well plates.

Genotype analysis of clones

Clones expanded to the 6-well stage were analyzed for genome editing via the CRISPR/Cas9 system. Genomic DNA was isolated and PCR amplified using the GeneArt cleavage detection kit (Thermo Fisher Scientific, Waltham, MA; A24372) according to the manufacturers' instructions. The primer set amplified a genomic region containing *SGCG* exon 6 along with a portion of the flanking introns (F: TAGGGAAAGAGTTGGGCCTATTT) (R: GAGGCAGATTGGAGAGGAAGAA). To test for clones edited through homology dependent repair (HDR), PCR-amplified products were subjected to Alu1 digest and restriction fragment length polymorphism (RFLP) analysis. In addition, PCR products from individual clones were

sequenced at the NUSeq Core at Northwestern University (Chicago, IL). Chromatograms and sequences were analyzed using SeqMan Pro (DNASTAR, Madison, WI).

RESULTS

Generation of urine-derived cells with inducible MyoD expression

Urine-derived cells were previously shown to be a useful source for the generation of iPSCs (T. Zhou et al., 2011). To test direct programming into myogenic lineages using urine cells, we used viral delivery of the muscle transcription factor MyoD. We used a previously characterized tamoxifen-inducible MyoD (iMyoD) lentivirus, which permits the culture and expansion of cells in an undifferentiated state until a reprogramming start point is determined (Kimura et al., 2008). The procedure includes urine cell isolation, proliferation, iMyoD transduction, tamoxifen induction, myogenic differentiation, and evaluation (Figure 2.1). Urine was isolated from multiple healthy individuals (n>8) and urine cells were isolated and cultured as described (Afzal & Strande, 2015; T. Zhou et al., 2012). Brightfield images from two typical urine cultures demonstrated characteristic urine cell morphology and growth (Figure 2.1). More than one cellular morphology was noted and independent cultures from the same individual were observed to have differential growth rates. In general, we selected clones demonstrating rapid expansion and displaying a type 1 morphology, characterized as a monolayer of polar cells with a “rice-grain” appearance, that maintained close cell-cell contact (Bharadwaj et al., 2011; Dorrenhaus et al., 2000; Felix, Sun, & Littlefield, 1980). Both fresh and freeze-thawed urine cells were used for lentiviral transduction with success.

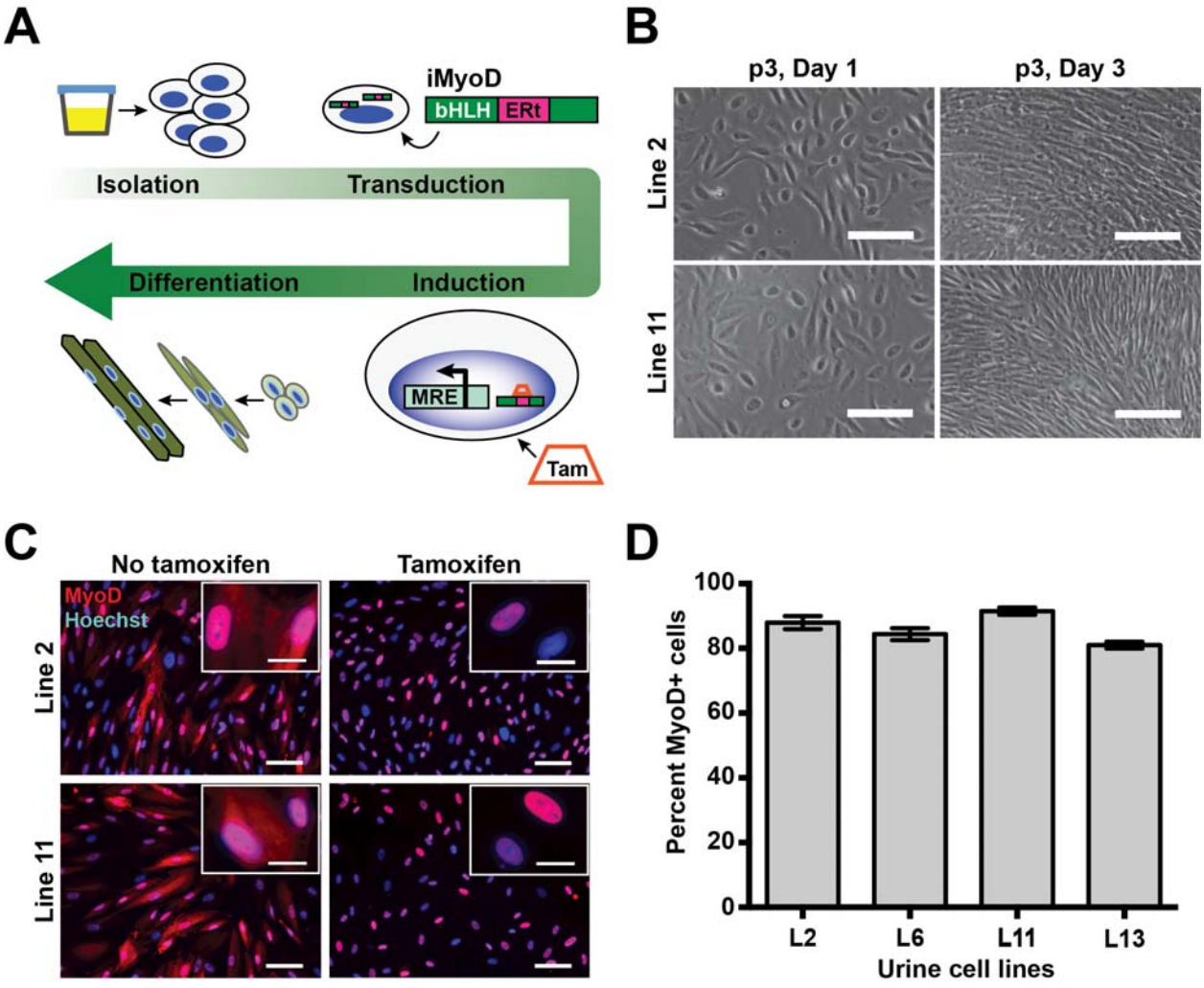

Figure 2.1 Transduction of urine-derived cells (UDCs) with an iMyoD lentiviral construct for myogenic reprogramming

(A) General overview for generating *in vitro* model of human skeletal muscle using UDCs and iMyoD construct. The cells were first isolated from urine samples and then transduced with lentivirus encoding an inducible MyoD. The construct includes a 4-hydroxytamoxifen (tamoxifen, TAM) response element from the estrogen receptor (ERt) downstream of the basic helix loop helix (bHLH) DNA binding domain of MyoD. After induction with tamoxifen, cells were placed in differentiation media. **(B)** Brightfield images of isolated urine cell cultures at passage 3. Scale bar = 25 μm. **(C)** Images of immunolabeled MyoD (red) in UDCs after transduction with the iMyoD lentivirus, and iMyoD transduced urine cells treated with tamoxifen (5 μM, 48h). Nuclei were marked with Hoechst 33342 (blue). Scale bar = 100 μm. Inset images show increased MyoD localization to the nuclei after tamoxifen. Inset of tamoxifen-treated line 2 cells shows one nuclei with MyoD localization (left) and one without (right). Inset scale bar = 25 μm. **(D)** Lentiviral iMyoD transduction efficiency across 4 control urine cell lines, shown as the percent of MyoD-positive cells relative the total number of cells.

Urine cells were transduced with the iMyoD lentivirus, regularly achieving >80% efficiency with an MOI of 50, as determined by immunofluorescence microscopy and image analysis for MyoD expression (Figure 2.1). In the absence of tamoxifen, MyoD was seen in cytoplasm. After tamoxifen exposure, MyoD staining also became nuclear (Figure 2.1). Because lentiviral transduction was of such high efficiency, nuclear MyoD staining was routinely evident in 80% of the cultures (Figure 2.1).

Morphological and molecular myogenic reprogramming of iMyoD urine-derived cells

After iMyoD transduction, urine cells underwent testing for myogenic reprogramming with or without tamoxifen followed by culture in differentiation media (HD media), a formulation previously shown to enhance the endogenous myogenic potential of untransduced urine cells (W. Chen et al., 2014). RT-PCR amplification showed upregulation of the *DES* transcript in tamoxifen-treated cells by the 7-day (7d) time point, and this was sustained throughout the differentiation time course (Figure 2.2). Low-level *DES* expression was detected in uninduced iMyoD urine cells cultured in HD media alone (Figure 2.2). Immunofluorescence microscopy showed desmin protein expression was evident in tamoxifen-induced iMyoD cells at the earliest time point (7d), and increased with extended culture in HD differentiation media (Figure 2.2). Desmin protein expression was observed concomitant with increased myotube organization and elongation (Figure 2.2). Desmin protein expression was not readily evident in uninduced iMyoD cells (Figure 2.2).

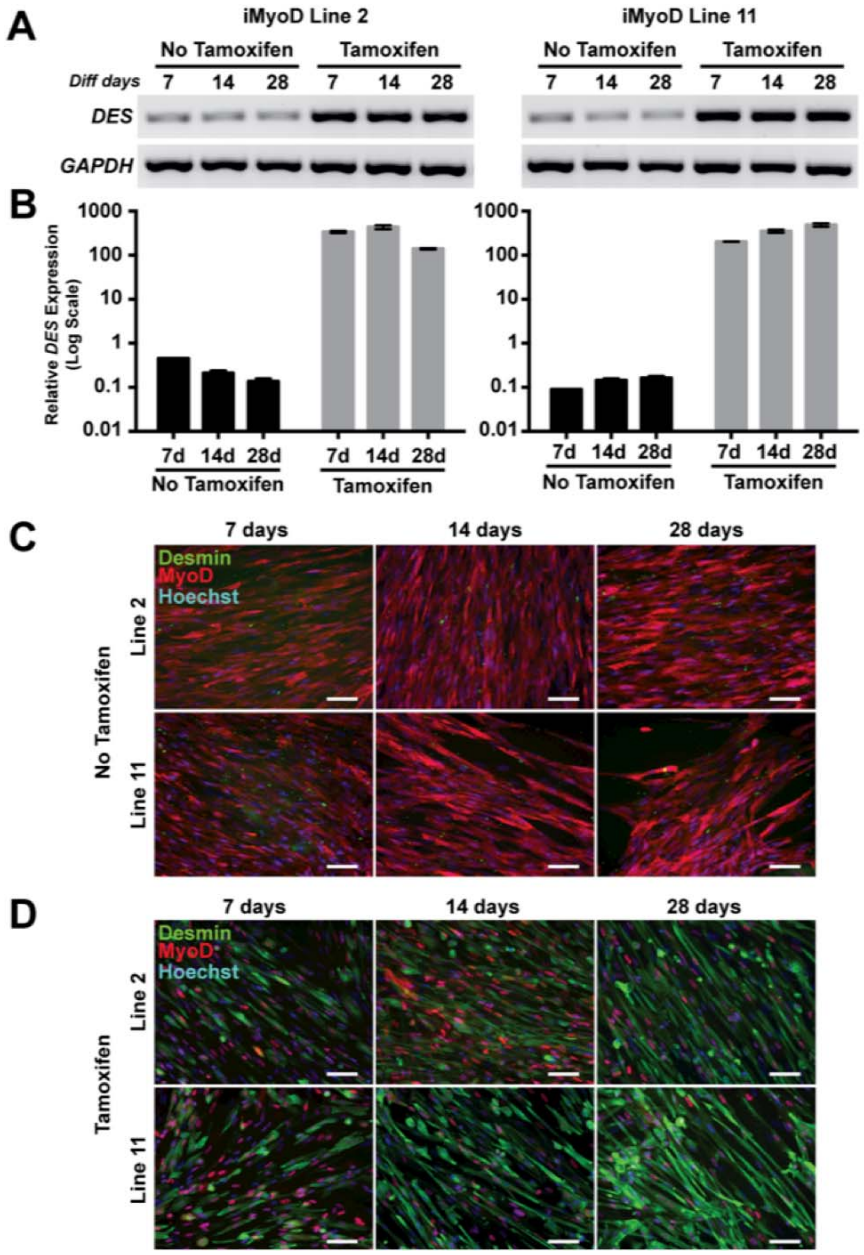

Figure 2.2 Tamoxifen-induced myogenic reprogramming of iMyoD-transduced UDCs

(A) RT-PCR time course evaluation of *DES* (desmin) mRNA expression in two UDC lines (2 and 11). iMyoD-transduced cells were treated with or without tamoxifen (2.5 μM, 24h), and then cultured in differentiation media as indicated (7, 14, and 28 days). *GAPDH* mRNA expression is shown as a control. **(B)** Real time semi-quantitative PCR results for *DES* mRNA expression in urine cell lines 2 and 11. **(C)** Immunofluorescence microscopy of MyoD (red) and desmin (green) protein expression in iMyoD-transduced control lines 2 and 11, without tamoxifen treatment. In the uninduced state, MyoD demonstrated a cytoplasmic distribution, and no appreciable desmin expression was observed. Nuclei (blue); Scale bar = 100 μm. **(D)** After induction, MyoD (red) became more nuclear concomitant with cytoplasmic desmin (green) protein expression. Myotube elongation progressed over time in culture. Scale bar = 100 μm.

Myogenic differentiation and maturation

We assessed myotube differentiation on alternative coated surfaces including collagen, laminin, fibronectin or poly-lysine. We also assessed the effectiveness of Matrigel overlay. We found that Matrigel overlay of cells on collagen I-treated plates prior to tamoxifen induction offered the most robust differentiation into myotubes based on morphological appearance. Matrigel overlay was applied when cells reached confluence, and this was followed by tamoxifen induction in DMEM with 10% FBS (2.5 μM, 24-48h), and culture in HD media for the indicated time course. The outline for this optimized protocol is depicted in Figure 2.3.

MyoD controls temporal expression of early and late genes in muscle development through a feed-forward mechanism (Berkes & Tapscott, 2005). To characterize myogenic marker expression, we tested tamoxifen-treated iMyoD cells by RT-PCR. Robust and sustained expression of *MYOG* (myogenin) and *MYH3* (embryonic myosin) was observed (Figure 2.3). In addition, there was a temporal increase in expression of *ACTN2* (α-actinin) and *DMD* (dystrophin) (Figure 2.3). Expression of *MYH2*, the adult form of skeletal myosin, was only detected when differentiation was extended to the 28d time point (Figure 2.3). Similarly, real-time PCR detected most transcripts after 7 days of differentiation, with sustained or moderately increased expression over time (Figure 2.3). However, *DMD* and *MYH2* demonstrated greater temporal increases in transcript expression as myogenic maturation progressed (Figure 2.3). Evaluation of myotubes by immunofluorescence microscopy showed accumulation of α-actinin, dystrophin, and fast myosin heavy chain (MHC), concordant with the mRNA data. Expression of these muscle proteins was associated with increased myotube formation, organization, and elongation, indicative of myogenic differentiation and maturation over time (Figure 2.3).

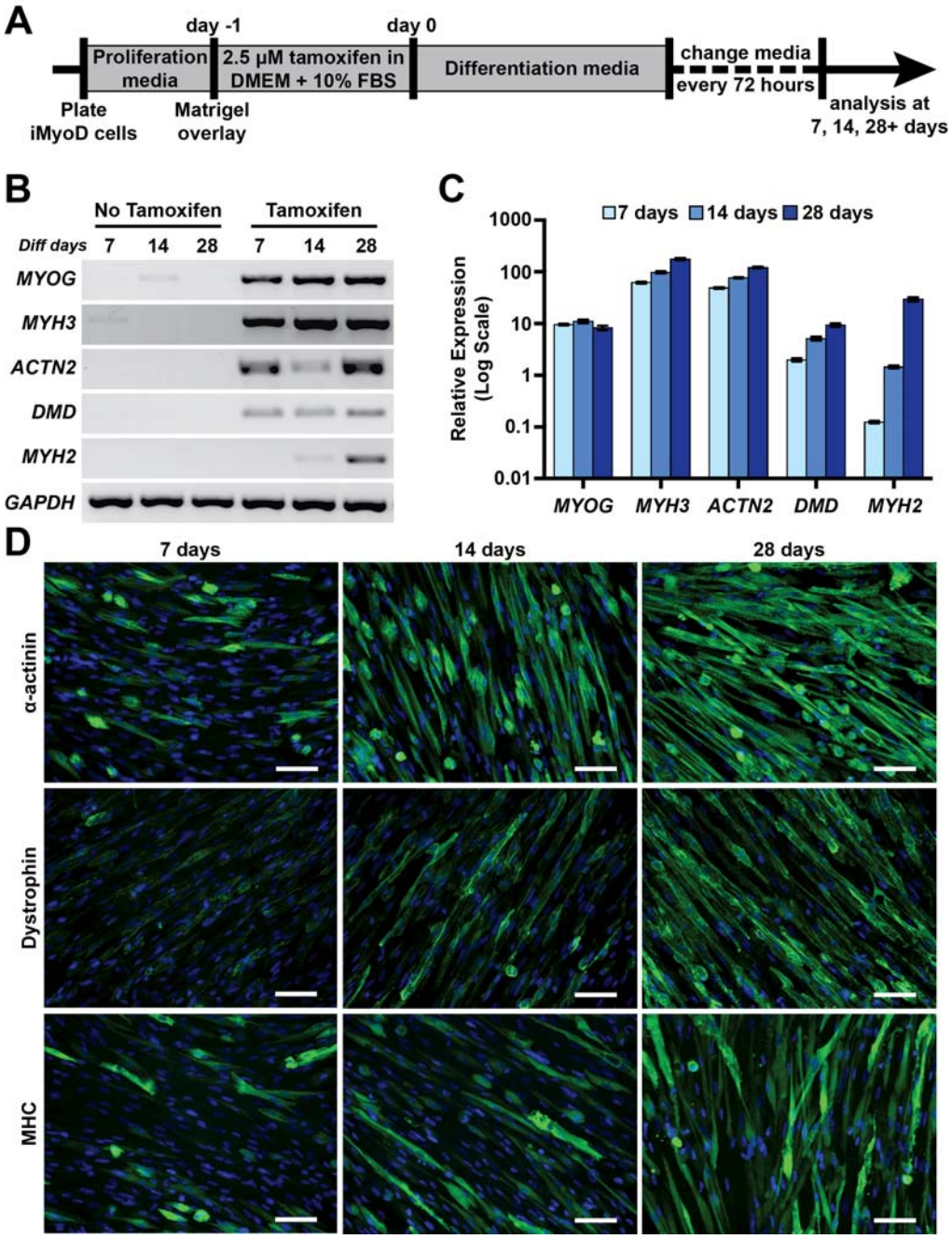

Figure 2.3 Myogenic differentiation and maturation of induced iMyoD UDCs

(A) Timeline for differentiation of iMyoD-transduced cells. **(B)** RT-PCR for myogenic maturation markers in iMyoD-transduced line 2, with or without tamoxifen (2.5 μM, 24h), and culture in differentiation media as indicated (7, 14, and 28 days). Myogenin (*MYOG*) and embryonic myosin heavy chain (*MYH3*) were the earliest markers detected. **(C)** Real time semi-quantitative PCR results demonstrated that dystrophin (*DMD*) and adult myosin heavy chain (*MYH2*) were detected with further differentiation. **(D)** Images of myogenic markers in iMyoD-transduced line 2. Increased muscle marker expression over time was accompanied by myotube elongation. Nuclei (blue); Scale bar = 100 μm.

To further characterize iMyoD-directed myogenic maturation of urine cells, we analyzed reprogrammed cultures differentiated for 28 and 35 days. Low magnification brightfield images of tamoxifen-treated iMyoD lines 2 and 11 demonstrated elongated myotube formation after 28 days in HD differentiation media (Figure 2.4) in which expression of α-actinin and dystrophin was observed throughout each fiber (Figure 2.4). Spontaneously twitching myotubes were observed in a subset of fields at both 28 and 35 days of culture, indicating sarcomere formation and function. Sarcomere formation was confirmed with expression of fast myosin, α-actinin, and titin, each localized internally to sarcolemmal dystrophin expression and in the expected pattern (Figure 2.4). These results demonstrated efficient myogenic reprogramming, differentiation, and maturation of iMyoD-transduced urine cells.

Direct reprogramming of urine cells to model muscular dystrophy

The iMyoD reprogramming strategy was applied to urine cells derived from two patients with Limb Girdle Muscular Dystrophy type 2C (LGMD2C), which results from loss of function mutations in the gene encoding γ-sarcoglycan (SGCG) (Figure 2.5). Urine-derived cells from each patient were successfully transduced with the iMyoD lentivirus. Real-time PCR analysis of tamoxifen-treated iMyoD LGMD2C cells demonstrated successful reprogramming into the myogenic lineage (Figure 2.5) associated with morphological myotube formation (Figure 2.5). RT-PCR analysis demonstrated full length *SGCG* transcript expression in reprogrammed control iMyoD cells and truncated mutant *SGCG* transcript expression in the reprogrammed iMyoD patient cells (Figure 2.5). Sarcolemmal associated γ-sarcoglycan protein was observed in control but not in LGMD2C cells, consistent with their mutation status (Figure 2.5).

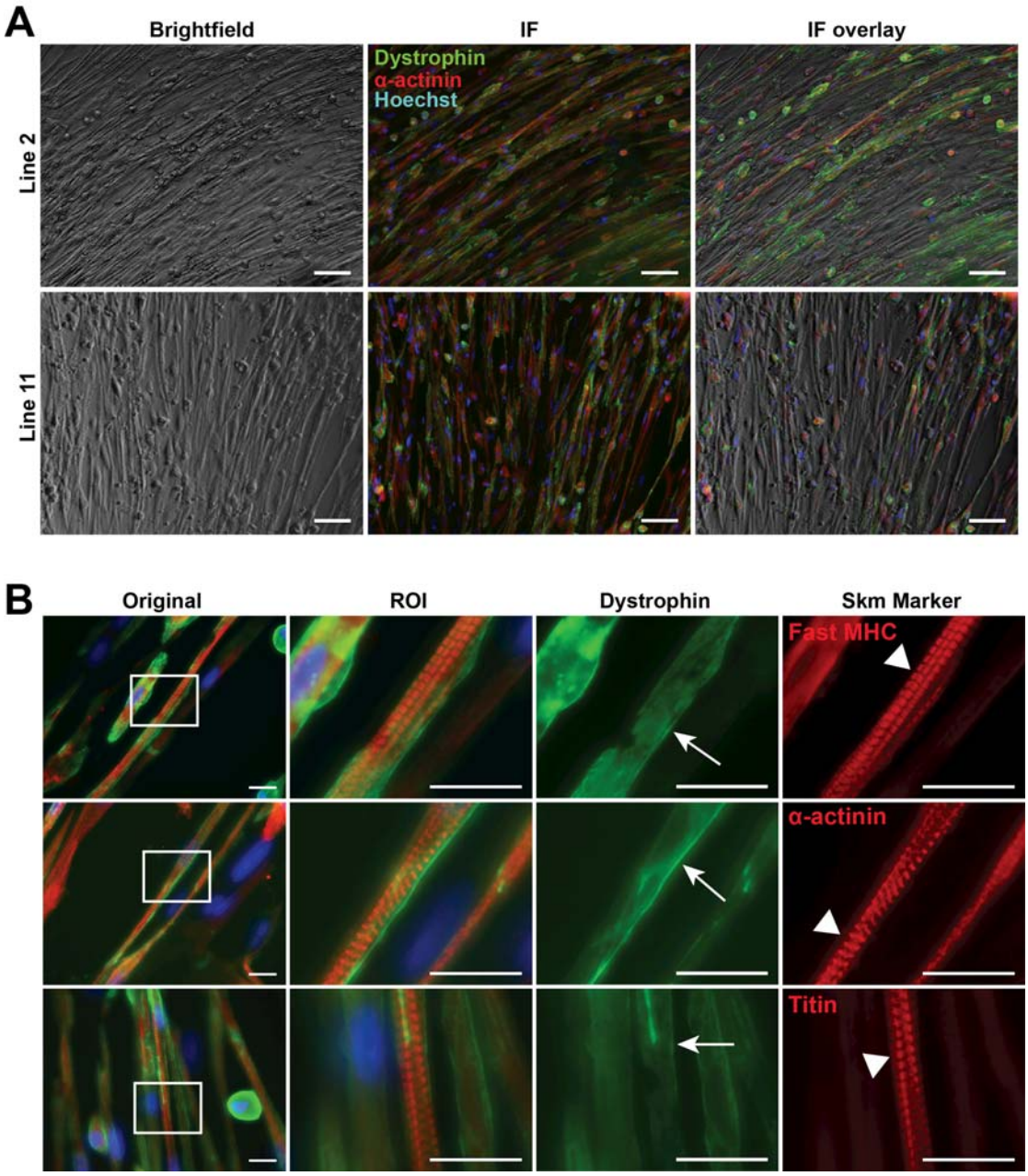

Figure 2.4 Maturation of myotubes at 28-day and 35-day time points

(A) Brightfield images of myotube formation at the 28-day time point in iMyoD lines 2 and 11 after induction and differentiation (left panels). Middle panels show images of dystrophin (green) and α-actinin (red) protein expression, taken in the same field as the brightfield panels. The right panels show the merged images revealing dystrophin and α-actinin expressions throughout the lengths of the myotubes. Scale bar = 100 μm. **(B)** Images of iMyoD-induced UDCs after 35 days of differentiation showing expresszon of fast MHC, α-actinin and titin. The magnified Region of Interest (ROI) is outlined in the first panels (white rectangles). White arrows highlight the membrane localization of dystrophin (green). White arrowheads highlight the formation of sarcomeres (red). Scale bar = 25 μm.

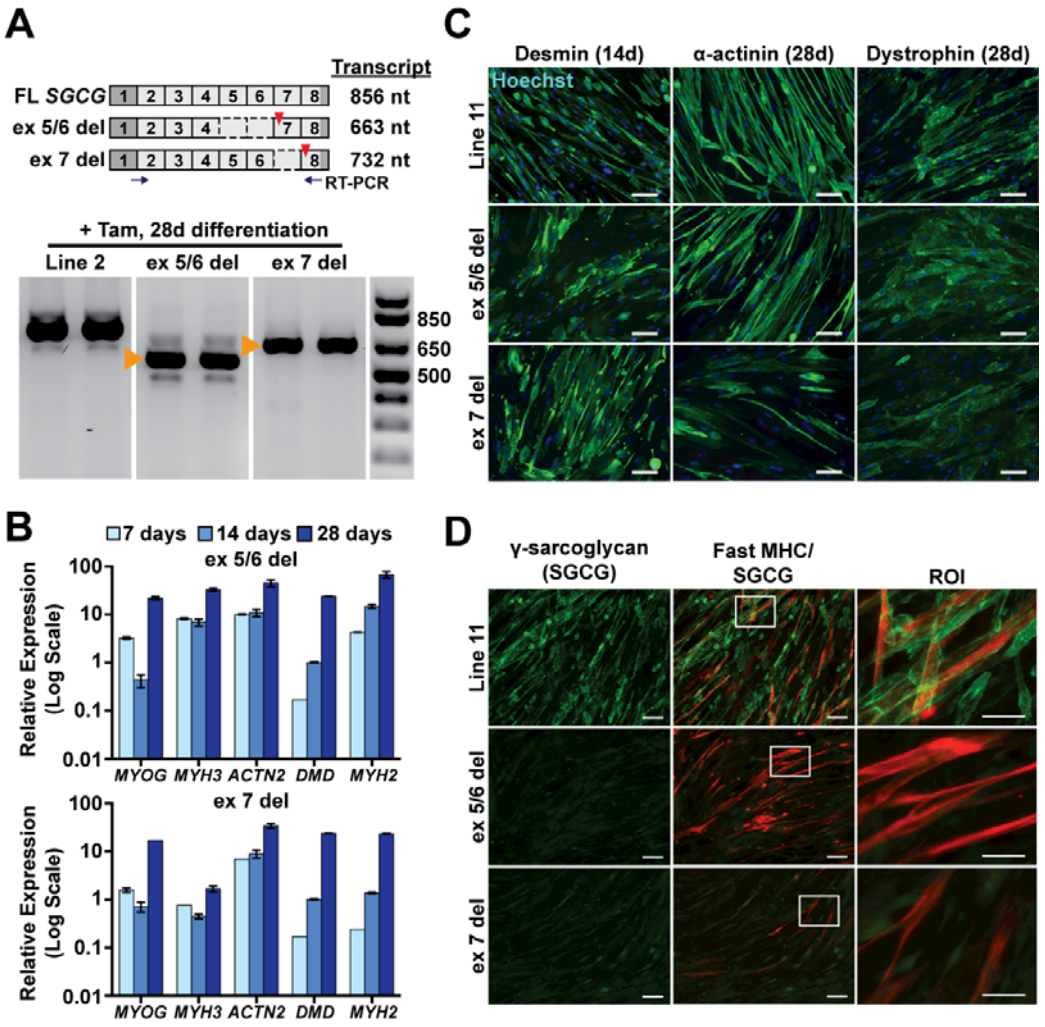

Figure 2.5 Myogenic reprogramming of LGMD2C UDCs

(A) Schematic showing exon organization of the γ-sarcoglycan (*SGCG)* mRNA transcript and two LGMD2C patients with frameshifting deletions affecting the *SGCG* locus that lead to premature stop codons (red triangles). One has a deletion of exons 5 and 6 (ex5/6del) and the other has a deletion of exon 7 (ex7del). RT-PCR demonstrated *SGCG* transcripts from UDCs after treatment with tamoxifen (2.5 μM, 24h) and culture in differentiation media for 28d. Orange arrowheads indicate the mutant transcripts lacking the expected exons. **(B)** Real time semi-quantitative PCR results demonstrate myogenic reprogramming of ex5/6del (top) and ex7del (bottom) after treatment with or without tamoxifen (2.5 μM, 24h) and culture in differentiation media as indicated (7, 14, and 28 days). **(C)** Images of myogenic markers in iMyoD control and LGMD2C ex5/6del and ex7del patient-derived lines. LGMD2C patient-derived cells formed myotubes comparable to those of control cells. Nuclei (blue); Scale bar = 50 μm. **(D)** Desmin, α-actinin, dystrophin and fast MHC were expressed in LGMD2C cells. **γ**-sarcoglycan (green) was not detected. White boxes outline double-labeled regions of interest (ROI) enlarged in far right panels. Images show **γ**-sarcoglycan expression and localization to the membrane in line 11, as opposed to no detectable expression of **γ**-sarcoglycan in LGMD2C patient myotubes. Scale bar = 100 μm in left and middle panels; 50 μm in right panels.

We applied the same iMyoD strategy to DMD urine cells. The DMD patient harbored a frameshift deletion of exons 46 and 47 (ex46/47del) (Figure 2.5). RT-PCR analysis demonstrated full-length *DMD* transcript expression in reprogrammed control iMyoD cells and truncated *DMD* mutant transcript expression in the reprogrammed iMyoD patient cells (Figure 2.5). Sequence analysis of the PCR-amplified transcripts confirmed the deletion of exons 46 and 47 in the reprogrammed patient-derived cells (Figure 2.6). Sarcolemma-associated dystrophin protein was observed in control cells (Figure 2.6). In contrast, dystrophin protein was not detected in reprogrammed DMD patient cells after 28d differentiation (Figure 2.6). Thus, the iMyoD strategy in urine cells replicated the primary LGMD and DMD phenotypes *in vitro*.

CRISPR/Cas9 mediated genome editing in single urine cell clones

Finally, we evaluated CRISPR (clustered regularly interspaced short palindromic repeats)/Cas9 (CRISPR-associated protein 9) mediated genome editing in urine cells. For these studies, the goal was to introduce the most common LGMD2C disease-causing mutation into control cell lines by deleting one thymine from *SGCG* exon 6 to disrupt the reading frame (McNally, Passos-Bueno, et al., 1996). To generate the 521ΔT mutation, we used a gRNA targeting downstream of five sequential thymine residues and a single stranded oligonucleotide (ssODN) to mediate homology directed repair (HDR). The ssODN targeting the minus strand contained a synonymous G>A transition to disrupt the protospacer adjacent motif (PAM) and introduce a novel Alu1 restriction site (Figure 2.7). CRISPR components were electroporated into control UDC lines 2 and 11, followed by FACS single cell sorting for GFP into 96 well plates. Approximately 20% of the clones derived from single sorted cells grew sufficiently so that they could be evaluated for CRISPR-mediated gene editing (Figure 2.7). The proliferation capacity of

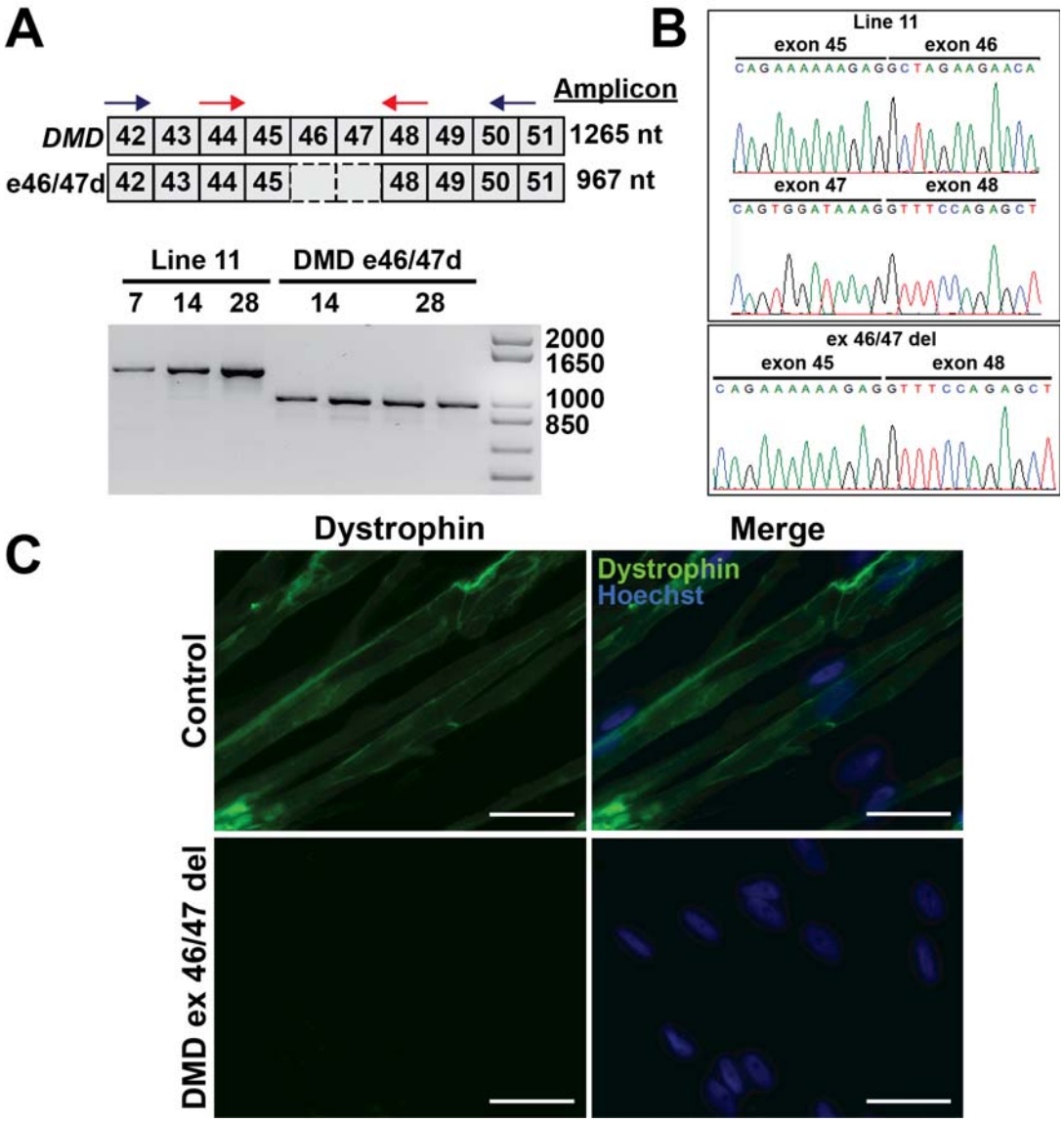

Figure 2.6 Myogenic reprogramming of DMD patient-derived urine cells

(A) Schematic showing organization of dystrophin exons 42 to 51 (top) and DMD patient with a frameshift deletion of exons 46 and 47 (bottom). RT-PCR demonstrated DMD transcript expression from iMyoD transduced line 11 control and DMD ex46/47del mutant cell lines, after tamoxifen induction (2.5 μM, 24h) and differentiation as indicated. Blue arrows indicate the location of the outer primers that produce the PCR products in the gel below. Red arrows indicate nested primers used to generate transcripts used for sequencing. **(B)** Sequencing results from RT-PCR products from iMyoD-reprogrammed urine-derived cells. The sequenced transcripts were generated from a set of nested primers (red) shown in A. Line 11 showed the expected exon45-exon46 and exon 47-exon48 junctions. The ex46/47del DMD individual shows the out-of-frame mutant exon45-exon48 junction. **(C)** Immunofluorescence images of iMyoD line 17 and DMD ex46/47del cells labeled with dystrophin using antibody to dystrophin. The antibody to dystrophin showed membrane localization of dystrophin in control cells (top). No dystrophin was detected in DMD patient-derived myotubes. Scale bar = 50 μm.

FACS-sorted clones was similar in untreated cells and cells electroporated with the Cas9 GFP plasmid alone.

The genomic region including *SGCG* exon 6 was PCR amplified to analyze the results of gene editing. Restriction digest of the PCR products revealed the presence of an Alu1 site in a subset of clones, indicative of HDR repair (Figure 2.7). Sequence analysis demonstrated efficient genome editing in UDCs with the expected variety of both heterozygous and homozygous mutations, including insertions and deletions from non-homologous end joining (NHEJ) repair and specific point mutations directed by HDR (Figure 2.7). Generation of clones with both heterozygous and homozygous 521ΔT mutations was evident in line 2 (Figure 2.7). Interestingly, a subset of HDR-edited clones contained a point mutation in the PAM region without the upstream thymine deletion, suggesting that this region is refractory to editing and/or required a gRNA target closer to the 5T region. A summary of the gene editing results is shown in Figure 2.7**.** Collectively, these data demonstrated the ability to edit the genome of urine-derived cells with CRISPR/Cas9, generating single cell clones with a specific point mutation.

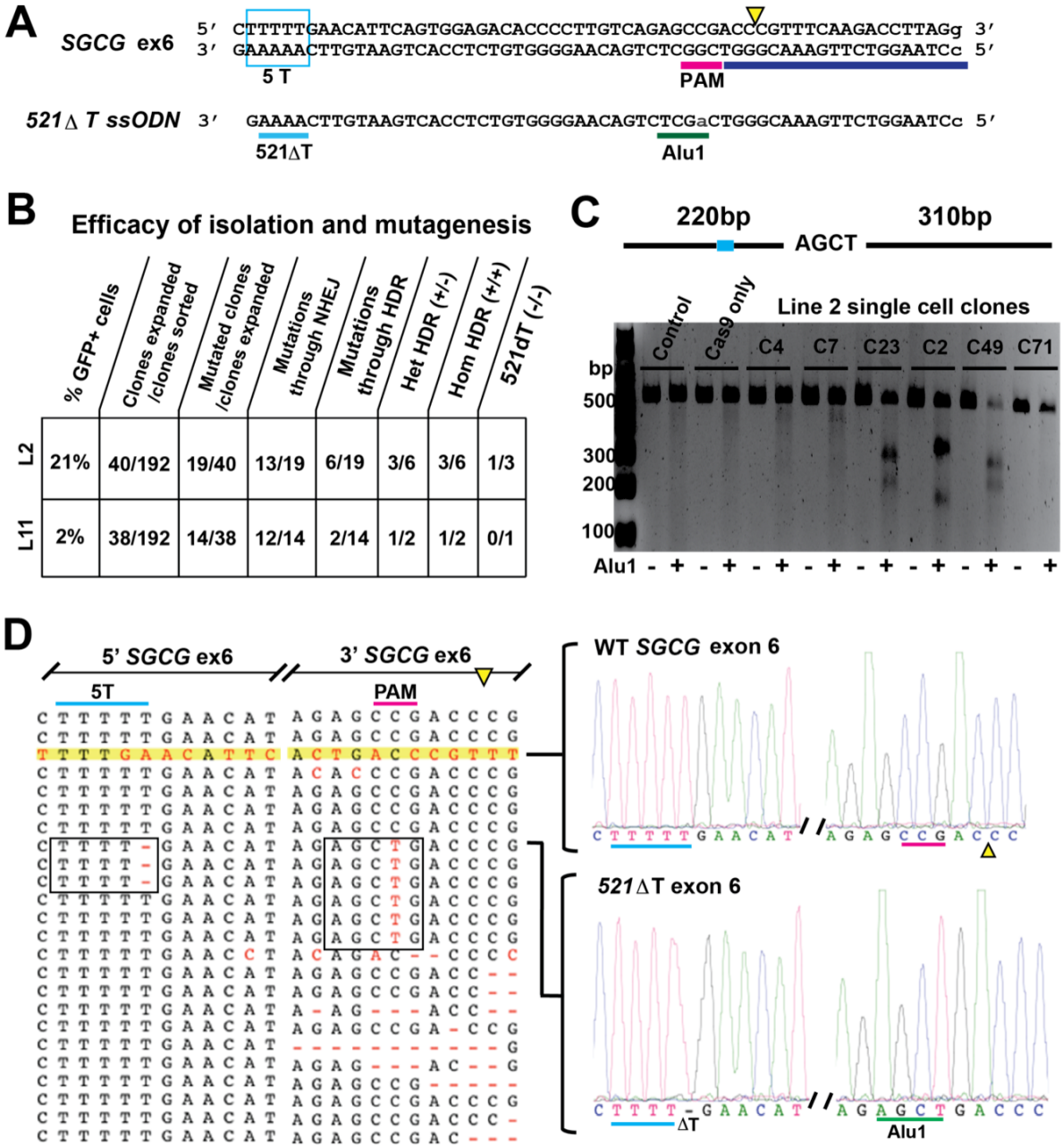

Figure 2.7 CRISPR/Cas9 mediated gene editing in UDCs

(A) Targeting strategy to introduce the 521ΔT point mutation into control *SGCG* exon 6 through gRNA guided, Cas9 nuclease generated double strand DNA break (DSB) with ssODN mediated HDR repair. A portion of the *SGCG* exon 6 coding region is shown; a single T was removed from the 5T sequence region (cyan box). The downstream gRNA target sequence is highlighted in blue, the PAM sequence in pink, and the Cas9 DSB indicated by a yellow triangle. Below it is a portion of the 142bp ssODN HDR repair template encoding the single T deletion along with a downstream G>A synonymous mutation (green) that destroys the PAM sequence and introduces

Figure 2.7 continued
an Alu1 restriction site. **(B)** Summary of efficiency of CRISPR/Cas9 protocol. **(C)** Alu1 restriction digest of a PCR-amplified genomic region including *SGCG* exon 6 and the flanking intronic sequences. **(D)** *Left*, partial summary of the Sanger sequencing results from individual line 2 edited clones. *Right*, is the DNA trace from an unedited control and a clone with a homozygous deletion of a single T from the 5T of *SGCG* exon 6, recreating the most common LGMD2C mutation.

DISCUSSION

The limited availability of human skeletal muscle tissue encumbers the study of muscle development and the pathology of muscle disease. Many novel strategies have been taken to overcome this limitation, relying on genetic engineering with direct and indirect reprogramming of cells. Regardless of strategy, a key component to success is the initial cell source, specifically the ease of acquisition and ability to reprogram. Urine is an underutilized, non-invasive, and cost effective source of primary human cells that has served as a platform for urothelial-based culture and iPSC reprogramming (Bharadwaj et al., 2013; Dorrenhaus et al., 2000; Y. Zhang et al., 2008). Recent advances in urine cell isolation have generated clonal populations of autologous human cells with a high proliferative capacity, evident telomerase activity, and plasticity for reprogramming into multiple lineages (Bharadwaj et al., 2013; Y. Zhang et al., 2008). These characteristics make urine-derived cells an attractive source of primary human cells for *in vitro* models. We now extended these findings showing that inducible expression of MyoD efficiently reprogrammed UDCs into the myogenic lineage, providing a simple strategy to generate an *in vitro* model of skeletal muscle from virtually any human subject.

Urine cells demonstrate an inclination towards the mesodermal lineage. A subpopulation of cells, classified as urine stem cells, express pericyte and mesenchymal stem cell markers and were able to differentiate into podocytes, smooth muscle, and urothelial cells (Bharadwaj et al., 2011; Bharadwaj et al., 2013; Y. Zhang et al., 2008). The ability of UDCs to differentiate into skeletal muscle is less defined. Studies showed growth on specific biomaterials, presence of specific growth factors, or defined media modifications promoted expression of myogenic markers such as MyoD, desmin, and myosin (W. Chen et al., 2014; Liu et al., 2013). However, these cells were not observed to form striations nor to display contractile properties. Given the

known expression of these markers, it is possible that without sufficient MyoD, UDCs differentiate more towards smooth rather than striated muscle lineages (Y. Zhang et al., 2008). The strategy with an induced MyoD pulse combined with media manipulation drove urine cells through the initial stages of myogenic development into a more mature phenotype, complete with expression of dystrophin, adult myosin, titin, and γ–sarcoglycan, along with the presence of functional sarcomeres. Despite these advancements, this cellular model still lacks major components of mature muscle such as transverse tubules and resident stem cell niches.

An alternative strategy to direct reprogramming with MyoD would be to first reprogram UDCs into iPSCs, and then use the iPSC lines for myogenic differentiation. This approach has the advantage of iPSC self-renewal, although immortalization of UDCs directly could obviate this need *in vitro*. DMD UDCs were previously successfully reprogrammed into iPSC and differentiated into cardiomyocytes, recapitulating cardiac phenotypes *in vitro* (Guan et al., 2014). Skeletal muscle differentiation of iPSCs has proven more challenging, although more efficient skeletal muscle differentiation from iPSC using small molecules has recently been reported (Chal et al., 2015). Interestingly, the ease of urine cell isolation, transduction with iMyoD virus, and reprogramming into iPSC suggest an ability to employ multiple parallel models for the study of muscle disease. A summary of cell types for modeling muscle disease and the timeline for generating these models in culture is shown in Figure 2.8.

We also showed that UDCs can be directly gene edited using CRISPR/Cas9 technology. The use of gene editing for muscle disease has focused intently on genetic correction strategies with significant success on the study of muscular dystrophy, as recent studies showed the ability to correct DMD disease-causing mutations in animal models and human cells (Li et al., 2015; Long et al., 2016; Long et al., 2014; Nelson et al., 2016; Ousterout et al., 2015; Tabebordbar et

al., 2016; Wojtal et al., 2016; Xu et al., 2016; Young et al., 2016). Nevertheless, gene editing in human iPSCs is challenged by the availability of patient cell lines, isolation of pure clonal populations, and low editing efficiency, especially when targeting precise mutations with homology-dependent repair (Bialk, Rivera-Torres, Strouse, & Kmiec, 2015; F. Chen et al., 2011; Yang et al., 2013). While some technical aspects of the CRISPR/Cas9 system are still undergoing improvement, the relative ease of urine cell isolation, coupled with the ability to generate single cell clones, makes this an attractive primary cell platform for CRISPR/Cas9 gene editing.

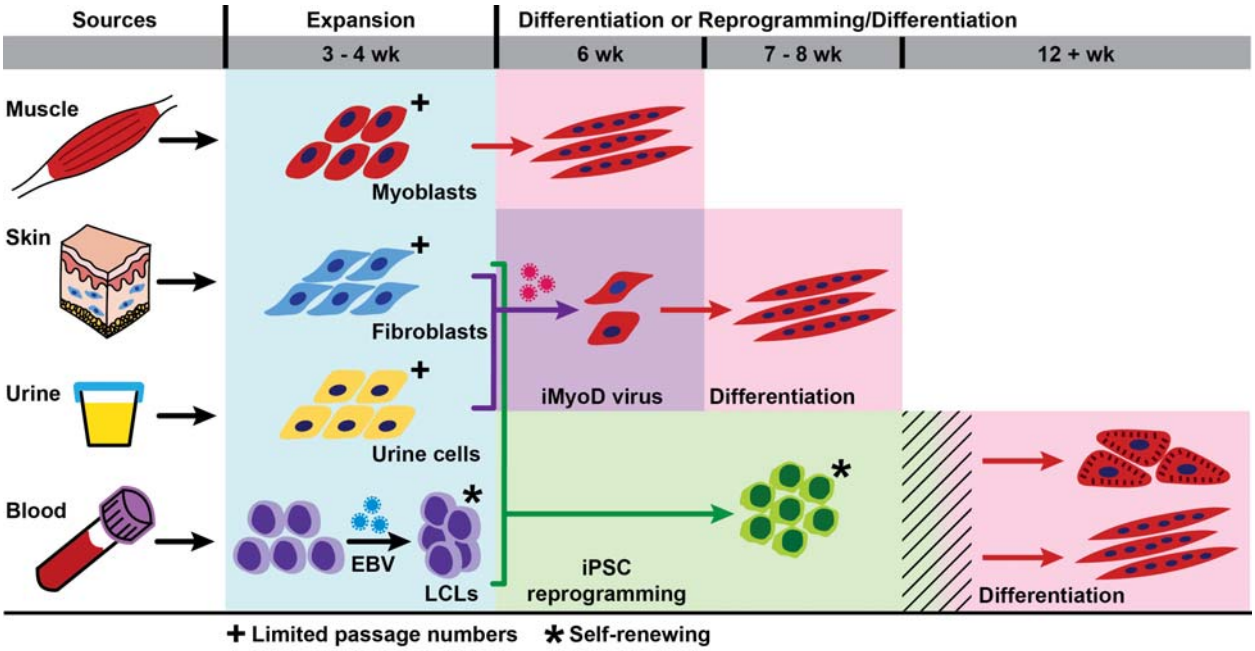

Figure 2.8 Overview of options for modeling skeletal muscle disease in cell culture

Primary cell sources for establishing cell cultures include: muscle, skin, urine, and blood. Myoblasts cultured from muscle biopsies require approximately three to four weeks for expansion and an additional two weeks of culture for myotube differentiation (Blau & Webster, 1981; Cheng et al., 2014; Rando & Blau, 1994). Primary dermal fibroblasts isolated from skin biopsies require three to four weeks for expansion. Fibroblasts can then be transduced with inducible MyoD (iMyoD) lentivirus, expanded, and differentiated to yield myotubes by approximately eight weeks (Kimura et al., 2008; Lattanzi et al., 1998). Urine cells require three to four weeks for expansion and a similar timeframe for iMyoD-induced myotube formation as dermal fibroblasts. Lymphocytes isolated from blood are typically transformed using Epstein-Barr virus (EBV) to generate lymphoblastoid cell lines (LCLs), which requires three to four weeks. Fibroblasts, urine derived cells, and LCLs can all be reprogrammed to induced pluripotent stem cells (iPSCs). Once generated and expanded, iPSCs will be subjected to quality control measures such as immunofluorescence for pluripotency markers, karyotyping, and embryoid body formation or teratoma formation for three germ layers. As each laboratory has its own quality control measures, this process will add variable amount of time for iPSC culture (indicated by hatch marks). iPSCs can be readily differentiated into cardiomyocytes (Burridge et al., 2014; Guan et al., 2014; Lian et al., 2013). Improved efficiency for myotube differentiation from iPSCs has been reported but additional advances are expected to enhance the efficiency of this process (Chal et al., 2015; R. Darabi & R. C. Perlingeiro, 2016)

CHAPTER 3

DISTINCT PHENOTYPES BETWEEN DISEASE SUBTYPES IN SKELETAL MUSCLE MODELS OF MYOTONIC DYSTROPHY

(modified from a manuscript in preparation)

OVERVIEW

Myotonic dystrophy (DM) is the most common autosomal dominant muscular dystrophy and encompasses both skeletal muscle and cardiac complications, including irregular heart rhythms. Myotonic dystrophy is caused by expansion of short nucleotide repeats with type 1 (DM1) due to a trinucleotide repeat expansion on chromosome 19, and type 2 (DM2) a tetranucleotide repeat expansion on chromosome 3. These repeat regions, once transcribed, form toxic RNA transcripts that can sequester RNA binding proteins such as muscleblind-1 (MBNL1). As MBNL1 normally serves as a splicing regulator to promote expression of adult transcript isoforms, sequestration of MBNL1 leads to a shift from adult to fetal splicing program and contributes to multisystemic manifestation of DM. As DM1 is thought to be the more common and severe subtype, most studies in the field have focused on DM1. Further, developing representative models of myotonic dystrophy in animals is challenging due to instability of repeat expansions. This is especially evident for DM2 in which the repeat expansions are often greater than 5,000 copies. To investigate mechanisms of human DM in the skeletal muscle, we generated cellular models of DM including both DM1 and DM2. We used regulated MyoD expression to reprogram urine-derived cells into myotubes. In this model, we found impaired dystrophin expression, MBNL1 foci, and aberrant splicing in DM1 but not in DM2 cells. These

data support that DM1 and DM2, despite some shared clinical and molecular features, have distinct pathological signatures in the skeletal muscle.

This chapter and Chapter 4 are modified from a manuscript in preparation titled, “Distinct pathological mechanisms in human cellular models of myotonic dystrophy.” I established myotube models, performed and imaged immunofluorescence, ran RT-PCR for alternative splicing analysis, and analyzed the data. Lisa Dellefave-Castillo recruited and consented patients. Alexis Demonbreun quantified dystrophin immunofluorescence. I wrote and edited the manuscript. Elizabeth McNally recruited patients, helped analyze the data, and edited the manuscript.

INTRODUCTION

The Myotonic Dystrophies (DMs) are autosomal dominant nucleotide repeat expansion disorders that share clinical features of skeletal muscle myotonia and weakness, as well as cardiac arrhythmias and heart failure (Meola & Cardani, 2017; Thornton, 2014; Udd & Krahe, 2012). Of the two subtypes, type 1 (DM1) is associated with a CTG trinucleotide expansion in 3' untranslated region of dystrophia myotonica protein kinase (*DMPK*) gene (Brook et al., 1992; Fu et al., 1992; M. Mahadevan et al., 1992), while type 2 (DM2) is associated with CCTG tetranucleotide expansion in intron 1 of CCHC-type zinc finger nucleic acid binding protein (*CNBP*, previously known as zinc finger 9, *ZNF9*) gene (Liquori et al., 2001; Ranum et al., 1998). In DM1, there is a correlation between number of repeats and disease age of onset. Those with 50 to 1,000 repeats typically have adult onset DM1, with a range of clinical features, and those with greater than 1,000 repeats will often have early onset congenital DM1 that displays many more systemic and profound clinical features (Meola & Cardani, 2015; Udd & Krahe, 2012). DM2 is characterized by an average repeat length of 5,000 (Liquori et al., 2001) and no reliable correlation between the number of repeats and disease onset (Day et al., 2003; Meola & Cardani, 2015). DM2 is considered an adult onset condition, as no congenital onset has been reported (Day et al., 2003).

The main mechanism thought to underlie DM is toxic RNA gain-of-function. RNA expression of nucleotide repeat expansions has been linked to the presence of double stranded RNA aggregates that can be detected in nuclei as ribonuclear foci (Mankodi et al., 2001; Taneja, McCurrach, Schalling, Housman, & Singer, 1995). Furthermore, these foci sequester splicing factors, such as muscleblind-1 (MBNL1) (B. M. Davis et al., 1997; Fardaei et al., 2002; Mankodi et al., 2003; Mankodi et al., 2001). Sequestration of MBNL1 and functional depletion of the

protein have been linked to missplicing of downstream genes such as *INSR* and *CLCN1*, which are thought to explain both insulin resistance and muscle myotonia in DM1, respectively (X. Lin et al., 2006; Mankodi et al., 2002; Savkur et al., 2001). In addition to MBNL sequestration, upregulation of RNA binding proteins like CUGBP1 has also been described, suggesting that multiple RNA regulatory proteins are implicated in DM pathogenesis (Wang et al., 2007). To date, most studies have been focused on DM1 rather than DM2, in part because features of myotonia are more prevalent in DM1 and the frequency of DM1 is generally thought to exceed that of DM2 (Udd & Krahe, 2012). Although DM1 and DM2 share the common theme of nucleotide repeat expansion and some clinical features, there are key clinical differences. Notably, DM2 typically has a later age of onset despite having a significantly larger nucleotide repeat expansion (Meola & Cardani, 2017). However, when considering all adult onset forms of DM1, including those associated with repeat expansions 50-100, there is considerable overlap between DM1 and DM2 in the progressive skeletal muscle weakness and their cardiac complications (Bhakta, Groh, Shen, Pascuzzi, & Groh, 2010; Groh et al., 2008; Schmacht et al., 2016; Tanawuttiwat, Wagner, Tomaselli, & Nazarian, 2017).

Generating animal models of DM is challenged by the instability of nucleotide repeat expansions, especially for DM2 with its very large tetranucleotide repeat expansion. A heterozygous *Cnbp*/*Znf9*$^{+/-}$ mouse model was previously described with multiorgan involvement including myotonia, cataracts, and cardiac conduction abnormalities, while a *Drosophila* model expressing a CCUG repeat expansion showed eye defects and ribonuclear foci formation (W. Chen et al., 2007; Z. Yu et al., 2015). However, whether ZNF9/CNBP expression levels change in DM2 has been debated, which may ultimately limit the use of *Znf9*$^{+/-}$ mouse as a disease model (Margolis et al., 2006; Raheem et al., 2010). Modeling DM1 in mice has been more

successful. The *Mbnl1*$^{\Delta 3/\Delta 3}$ model recapitulates MBNL1 depletion and display myotonic discharges and splicing aberrations (Kanadia et al., 2003). The HSA^{LR} and EpA960 models recapitulate repeat expansions of 250 and 960, respectively, and exhibit disease phenotypes such as myotonia, muscle weakness, and missplicing (Mankodi et al., 2000; Orengo et al., 2008). While these mouse models have elucidated critical aspects of DM, inherent differences between mouse and human physiology could limit their use. Furthermore, DM2 remains significantly understudied.

In this study, we modeled human DM using a cell-based model derived from both DM1 and DM2 patients to investigate skeletal muscle phenotypes. We first generated a skeletal muscle-like model relying on an inducible MyoD system on urine-derived cells isolated from control and DM patients. After differentiation, DM1 myotubes displayed intranuclear MBNL1 foci and associated shift in splicing, whereas DM2 myotubes exhibited very few MBNL1 clusters and splicing patterns similar to those of control myotubes. These findings confirmed previously described features of DM1 but suggested that DM2 may have alternative pathological mechanisms.

MATERIALS AND METHODS

Human subjects

Written and informed consent was obtained from all human subjects included in the study. All work was conducted under the University of Chicago and Northwestern University's Institutional Review Boards.

Urine-derived cells isolation and culture

Cells were isolated from urine samples and maintained as described previously (E. Y. Kim et al., 2016).

Lentiviral transduction and myotube differentiation

The tamoxifen-inducible MyoD lentiviral construct (p-Lv-CMV-MyoD-ER(T)), referred to as iMyoD in this paper, was previously described (Kimura et al., 2008) and was kindly provided by the laboratory of Dr. Jeffrey Chamberlain (University of Washington; Addgene plasmid # 26809). Lentiviral construct was packaged by the Skin Disease Research Center DNA/RNA Delivery Core at Northwestern University (Chicago, IL). Urine-derived cells transduction with iMyoD, transduction efficiency estimations, and myotube differentiation were done as previously described (E. Y. Kim et al., 2016).

Splice form analysis

Differentiated myotubes at day 28 and 35 post-differentiation were collected for RNA. The cells were washed once with cold PBS. RNA was isolated using TRIzol (Thermo Fisher Scientific, Waltham, MA; 15596-018) following the manufacturer's instructions. Glycogen (Thermo Fisher Scientific, Waltham, MA; AM9510) was added to the isopropanol at 50-100 μg/mL prior to RNA precipitation. The RNA pellets were washed once in 70% ethanol and resuspended in UltraPure Distilled Water. RNA concentration was measured using NanoDrop 2000 (Thermo Fisher Scientific, Waltham, MA; ND-2000) and up to 1000 ng of RNA was reverse transcribed using qScript cDNA SuperMix (Quanta Biosciences, Gaithersburg, MD; 95048-025). cDNA (30-60 ng) was used per PCR reaction and the products were separated on 1.5% agarose gel with

ethidium bromide. All gels were visualized and imaged on UVP Transilluminator (UVP, Upland, CA). All primers were purchased from Integrated DNA Technologies (IDT, Skokie, IL) and primer sequences used for RT-PCR are listed in Table 3.1.

Table 3.1 Primers used for splicing analysis

Gene target	Primer sequence	Template or Source
INSR	F: CCAAAGACAGACTCTCAGAT	(Savkur et al., 2001)
	R: AACATCGCCAAGGGACCTGC	
CAPN3	F: TCATCCTCCGGGTCTTCTCTG	(X. Lin et al., 2006)
	R: GTTCACGACTGTGTTAAGGACCTTC	
mTTN	F: CCGCTCCAGAAATGTATACTCCC	(X. Lin et al., 2006)
	R: TCCACCATCTTGTTTCTGTACG	
zTTN	F: GAAACAAGATGCTGACAAAAGTGC	(X. Lin et al., 2006)
	R: GGTCTGCTGAGCATAGGATTCTTC	
MBNL1	F: GCTGCCCAATACCAGGTCAAC	(X. Lin et al., 2006)
	R: TGGTGGGAGAAATGCTGTATGC	
MBNL2	F: ACAAGTGACAACACCGTAACCG	(X. Lin et al., 2006)
	R: TTTGGTAAAGGATGAAGAGCACC	
ATP2A1 (SERCA1)	F: GCTCATGGTCCTCAAGATCTCAC	(X. Lin et al., 2006)
	R: AGCTCTGCCTGAAGATGTGTCAC	
ZASP	F: GCAAGACCCTGATGAAGAAGCTC	(X. Lin et al., 2006)
	R: GACAGAAGGCCGGATGCTG	

Splice form band densitometry

To quantify band densities of differentially spliced transcripts, the gel images were analyzed using Fiji (NIH, Bethesda, MD). Each lane was selected using Select Lane function of Gel analysis tool in Fiji, and then the lanes were plotted. Areas under the curve calculated by Fiji were used as band densities. Ratios are reported as band density of embryonic transcript divided by band density of adult transcript.

Immunofluorescence microscopy (IFM)

After 28 days of differentiation, myotubes were washed quickly 3 times with room temperature PBS then fixed in 4% paraformaldehyde at room temperature for 15 minutes. Cells were washed quickly once with room temperature PBS then permeabilized in 0.25% Triton-X (Sigma Aldrich, St. Louis, MO; T8787) for 20 minutes at room temperature. Cells were then blocked in 10% horse serum 30 minutes to 1 hour at 4°C. Primary antibody incubations were done overnight at 4°C. After primary antibody incubation, myotubes were washed 3 times at room temperature, 10 minutes per wash. The first and third washes were done using PBS and the second wash was done using 0.1% Triton-X. Secondary antibody incubations were done at room temperature for 1 hour, followed by 3 washes as described above. Nuclei were stained with Hoechst 33342 (Thermo Fisher Scientific, Waltham, MA; H3570), used at final concentration of 1:10,000. All antibodies were diluted in 0.1% Triton-X and 2% horse serum, and all solutions were made with 1x PBS. All myotubes were imaged on Zeiss Axio Observer Z.1 inverted microscope. Primary antibodies and dilutions used are as follows: MyoD (C-20) at 1:1,000 (Santa Cruz Biotechnology, Dallas, TX; sc-304), α-actinin at 1:1,000 (Sigma Aldrich, St. Louis, MO; A7811), dystrophin at 1:1,000 (Thermo Fisher Scientific, Waltham, MA; PA1-37587). MBNL1 (A2764) was used at 1:3,000 and was a kind gift from the laboratory of Dr. Charles Thornton (University of Rochester) (X. Lin et al., 2006). Secondary antibodies were all from Thermo Fisher Scientific and was used at 1:1,000. These are as follows: Alexa Fluor 488 donkey anti-rabbit (A21206), Alexa Fluor 488 donkey anti-mouse (A21202), Alexa Fluor 594 donkey anti-rabbit (A21207), Alexa Fluor 594 donkey anti-mouse (A21203).

Dystrophin quantification

All images were acquired identically on Zeiss Axio Observer Z.1 inverted microscope with Zen Software. Images were post-processed using FIJI (NIH, Bethesda, MD). Background was subtracted from all images using rolling ball filter set at 200 pixels. Dystrophin and α-actinin mean fluorescence intensity were measured in individual channels across the entire field, n≥2 images per condition, with multiple fibers present per image. Dystrophin mean fluorescence intensity was calculated as dystrophin mean fluorescence intensity divided by α-actinin mean fluorescence intensity. A one-way ANOVA was performed using GraphPad Prism 7.

RESULTS

Myotube differentiation of DM1 and DM2 urine-derived cells

Urine-derived cells can be directly reprogramed into myotubes using MyoD (E. Y. Kim et al., 2016). This system relies on a tamoxifen inducible, lentiviral delivered MyoD (iMyoD) (Kimura et al., 2008). Urine-derived cells were isolated and cultured from DM1, DM2, and healthy controls and then transduced with iMyoD lentivirus (Table 3.2).

Table 3.2 Demographic features of subjects included in myotube study

Disease type	Age at cell collection	Sex	Repeat number
DM1	51	M	150 CTG
DM2	31	F	>10,000 CCTG
Control	24	M	n.d.
Control	25	F	n.d.

Following induction of MyoD with tamoxifen, cells acquired a myotube-like appearance and were then analyzed at 28 days after induction (Figure 3.1). Immunostaining using an anti-MyoD antibody demonstrated intranuclear localization of MyoD after tamoxifen treatment (Figure 3.1).

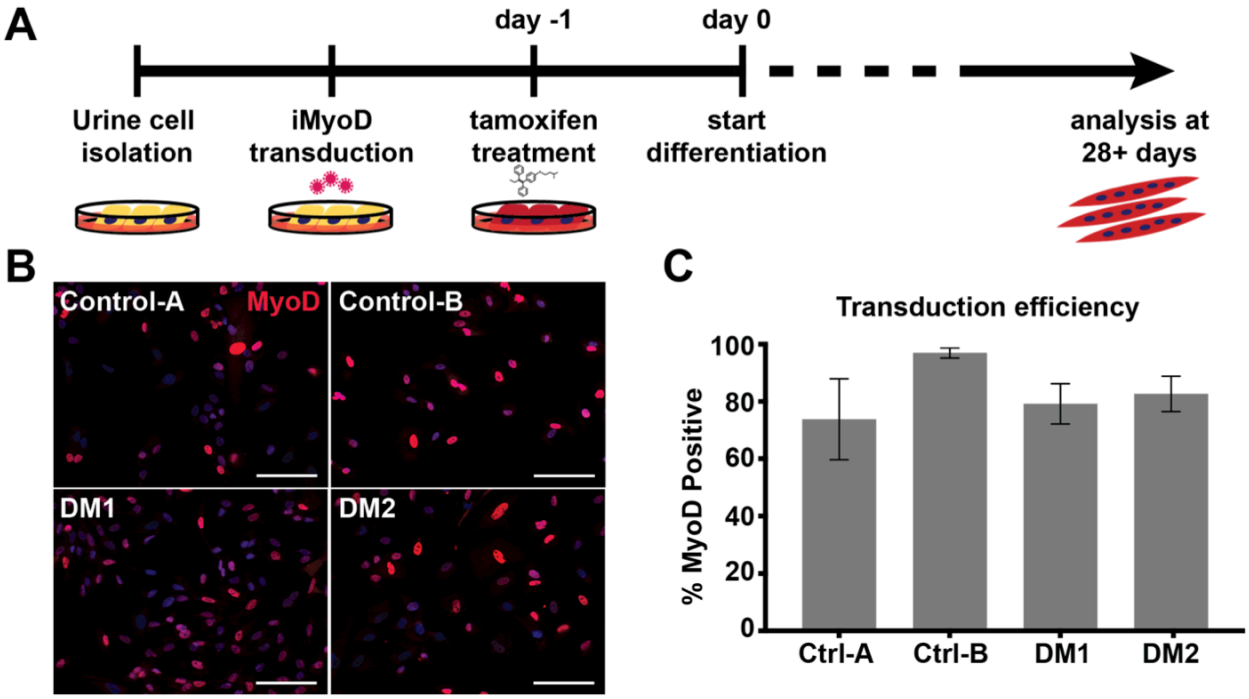

Figure 3.1 MyoD directed reprogramming to create a skeletal muscle model of DM1 and DM2 from urine-derived cells

(A) Urine-derived cells were isolated and cultured from healthy controls, DM1 and DM2 subjects. Cell cultures were transduced with lentivirus expressing an inducible form of Myod (iMyoD) and then induced with tamoxifen to express MyoD and stimulate myotube differentiation. **(B)** MyoD (red) was detected in the nucleus of tamoxifen-treated cells. Nuclei were labeled with Hoechst 33342 (blue). Scale bar = 100 μm. **(C)** Transduction efficiency of control, DM1, and DM2 cell lines was comparable and was greater than 70%. Efficiencies are represented as percentages of MyoD positive nuclei relative to total number of nuclei.

Transduction efficiency typically exceeded 70% at the initiation of differentiation and was comparable among DM1, DM2, and healthy controls (Figure 3.1). At 28 days post-differentiation, myotubes were seen in control, DM1 and DM2 lines (Figure 3.2), and α-actinin, a marker of muscle differentiation, was readily detected in the expected sarcomeric pattern in all lines (Figure 3.2). Immunostaining with anti-dystrophin, a marker of mature muscle membrane, reproducibly showed diminished sarcolemma localization in DM1 myotubes compared to control and DM2 myotubes (Figure 3.2). These data are consistent with prior reports that DM1 myotubes have impaired differentiation (Amack & Mahadevan, 2004; Timchenko, Iakova, et al., 2001).

MBNL1 foci and splicing defects in DM1

In myotonic dystrophy, RNA expression nucleotide repeat expansions are thought to promote missplicing via sequestration of RNA binding splicing regulators such as muscleblind-like 1 (*MBNL1*) (Mankodi et al., 2001). To determine whether MyoD-reprogrammed urine-derived cells recapitulated this same pattern of MBNL1 sequestration, immunostaining for MBNL1 was performed. DM1 myotubes showed readily evident intranuclear MBNL1-positive foci (Figure 3.3**)**. This pattern of MBNL1 foci was accompanied by a loss of diffuse MBNL1 nucleoplasmic staining observed in control myotubes (Figure 3.3). In contrast, DM2 myotubes were more similar to control cells (Figure 3.3). Specifically, both DM2 and control myotubes showed the diffuse nucleoplasmic MBNL1 pattern. In DM2, very rare small discrete, intranuclear MBNL1-positive foci were occasionally observed (Figure 3.3), whereas foci were never detected in control myotubes (Figure 3.3).

The recruitment of MBNL1 to ribonuclear foci results in a functional depletion of the MBNL1 protein, which is associated with a shifted splicing pattern from adult splice forms to

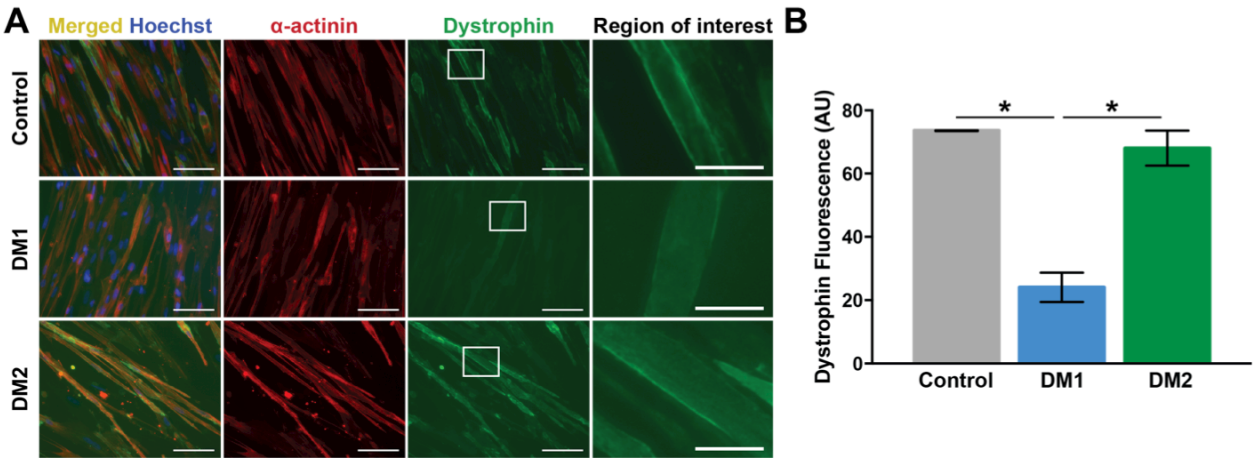

Figure 3.2 DM1 myotubes have reduced dystrophin expression compared to DM1 and control cells

MyoD-reprogrammed myotubes from control, DM1 and DM2 were established. **(A)** Myotubes were immunostained with α-actinin (red) and dystrophin (green). Nuclei were labelled with Hoechst (blue). Higher magnification images of the white dotted box are shown on the far right. Scale bar = 100 μm (all panels but region of interest), scale bar = 25 μm (region of interest). **(B)** DM1 myotubes have decreased dystrophin sarcolemmal staining, and dystrophin fluorescence was reduced (AU) compared to control and DM2 myotubes (*$p<0.05$, one-way ANOVA)

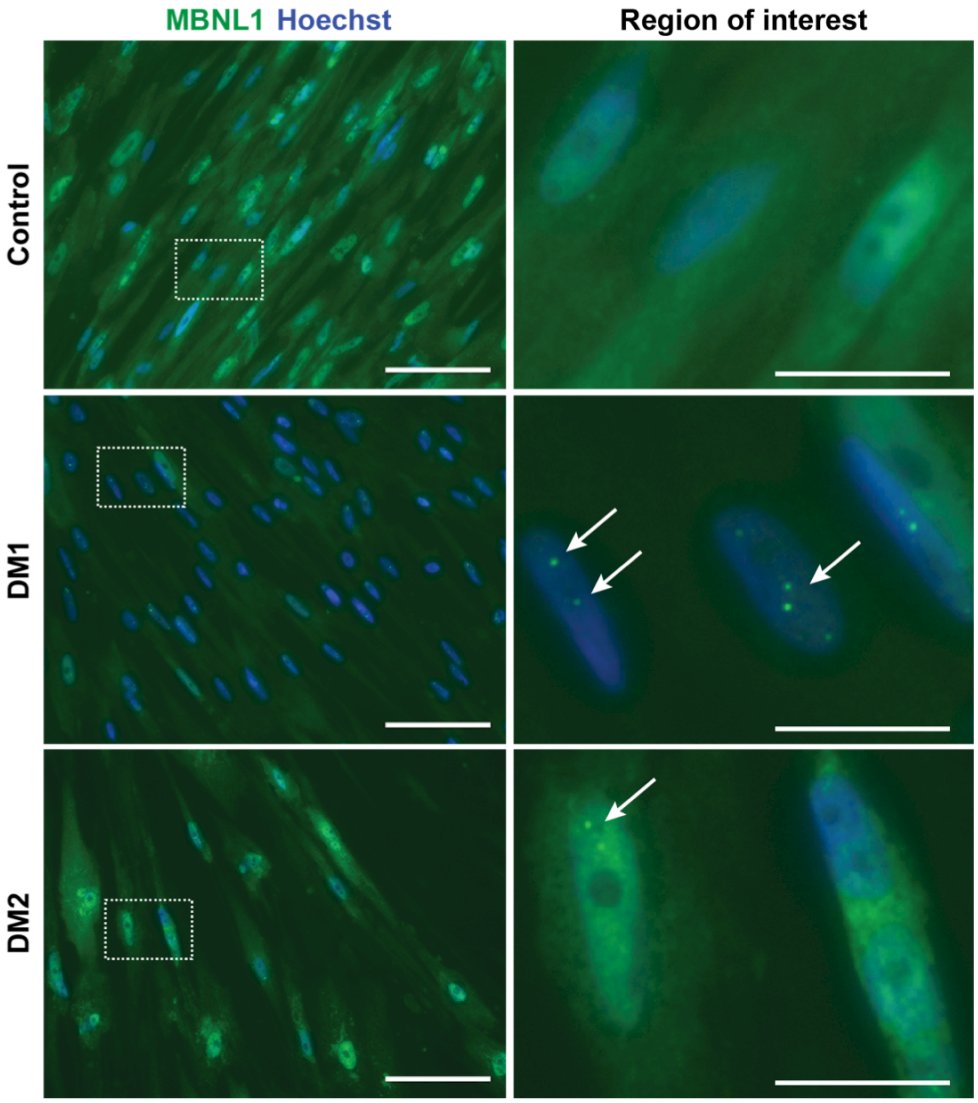

Figure 3.3 Intranuclear MBNL1 foci in DM1 myotubes

MyoD reprogrammed myotubes were immunostained with α-MBNL1 (green) and nuclei were labelled with Hoechst (blue). DM1 myotubes had readily detectable MBNL1-positive intranuclei foci (middle panel, white arrow). In DM1, MBNL immunoreactivity displayed a reduction in the diffuse nucleoplasmic pattern. This is in contrast to control and DM2 cells in which MBNL was diffuse throughout the nucleoplasm. Only very rare MBNL positive nuclei were seen (bottom panel, white arrow). Higher magnification images of the white dotted box are shown on the right. Scale bar (left panel) = 100 μm. Scale bar (right panel) = 25 μm.

embryonic splicing forms (X. Lin et al., 2006; Savkur et al., 2001). Missplicing in DM1 results in both inclusion or exclusion of exons in a cascade of genes (X. Lin et al., 2006; Savkur et al., 2001), including *INSR*, *CAPN3*, *mTTN*, *zTTN*, *MBNL1*, *MBNL2*, *SERCA*, and *ZASP*. RT-PCR analysis of these genes in DM1 myotubes displayed the expected increase in embryonic transcripts compared to control myotubes (Figure 3.4). In contrast, the pattern of splicing in DM2 myotubes was similar to those of control myotubes (Figure 3.4). DM1 myotubes showed a statistically significant increase in embryonic transcripts in all eight genes studied when compared to both control and DM2 myotubes (Figure 3.4). These findings suggest that MBNL1-related missplicing characterizes DM1 but not DM2 iMyoD-induced myotubes.

DISCUSSION

DM1 is thought to be more prevalent subtype than DM2, which has in part contributed to focus on elucidating DM1 pathogenetic mechanisms (Day et al., 2003; Udd & Krahe, 2012). Additionally, DM1 typically displays an earlier age of onset, especially when it manifests as congenital muscular dystrophy. More recently, it has been suggested that DM2 may be more prevalent than previously thought; a study showed the repeat expansion for DM2 was present in 1:1800 in the Finnish population (Suominen et al., 2011). Additionally, the smaller repeat expansions that characterize DM1 compared to DM2 has made animal models easier to generate. Here we established skeletal muscle models of DM, modeling both DM1 and DM2 and highlighting the differences in their molecular sequelae. These models have the advantage of being derived from human samples, but have the disadvantage in that cellular models do not fully replicate mature skeletal muscle. Nonetheless, these models are useful for delineating aspects of clinical disease phenotypes.

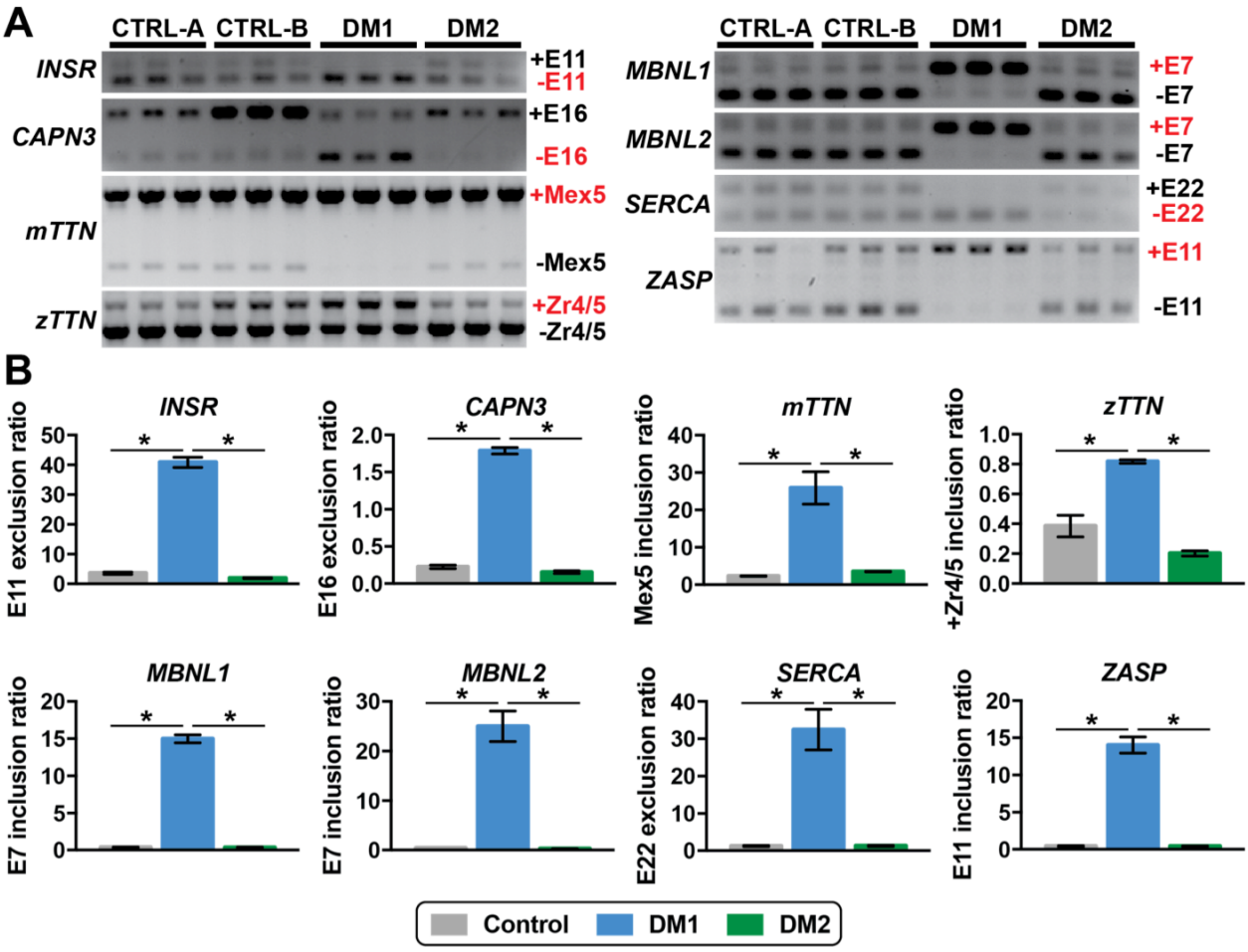

Figure 3.4 Aberrant splicing in DM1 myotubes but not DM2 myotubes

(A) RT-PCR of *INSR*, *CAPN3*, *mTTN*, *zTTN*, *MBNL1*, *MBNL2*, *SERCA*, and *ZASP* revealed an increase in embryonic transcripts (marked in red) in DM1. DM2 myotubes displayed similar splicing profiles as control myotubes. Each lane indicates technical replicate. **(B)** Quantification of band densities show an increase in ratios of transcripts with embryonic exons in DM1 when compared to DM2 and control myotubes (*$p<0.05$, One-way ANOVA).

Generating reproducible skeletal muscle lineages from iPSCs requires multiple selection steps (Chal et al., 2016; R. Darabi & R. C. R. Perlingeiro, 2016; Magli et al., 2017). In order to reduce the variability that arises from these steps, we used direct reprogramming by MyoD to generate a human skeletal muscle model. Direct reprogramming by MyoD is an effective means of inducing myogenesis and the ready access to urine-derived cells makes this an attractive option for human disease modeling (Kimura et al., 2008; Lattanzi et al., 1998). MyoD induction produced successful myotube generation from both DM1 and DM2, but in this skeletal muscle model, only DM1 recapitulated robust MBNL1 cluster formation and abnormal splicing.

Very rare MBNL1 clusters were observed in DM2 myotubes compared to DM1 myotubes, and consistent with this, the splicing profiles of DM2 myotubes resembled those of control cells. Previously, skeletal muscle biopsies from DM2 patients were examined and found to have MBNL1 clusters (X. Lin et al., 2006; Lukas et al., 2012; Mankodi et al., 2001), although relatively few clusters were noted. A recent study using immortalized myoblasts from DM1 and DM2 patients revealed MBNL1 cluster in both subtypes (Arandel et al., 2017). Notably, primary and immortalized myoblasts from DM1 patients displayed missplicing in *BIN1*, *DMD,* and *LDB3* upon differentiation into myotubes (Arandel et al., 2017). On the contrary, myotubes differentiated from primary and immortalized myoblasts isolated from DM2 patients exhibited splicing profiles similar to those of control myotubes (Arandel et al., 2017), similar to what we have observed in this current study. Missplicing events in DM2 have previously been reported in studies conducted with patient skeletal muscle biopsies (X. Lin et al., 2006). As myotube models represent a more immature state of skeletal muscle, the absence of missplicing in DM2 myotubes could suggest that the shift in splicing occurs later in myotube development, potentially after maturation of the myotubes into skeletal muscle. DM2 is also a later onset disease than DM1,

thus missplicing observed in DM1 at the myotube stage may be reflective of the earlier disease onset. MBNL1 clusters and missplicing events may be especially important for myotonia symptoms since overexpression of MBNL1 can correct aspects of myotonia in the mouse model of DM1 that expresses 250 CTG repeats in skeletal-muscle specific manner (Kanadia et al., 2006). Myotonia symptoms are less prevalent in DM2 compared to DM1, and therefore the difference in MBNL1 cluster formation observed in this study may reflect this distinct aspect of pathology (Udd & Krahe, 2012).

A decreased expression of dystrophin was observed in DM1 myotubes when compared to control and DM2 myotubes. A previous study reported that myoblasts isolated from two DM1 patients, one harboring 500 repeats and the other 1,200 repeats, fail to upregulate MyoD upon differentiation (Timchenko, Iakova, et al., 2001). Notably, overexpression of MyoD was insufficient to overcome the myogenic defects in DM1 myotubes as the system used in this current study results in high level of sustained MyoD expression. One study of satellite cells isolated from DM2 patients revealed MyoD and myogenin expression comparable to those of control cells upon differentiation (Pelletier et al., 2009), providing additional support that a development defect characterizes DM1 but not DM2.

CHAPTER 4

CARDIAC MODELS HIGHLIGHT PHENOTYPIC DIFFERENCES OF MYOTONIC DYSTROPHY DISEASE SUBTYPES

(modified from a manuscript in preparation)

OVERVIEW

Myotonic dystrophy exhibits both skeletal and cardiac muscle features. While skeletal muscle phenotypes of DM1 have been studied extensively, cardiac features of DM1 and DM2 have received less attention. DM1 and DM2 patients display arrhythmias and conduction defects that can lead to sudden death. Only a few DM mouse models with cardiac phenotypes exist, and these models recapitulate a subset of symptoms observed in DM patients. Thus, a model system that allow investigation of cardiac phenotypes in DM is needed. We generated induced pluripotent stem cells (iPSCs) from both DM1 and DM2 patients, and demonstrated an increase in RNA foci concomitant with cellular differentiation into cardiomyocytes for both DM1 and DM2. Cardiomyocytes that were differentiated from patient iPSCs displayed aberrant splicing and MBNL1 sequestration in DM1 cells, while those from DM2 did not. Investigation of Ca^{2+} handling in iPSC-derived cardiomyocytes from DM1 and DM2 revealed abnormal Ca^{2+} transients compared to controls. Finally, RNA-sequencing from DM1 and DM2 iPSC-derived cardiomyocytes implicated misregulation of potassium channels as a potential mediator of cardiac dysfunction.

This chapter and Chapter 3 are modified from a manuscript in preparation titled, “Distinct pathological mechanisms in human cellular models of myotonic dystrophy.” I established cardiomyocyte models, performed and imaged immunofluorescence, ran RT-PCR for alternative

splicing analysis, recorded calcium transients, and analyzed the data. David Barefield helped analyze calcium transient data. Andy Vo ran RNA-sequencing analysis. Emma Schuster assisted with alternative splicing analysis. Lisa Dellefave-Castillo recruited and consented patients. I wrote and edited the manuscript. Elizabeth McNally recruited patients, helped analyze the data, and edited the manuscript.

INTRODUCTION

In myotonic dystrophy type 1, progressive skeletal muscle weakness, especially targeting the respiratory muscles, and cardiac manifestations contribute to mortality (Groh et al., 2008; Mathieu, Allard, Potvin, Prevost, & Begin, 1999). The most common cardiac symptoms observed in DM1 patients are conduction blocks, such as atrioventricular block and bundle branch blocks, followed by premature ventricular contractions, and atrial fibrillation (Petri et al., 2012). Left ventricular systolic dysfunction can also develop in DM1 (Petri et al., 2012). These disturbances could lead to sudden death, where one study reported that about 30% of the deaths reported during a 10-year follow-up period were attributed to sudden death (Groh et al., 2008). While there are fewer studies investigating cardiac phenotypes of DM2 patients, those that are available report conduction defects as the most common cardiac feature, followed by supraventricular arrhythmias and left ventricular systolic dysfunction (Wahbi et al., 2009). Notably, the prevalence of cardiac dysfunction in DM1 and DM2 patient cohorts were similar, with conduction defects found in about 30% of the patients (Petri et al., 2012; Wahbi et al., 2009). While the small size of DM2 patient cohorts limits the interpretation of these findings, they still illustrate that cardiac symptoms are relatively common in both DM1 and DM2 and that they can impose a disease burden on patients.

Similar to skeletal muscle pathogenesis, expression of toxic RNA and subsequent missplicing in the heart is thought to contribute to the cardiac phenotypes, as ribonuclear foci are observed in the hearts of DM patients (Mankodi et al., 2005). Missplicing of cardiac troponin T, *TNNT2,* is one splicing anomaly implicated in cardiac pathology of DM (Philips et al., 1998). More recently, missplicing of *SCN5A*, which encodes the major sodium channel in the heart, was implicated in DM cardiac pathogenesis (Freyermuth et al., 2016). While there are likely shared

mechanisms between the cardiac and skeletal muscle pathology of DM1 and DM2, there may also be cardiac-specific effects accounting for development of arrhythmias. Moreover, the degree to which DM1 and DM2 share mechanisms has not been adequately addressed.

A few DM mouse models develop cardiac symptoms. Tg26 mice that overexpress *Dmpk* gene and TRECUGBP1 mice that overexpress *CUGBP1* in the heart both show cardiac conduction defects (Koshelev et al., 2010; O'Cochlain et al., 2004). DMSXL mice that express >1,000 CTG repeats and *Mbnl1*$^{\Delta 3/\Delta 3}$ mice both develop missplicing but no conduction defects (Huguet et al., 2012; Kanadia et al., 2003). EpA960 mice that express 960 CTG repeats specifically in the heart recapitulate many of the DM1 features, such as conduction defects, ribonuclear foci and MBNL1 sequestration, as well as missplicing (Wang et al., 2007). However, while repeat expansions are usually uninterrupted in DM1, these mice carry interrupted CTG repeats, which can potentially limit their relevance to human DM1 (Wang et al., 2007). *Znf9*$^{+/-}$ model develops conduction defects and cardiac hypertrophy, and is the only available mouse model for DM2 (W. Chen et al., 2007). This low availability of mouse models demonstrates the difficulty of modeling cardiac phenotypes in DM. Here, patient-derived cardiac models could provide a complementary system where disease mechanisms could be investigated.

In this study, we modeled the cardiac features of human DM using cardiomyocytes derived from induced pluripotent stem cells (iPSCs) of DM1 and DM2 patients. We found that DM1 iPSC-CMs readily displayed intranuclear MBNL1 clusters while DM2 cells showed very few, if any, MBNL1 clusters in the cardiac model. Correspondingly, DM1 iPSC-CMs recapitulated pathogenic alternative splicing, whereas DM2 cells did not. Finally, both DM1 and DM2 iPSC-CMs exhibited altered Ca^{2+} handling consistent with the known cardiac

complications that accompany these disorders. These finding support distinct pathogenic mechanisms underlying DM1 and DM2.

MATERIALS AND METHODS

Human subjects

Written and informed consent was obtained from all human subjects included in the study. All work was conducted under the University of Chicago and Northwestern University's Institutional Review Boards.

Urine-derived cells isolation and culture

Cells were isolated from urine samples and maintained as described previously (E. Y. Kim et al., 2016).

Reprogramming to induced pluripotent stem cells (iPSCs)

Urine-derived cells were reprogrammed to iPSCs by electroporating four plasmids described previously (Okita et al., 2011). The three reprogramming plasmids were pCXLE-hOCT3/4-shp53-F (Addgene plasmid # 27077), pCXLE-hSK (Addgene plasmid # 27078), and pCXLE-hUL (Addgene plasmid # 27080). The fourth plasmid, pCXLE-EGFP (Addgene plasmid # 27082) monitored successful electroporation. Plasmids were prepared using EndoFree Maxi Kit (Qiagen, Germantown, MD; 12362) and resuspended in UltraPure Distilled Water (Thermo Fisher Scientific, Waltham, MA; 10977-023). One day prior to electroporation, plasmids were precipitated with 0.3 M sodium acetate (Sigma Aldrich, St. Louis, MO; S8750) and at least 70% ethanol at -20°C overnight. On the day of electroporation, plasmids were centrifuged at 13,200

rpm for 10 minutes at 4°C. Supernatant was removed, and plasmids were washed with 70% ethanol twice, first time centrifuged for 2 minutes and second time for 10 minutes at 13,200 rpm, 4°C. Plasmid pellets were then dried and resuspended in UltraPure Distilled Water. Five μg of each plasmid was combined to create plasmid cocktail for each electroporation.

For electroporation, cells were washed once in 1x PBS (Thermo Fisher Scientific, Waltham, MA; 14190-250), counted, and then resuspended in 200 μL of electroporation buffer (Bio-Rad, Hercules, CA; 1542677). Electroporation used 100,000 cells. Cell suspensions were combined with the plasmid cocktails and then placed in electroporation cuvette with 0.4 cm gap (Bio-Rad, Hercules, CA; 1542088). The Gene Pulser Xcell Electroporation System was used (Bio-Rad, Hercules, CA; 1652660) with the following electrical setting: exponential decay at 300 V, 200 μFD, 100 Ω. After electroporation, cells were plated directly onto 12-well and 6-well plates pre-plated with primary mouse embryonic fibroblasts (PMEF, Millipore, Burlington, MA; PMEF-CF). MEFs were plated one day prior to electroporation on wells coated with 0.1% gelatin (Millipore, Burlington, MA; ES-006-B). Electroporated cells were placed in WiCell media with 50 μg/mL ascorbic acid on the day of electroporation. Fresh media was added the next day. On the second day, media was replaced with WiCell with 50 μg/mL ascorbic acid (Santa Cruz Biotechnology, Dallas, TX; sc-228390) and 0.5 mM sodium butyrate (Stemgent, Lexington, MA; 04-005). Media was switched every other day until colonies appeared. Colonies were picked manually and subsequently expanded on feeder plates until at least passage 5, and then adapted to feeder-free system using plates coated with hES-qualified Matrigel (Corning, Corning, NY; 354277) and grown in mTeSR1 (Stemcell Technologies, Vancouver, BC, Canada; 05875). WiCell media was composed of DMEM/F-12 50/50 mix (Corning, Corning, NY; 10-092-CV) with 20% KnockOut Serum Replacement (Thermo Fisher Scientific, Waltham, MA;

10828-028), 1% Non Essential Amino Acids (Thermo Fisher Scientific, Waltham, MA; 11140-050), 1% GlutaMax (Thermo Fisher Scientific, Waltham, MA; 35050-061), 0.1 mM beta-mercaptoethanol (BME, Thermo Fisher Scientific, Waltham, MA; 21985-023), and 12.5 ng/mL fibroblast growth factor (bFGF, Miltenyi Biotec, Auburn, CA; 130-093-842).

Cardiomyocyte differentiation and replating

Reprogrammed iPSCs were differentiated to cardiomyocytes according to previously described protocol (Barefield et al., 2017), with the starting densities between 100,000-320,000 cells/cm^2. Differentiated cardiomyocytes were replated 5 to 7 days after beating was observed to 12 mm No. 1.5 thickness coverslips (Fisher Scientific, Waltham, MA; 12-545-81) or 35 mm dish fitted with No. 1.5 coverslip (MatTek Corporation, Ashland, MA; P35G-1.5-14-C). Both types of coverslips were coated with hES-qualified Matrigel (Corning, Corning, NY; 354277) prior to seeding cardiomyocytes. Cells were placed in PBS for 20 minutes at 37°C and then dissociated with TrypLE Select (Thermo Fisher Scientific, Waltham, MA; 12563-011) for 15 minutes at 37°C. Cells were then collected and centrifuged at 300x*g* for 5 minutes. The supernatant was removed and cells were triturated 15 to 20 times using 1 mL of RPMI 1640 supplemented with 1x B-27 supplement, 40% FBS, and 2 μM thiazovivin. Resuspended cells were then passed through 100 μm strainers (Fisher Scientific, Waltham, MA; 08-771-19). Cells were counted and replated at 140,000 cells/cm^2 for downstream applications as specified in following sections. For 35 mm dishes fitted with coverslips, only the coverslips were coated with Matrigel and plated with cardiomyocytes.

Splice form analysis

IPSC-derived cardiomyocytes were collected for RNA. The cells were washed once with cold PBS. RNA was isolated using TRIzol (Thermo Fisher Scientific, Waltham, MA; 15596-018) following the manufacturer's instructions. Glycogen (Thermo Fisher Scientific, Waltham, MA; AM9510) was added to the isopropanol at 50-100 µg/mL prior to RNA precipitation. The RNA pellets were washed once in 70% ethanol and resuspended in UltraPure Distilled Water. RNA concentration was measured using NanoDrop 2000 (Thermo Fisher Scientific, Waltham, MA; ND-2000) and up to 1000 ng of RNA was reverse transcribed using qScript cDNA SuperMix (Quanta Biosciences, Gaithersburg, MD; 95048-025). cDNA (30-60 ng) was used per PCR reaction and the products were separated on 1.5% agarose gel with ethidium bromide. For *SCN5A* analysis, PCR products were digested with BstBI (New England Biolabs, Ipswich, MA; R0519S) at 65°C for 15 minutes as described previously (Freyermuth et al., 2016). For PCR reactions run on polyacrylamide gels, 8% Novex TBE gels (Thermo Fisher Scientific, Waltham, MA; EC6215BOX) were used. The gels were stained with ethidium bromide diluted in TBE buffer for 1-2 minutes at room temperature. All gels were visualized and imaged on UVP Transilluminator (UVP, Upland, CA). All primers were purchased from Integrated DNA Technologies (IDT, Skokie, IL) and primer sequences used for RT-PCR are listed in Table 4.1.

Table 4.1 Primers used for splicing analysis

Gene	Primer sequence	Template or Source
SCN5A	F: CTTCTGCCTGCACGCGTTCAC	(Freyermuth et al., 2016)
	R: CAGAAGACTGTGAGGACCATC	
ANK3	F: CCCTGTGGTCGTCTGTCTTT	(Freyermuth et al., 2016)
	R: CCAGGCTCAGTCAAGTAGCTG	
RYR2	F: TTCCAAGAATGTGCCCCCAG	NM_001276345.1
	R: GTGGACAGGCAGCACAGATA	
TNNT2	F: GTTCTGAGGGAGAGCAGAGAC	NM_001330272.1
	R: TTTGGACTCCTCCATTGGGC	

Splice form band densitometry

To quantify band densities of differentially spliced transcripts, the gel images were analyzed using Fiji (NIH, Bethesda, MD). Each lane was selected using Select Lane function of Gel analysis tool in Fiji, and then the lanes were plotted. Areas under the curve calculated by Fiji were used as band densities. Ratios are reported as band density of embryonic transcript divided by band density of adult transcript.

RNA fluorescence in situ hybridization (FISH) and quantification

IPSCs and iPSC-derived cardiomyocytes were plated on coverslips coated with Matrigel. IPSCs were cultured on coverslips until the colonies reached about 70-80% confluence and IPSC-derived cardiomyocytes were plated at 140,000 cells/cm^2 and cultured until beating was observed. FISH was performed following a protocol described previously with modifications to wash steps (de Mezer, Wojciechowska, Napierala, Sobczak, & Krzyzosiak, 2011). Cells were washed once with room temperature PBS then fixed in 4% paraformaldehyde (Electron Microscopy Sciences, Hatfield, PA; 15710) diluted in PBS at room temperature for 30 minutes. After fixation, cells were quickly washed 3 times with PBS then permeabilized in pre-chilled 2% acetone (Sigma Aldrich, St. Louis, MO; 34850) in PBS for 5 minutes. Pre-hybridization was done with 30% formamide (Sigma Aldrich, St. Louis, MO; F7503) diluted in 2x saline sodium citrate (SSC) for 10 minutes at room temperature. Hybridization was done in 2x SSC buffer with 30% formamide (Sigma Aldrich, St. Louis, MO; F7503), 0.02% bovine serum albumin (BSA, Sigma Aldrich, St. Louis, MO; A7906), 66 μg/mL yeast tRNA (Thermo Fisher Scientific, Waltham, MA; 15401-011), 10% dextran sulfate (Sigma Aldrich, St. Louis, MO; D8906), and 2mM vanadyl ribonucleoside complex (New England BioLabs, Ipswich, MA; S1402S).

Fluorescence probes (IDT, Skokie, IL) were diluted in the hybridization buffer at final concentration of 2 ng/μL, and cells were incubated with probes overnight at 37°C. The first post-hybridization wash was done 3 times, 10 minutes per wash in 2x SSC buffer with 30% formamide at 55°C. This was followed by second post-hybridization wash, which was done 3 times, 10 minutes per wash in 2x SSC buffer with 30% formamide at 37°C. IPSC-derived cardiomyocytes were then subjected to immunofluorescence labeling starting from blocking step as described below. 2x SSC buffer was made by diluting 20x SSC with water. 20x SSC was made by dissolving 175.3 g NaCl (Fisher Scientific, Waltham, MA; BP358-10) and 88.2 g of sodium citrate (Sigma Aldrich, St. Louis, MO; W302600) in water to final concentration of 3M NaCl and 300 mM sodium citrate. 20x SSC was then autoclaved for sterilization. The RNA probe used to detect repeats in DM1 patient cells was $(CAG)_{10}$ and in DM2 patient cells was $(CAGG)_5$. Both probes were labeled at 5' end with Cy3 and were resuspended in UltraPure Distilled Water to stock concentration of 1 μg/μL.

Cells probed with RNA FISH were imaged on Zeiss Axio Observer epifluorescence microscope with Apotome 2. Z-stack images at 0.15 to 0.25 μm gap between slices were taken from three random fields per coverslip. Z-stacks were collapsed using Z project function for maximum intensity in Fiji (NIH, Bethesda, MD). FISH foci were counted using Find Maxima function in Fiji with noise tolerance set to 25. The number of FISH foci was divided by the number of total nuclei in the field to calculate average number of foci per nucleus. The averages were graphed using GraphPad Prism 7 (GraphPad Software, La Jolla, CA).

Immunofluorescence microscopy (IFM)

IPSC-CMs were washed quickly 3 times with room temperature PBS then fixed in 4% paraformaldehyde at room temperature for 15 minutes. Cells were washed quickly once with room temperature PBS then permeabilized in 0.25% Triton-X (Sigma Aldrich, St. Louis, MO; T8787) for 20 minutes at room temperature. Cells were then blocked in 10% horse serum 30 minutes to 1 hour at 4°C. Primary antibody incubations were done overnight at 4°C. After primary antibody incubation, myotubes were washed 3 times at room temperature, 10 minutes per wash. The first and third washes were done using PBS and the second wash was done using 0.1% Triton-X. Secondary antibody incubations were done at room temperature for 1 hour, followed by 3 washes as described above. Nuclei were stained with Hoechst 33342 (Thermo Fisher Scientific, Waltham, MA; H3570), used at final concentration of 1:10,000. All antibodies were diluted in 0.1% Triton-X and 2% horse serum, and all solutions were made with 1x PBS. Coverslips were mounted using Vectashield Antifade Mounting Medium (Vector Laboratories, Burlingame, CA; H-1000) or ProLong Gold Antifade Mountant (Thermo Fisher Scientific, Waltham, MA; P36930). All iPSC and iPSC-derived cardiomyocytes were imaged on Zeiss Axio Observer epifluorescence microscope with Apotome 2. IF images in Figure 4.4 were obtained as z-stacks and flattened using Fiji (NIH, Bethesda, MD) z projection function. Primary antibodies and dilutions used were as follows: SSEA-4 at 1:1,000 (Santa Cruz Biotechnology, Dallas, TX; sc-21704), Tra-1-60 at 1:1,000 (Santa Cruz Biotechnology, Dallas, TX; sc-21705), MYBPC3 (E-7) at 1:1,000 (Santa Cruz Biotechnology, Dallas, TX; sc-137180), MBNL1 (4A8) at 1:1,000 (Millipore, Burlington, MA; MABE70). Actin was labeled with Alexa Fluor 488 Phalloidin at 1:1,000 (Thermo Fisher Scientific, Waltham, MA; A12379). Secondary antibodies were all from Thermo Fisher Scientific and were used at 1:1,000. These are as follows: Alexa Fluor 594 goat

anti-mouse IgM (A21044), Alexa Fluor 488 donkey anti-rabbit (A21206), Alexa Fluor 488 donkey anti-mouse (A21202), Alexa Fluor 594 donkey anti-rabbit (A21207), Alexa Fluor 594 donkey anti-mouse (A21203).

RNA ribonuclear foci quantification

IF images of iPSC and iPSC-CMs were acquired as z-stacks and flattened using z projection function on Fiji. The number of RNA foci were counted on Fiji using Find Maxima function with noise tolerance set between 25 to 30. Noise tolerance that allowed for the most accurate identification of foci by Fiji was chosen for each image. The total number of nuclei were counted manually. Then the total number of foci were divided by the total number of nuclei to calculate foci per nucleus.

Calcium transient measurements

IPSC-derived cardiomyocytes were replated on MatTek dishes as described above. Cells were washed once with room temperature PBS and loaded with 5 μM Indo-1 Leakage Resistant dye (TEFLabs, Austin, TX; 0145) with 0.02% pluronic F-127 (Sigma Aldrich, St. Louis, MO; P2443) in Tyrode's solution for 45 minutes at 37°C. After loading, cells were placed in Tyrode's solution. Tyrode's solution contained 119 mM NaCl, 5 mM KCl (Sigma Aldrich, St. Louis, MO; P9541), 25 mM HEPES (Sigma Aldrich, St. Louis, MO; H3375), 2 mM $CaCl_2$ (Sigma Aldrich, St. Louis, MO; C1016), and 2 mM $MgCl_2$ (Sigma Aldrich, St. Louis, MO; M8266), and was pH adjusted to 7.6. D-glucose (Sigma Aldrich, St. Louis, MO; G7021) was freshly added to Tyrode's solution at 6 mg/mL on the day of calcium measurements. Cells were imaged on Nikon Diaphot inverted microscope fitted with custom stage and photomultiplier tubes (PMT, Ionoptix,

Westwood, MA). Cells were paced at 0.25, 0.5, 0.75, and 1 Hz using 2 msec pulse width and voltage between 18-20 V. Pacer had electrodes at fixed width and was powered by a stimulator (Aurora Scientific, Aurora, ON, Canada; 701C). 10 to 20 transients were recorded per trace. Video Sarcomere Length 900B software (Aurora Scientific, Aurora, ON, Canada) was used to visualize the imaged fields and 950A Calcium Fluorescence System (Aurora Scientific, Aurora, ON, Canada) was used to record the traces and analyze the parameters of average transients. The average transients were plotted using GraphPad Prism 7, and one-way ANOVA statistical tests were run on GraphPad Prism 7 with $p<0.05$ set as statistically significant.

Cardiomyocyte differentiation efficiency estimation

After calcium transients were measured, coverslips were separated from 35 mm dishes and probed for cMyBP-C protein using IFM as described above. Coverslips were mounted using Vectashield Antifade Mounting Medium or ProLong Gold Antifade Mountant and imaged on Zeiss Axio Observer epifluorescence microscope with Apotome 2. Z-stack images were taken from three random fields per coverslip. Z-stacks were collapsed using Fiji (NIH, Bethesda, MD). The number of cells that show expression of cMyBP-C were counted manually and this number was divided by the number of total nuclei in the field to estimate differentiation efficiency. Samples with at least 90% efficiency were chosen for RNA sequencing.

RNA-seq sample preparation

IPSC-derived cardiomyocytes were replated as described above. Cells were washed once with cold PBS and collected in TRIzol. 200µL of chloroform was added per 1 mL of TRIzol used to collect the cells. Tubes were shaken vigorously for 15 seconds and incubated at room

temperature for 5 minutes. Tubes were then centrifuged at 12,000x*g* for 15 minutes at 4°C. Clear aqueous phase (about 400-450μL) was collected and moved to a new tube and equal volume of 70% ethanol was added. RNA was then isolated using Aurum Total RNA Mini Kit (Bio-Rad, Hercules, CA; 7326820) as described here. RNA was bound to columns by centrifuging at 12,000x*g* for 60 seconds at room temperature. Seven hundred μL of low stringency was solution was added to the columns, and samples were centrifuged for 30 seconds at 12,000x*g*. Eighty μL DNase solution was added to the columns and the samples were incubated at room temperature for 15 minutes. Columns were centrifuged for 30 seconds at 12,000x*g*. Seven hundred μL high stringency wash solution was added to the columns, and samples were centrifuged for 30 seconds at 12,000x*g*. Finally, 700 μL of low stringency wash solution was added to the columns and the samples were centrifuged at 12,000x*g* for 60 seconds. The flow-through was discarded and the columns were centrifuged again for 2 minutes at 12,000x*g*. RNA was eluted with UltraPure Distilled Water. RNA samples that were submitted for RNA sequencing were chosen from differentiations that showed at least 90% differentiation as measured by counting the number of cells that showed cMyBP-C expression through IFM. RNA quality check, cDNA library preparation, and sequencing were performed at the NUSeq Core Facility at Northwestern. Sample were sequenced on Illumina HiSeq 4000 for 150bp paired-end sequencing.

RNA-seq analysis

RNA-seq reads were aligned using STAR 2.5.2 to the human genome assembly hg38. Transcripts were assessed and quantitated using HT-seq and analyzed for differential expression using EdgeR. Counts per million (CPM) were used to calculate differential expression. Comparisons were done pairwise in the following groups: control vs DM1, control vs DM2, and

DM1 vs DM2. The lists were then filtered for genes that have *p*-value<0.15 and absolute log fold change greater than 1. The filtered gene list from each comparison were run through GO analysis using Gene Ontology Consortium with false discovery rate (FDR)<0.05. From GO term list, GO terms that contain less than 5 genes per category was excluded. Genes that fall under GO categories relating to cardiac conduction, ion transport, or cardiac development were used to generate a candidate list of genes. GO terms used for candidate list generation are listed in Table 4.3. The list was further reduced by selecting for genes that participate in channel formation, cardiac structure, ion transport, or developmental processes. Heatmaps were generated on GraphPad Prism using Z-scores calculated from log transformed CPM values per gene.

RESULTS

DM iPSC-derived cardiomyocytes have increased RNA repeat foci

The degree to which MBNL sequestration and missplicing characterizes the myotonic heart has been difficult to monitor given the scarcity of cardiac tissue from DM patients (Mankodi et al., 2005). In order to better understand the pathogenic mechanism of cardiac phenotypes in DM, urine-derived cells were reprogrammed to iPSCs and then differentiated into cardiomyocytes (Table 4.2). IPSCs derived from urine cells exhibited expression of embryonic stem cell markers such as SSEA4 and Tra-1-60, reflecting pluripotency and successful reprogramming (Figure 4.1). IPSC-derived cardiomyocytes (iPSC-CMs) expressed cardiac specific myosin binding protein C (cMyBP-C) in a sarcomeric, doublet pattern alternating with actin, indicating cardiomyocyte differentiation in both control and DM cells (Figure 4.2).

Table 4.2 Demographic features of subjects included in cardiac study

Disease type	Age at cell collection	Sex	Repeat number
DM1	51	M	150 CTG
DM1	28	F	430 CTG
DM2	31	F	>10,000 CCTG
DM2	57	M	>10,000 CCTG
DM2	28	F	>10,000 CCTG
DM2	41	M	>10,000 CCTG
Control	25	F	n.d.
Control	29	F	n.d.

RNA expression of nucleotide repeat expansions can be detected as ribonuclear foci using RNA FISH. We assessed the presence of RNA foci using RNA FISH on iPSCs ascertained as undifferentiated iPSCs and iPSC-CMs. RNA FISH using probes specific to repeat region in either DM1 or DM2 was conducted and demonstrated the formation of intranuclear foci in both DM1 and DM2 undifferentiated iPSCs as well as differentiated iPSC-CMs (Figure 4.3). Quantitation of FISH foci demonstrated an increased number of intranuclear foci in DM1 as compared to control cells (Figure 4.3). DM2 iPSCs had an increased number of RNA foci that trended towards significance ($p<0.07$) when compared to control cells (Figure 4.3). IPSC-CMs exhibited a further increase in foci per nucleus in both DM1 and DM2, indicating that differentiation promotes the formation of RNA foci (Figure 4.3).

MBNL1 sequestration results in aberrant splicing patterns in DM1 iPSC-CMs

We next queried whether differentiated iPSC-CMs similarly displayed MBNL1 sequestration into foci and aberrant splicing, as this same mechanism is thought to contribute to pathology in the myotonic heart (Mankodi et al., 2005). DM1 iPSC-CMs displayed distinctive

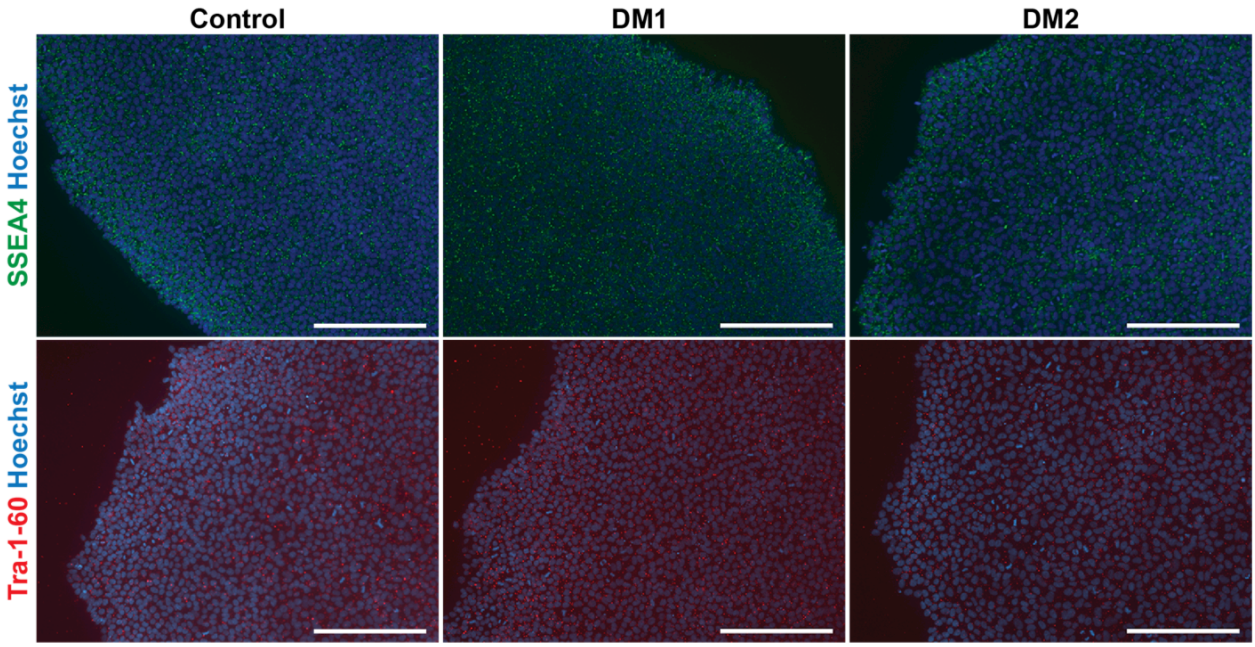

Figure 4.1 Urine-derived iPSCs express pluripotent markers

Immunostaining of iPSCs show expression of pluripotency markers SSEA4 (green) and Tra1-60 (red). Nuclei were labelled with Hoechst (blue). Scale bar = 250 µm.

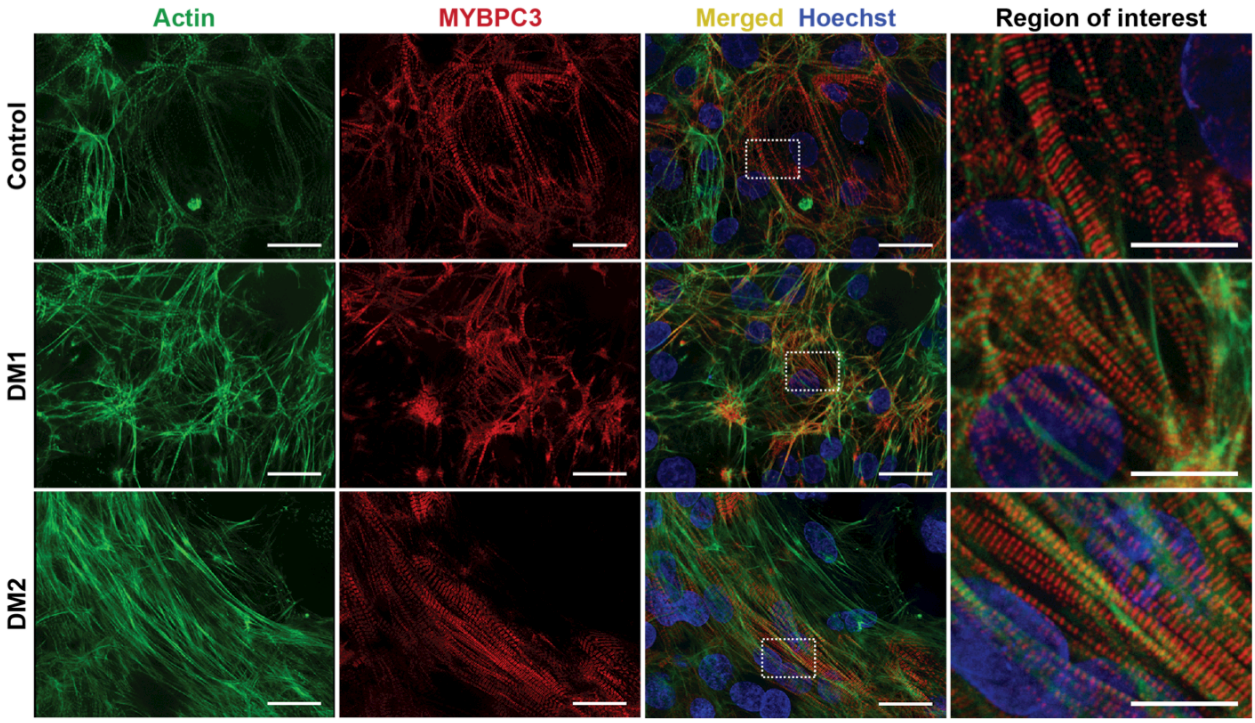

Figure 4.2 IPSC-derived cardiomyocytes from DM1 and DM2 subjects

Urine-derived cells were isolated from healthy control, DM1 and DM2 subjects and induced pluripotent stem cells (iPSCs) were generated using episomal delivery of Yamanaka factors. IPSCs were then differentiated into cardiomyocytes (iPSC-CM). To monitor differentiation status, cells were immunostained with α-actin (green) and α-MYBPC3 (red). Nuclei were labelled with Hoechst (blue). DM1, DM2, and control cells successfully differentiated into iPSC-CMs evidenced by an cMyBP-C, the major cardiac isoform of myosin binding protein C, which demonstrate the expected sarcomeric pattern. Higher magnification images of the white dotted box are shown on the right. Scale bar (all panels except region of interest) = 25 μm. Scale bar (region of interest) = 10 μm.

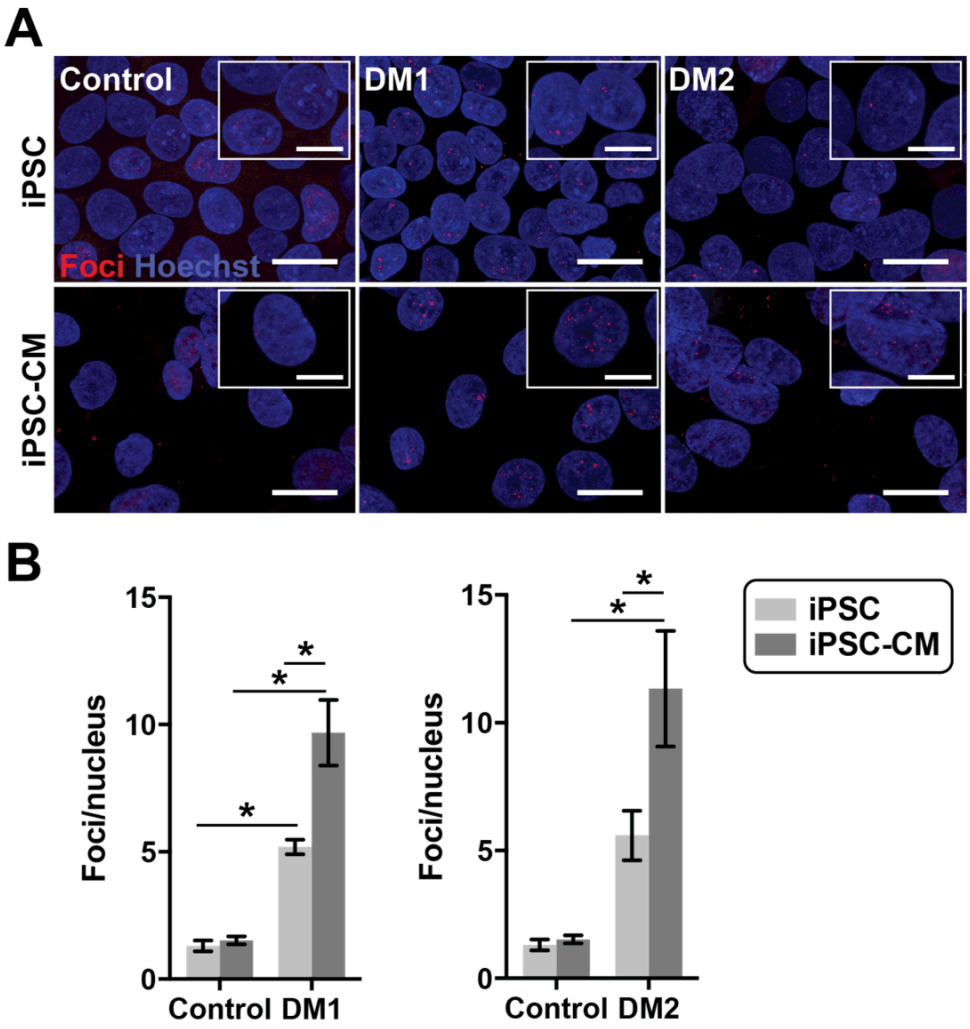

Figure 4.3 RNA FISH to detect the formation of RNA foci expressed from the repeat expansions before and after cardiomyocyte differentiation. RNA foci increase with differentiation in DM1 and DM2

RNA foci were detected with either $(CAG)_{10}$ (DM1) or $(CAGG)_5$ (DM2) probes labeled with Cy3 and quantified in undifferentiated iPSCs and those differentiated to cardiomyocytes (iPSC-CM). **(A)** RNA foci (red) were visualized using RNA FISH specific for the repeat subtype. Nuclei were labelled with Hoechst (blue). Magnified images are shown in the insets. Scale bar = 20 μm. Scale bar (inset) = 10 μm. **(B)** DM1 iPSCs and iPSC-CMs have an increased number of RNA foci compared to controls (p=0.04, p=0.0008, respectively; for control: n=148 for iPSC, n=53 for iPSC-CM; for DM1: n=305 for iPSC, n=93 for iPSC-CM). DM2 iPSC-CMs have an increased number of RNA foci compared to controls (p=0.03, n=144), while iPSC cells were trended toward significance when compared to control cells (p<0.07, n=501). For both DM1 and DM2, differentiation of iPSCs into iPSC-CMs resulted in an increase number of RNA repeat foci in iPSC-CMs (p=0.008, p=0.04, respectively; n=93 for DM1, n=144 for DM2). The number of RNA foci did not change with differentiation in control cells.

intranuclear foci of MBNL1 (Figure 4.4). In contrast, MBNL1-positive foci were not readily observed in either DM2 or control iPSC-CMs (Figure 4.4**)**. Moreover, the similar pattern of diffuse nucleoplasmic MBNL1 staining was evident in both control and DM2 iPSC-CMs, where MBNL1 was more diffusely distributed throughout the nucleus (Figure 4.4). Similar to what was observed in directly reprogrammed myotubes, DM1 cells displayed MBNL1 foci, a molecular signature of myotonic dystrophy, while DM2 cells appeared more similar to control.

Like skeletal muscle, myotonic hearts are characterized by aberrant splicing. In DM1 hearts, it has been shown that *SCN5A* transcripts favor inclusion of exon 6A, an embryonically expressed exon, over exon 6B (Freyermuth et al., 2016). In mice lacking MBNL1, a model of myotonic dystrophy, *RYR2* and *TNNT2* were each described with alternative splicing (Dixon et al., 2015). Examination of MBNL1 targets in iPSC-CMs revealed an increased inclusion of fetal exons in DM1 cells (Figure 4.5). For *SCN5A* the ratio of exon 6A to 6B increased 2.5 fold in DM1 iPSC-CMs compared to controls (Figure 4.5). Similarly, in control cells *ANK3* transcripts exhibited minimal exon 40 inclusion, whereas the ratio of transcripts including exon 40 to those excluding exon 40 (+E40/-E40) ratio was significantly increased in DM1 iPSC-CMs (Figure 4.5). *TNNT2* transcripts also showed a significant increase in transcripts with exon 5 compared to those without exon 5 (+E5/-E5 ratio) in DM1 compared to control cells (Figure 4.5). The ratio of full length transcript (+E3,4) to transcripts excluding exon 4 (+E3,4/-E4) in *RYR2* decreased 3 fold in DM1 iPSC-CMs ($p<0.05$). (Figure 4.5). In contrast, DM2 iPSC-CMs showed splicing patterns similar to those of control cells for *SCN5A* and *ANK3* (Figure 4.5). The splicing patterns for *RYR2* and *TNNT2* in DM2 were variable depending on the individual patient (Figure 4.5). The ratios of embryonic to adult splice isoforms were not statistically different between DM2

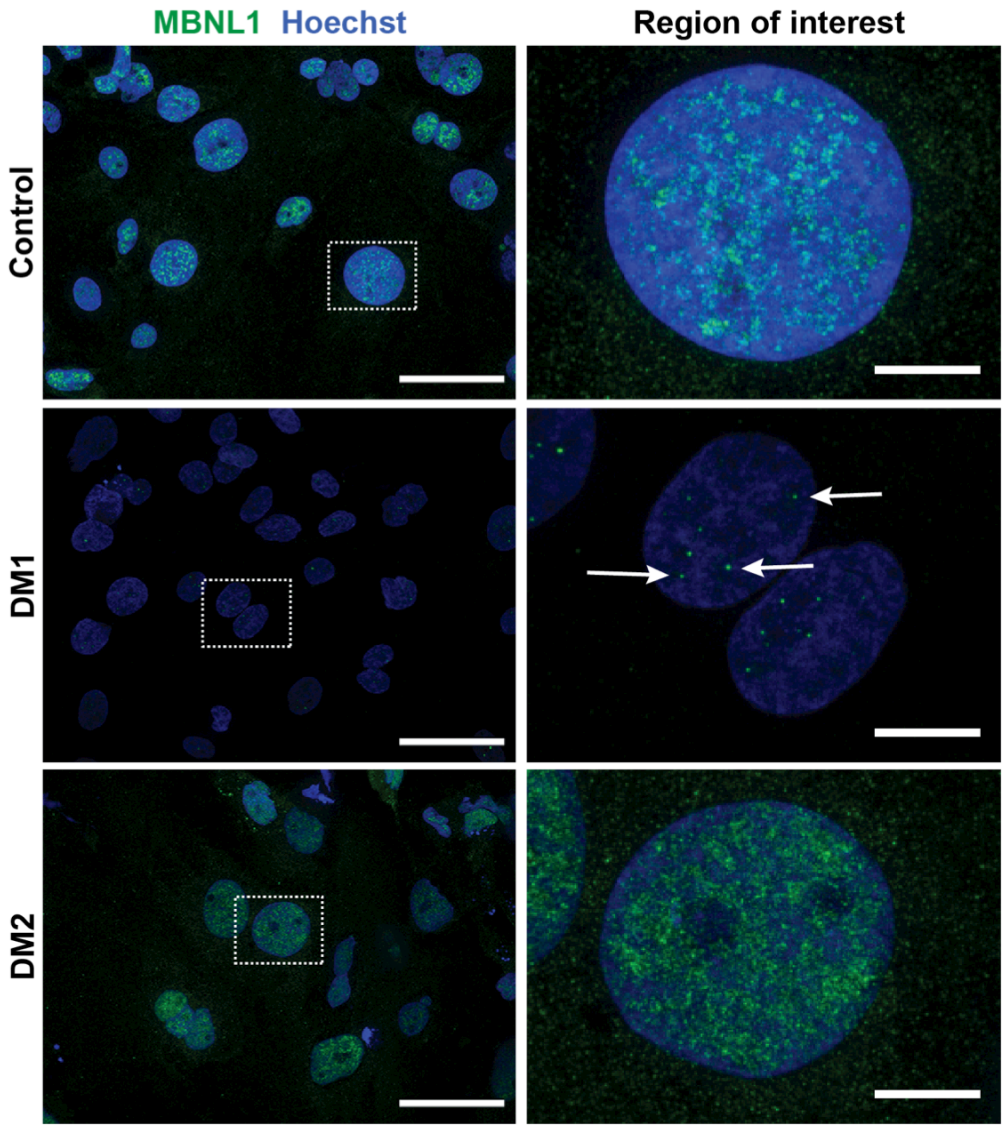

Figure 4.4 Intranuclear MBNL foci characterize DM1 iPSC-cardiomyocytes but not DM2

IPSC-CMs were immunostained with α-MBNL1 (green) and nuclei were labelled with Hoechst (blue). DM1 iPSC-CMs had readily detectable MBNL1-positive intranuclei foci (middle panel, white arrows) and reduced nucleoplasmic MBNL staining compared to control and DM2 iPSC-CMs. Higher magnification images of the white dotted box are shown on the right.
Scale bar (left panel) = 50 μm. Scale bar (right panel) = 10 μm.

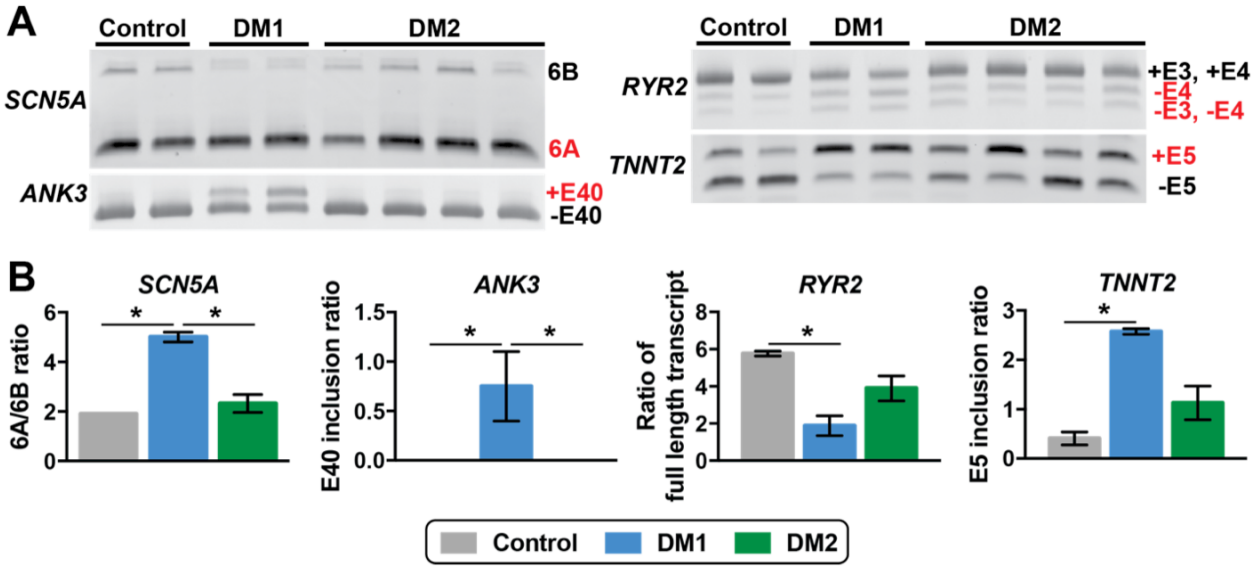

Figure 4.5 Distinct splicing profiles between DM1 and DM2 iPSC-cardiomyocytes

A & B) RT-PCR of *SCN5A*, and *ANK3* revealed an increase in embryonic transcripts from DM1 iPSC-CMs compared to control and DM2 iPSC-CMs. *RYR2*, and *TNNT2* transcripts in DM1 iPSC-CMs were significantly different from control iPSC-CMs. *p<0.05, one-way ANOVA. Each lane in **A** indicates a study subject.

and DM1 or control iPSC-CMs. These findings are consistent with the role of MBNL1 sequestration and specific aberrant splicing in DM1 but not in DM2.

DM iPSC-CMs exhibit changes in calcium handling

Clinical cardiac complications in both DM1 and DM2 include arrhythmias and even heart failure (Bhakta et al., 2010; Lau et al., 2015). In order to study functional cellular cardiac phenotypes of DM, Ca^{2+} handling in DM1 and DM2 iPSC-CMs was assessed. IPSC-CMs were loaded with Indo-1, a ratiometric dye that is sensitive to intracellular Ca^{2+} levels. Cells were paced at four different frequencies (0.25, 0.5, 0.75, and 1 Hz) and transients at each frequency were averaged and analyzed (Figure 4.6). Diastolic Ca^{2+} levels were decreased in DM2 iPSC-CMs at every frequency when compared to control and DM1 cells (Figure 4.6). However, the transient peak heights, which measures the difference between peak height and diastolic Ca^{2+}, were not different between DM and control cells (Figure 4.6). At each frequency, rates of Ca^{2+} release and reuptake were significantly different in DM2 iPSC-CMs compared to control cells (Figure 4.6). The time to the peak of the Ca^{2+} transient was significantly decreased in DM1 cardiomyocytes (Figure 4.6). Time to 50% Ca^{2+} release was increased (Figure 4.6) and the time from peak to 50% Ca^{2+} reuptake was decreased in DM2 iPSC-CMs (Figure 4.6). These differences in release and reuptake kinetics between DM1 and DM2 can be seen in the representative Ca^{2+} transients (Figure 4.6). These findings suggest that Ca^{2+} handling differs between DM1 and DM2 and from controls.

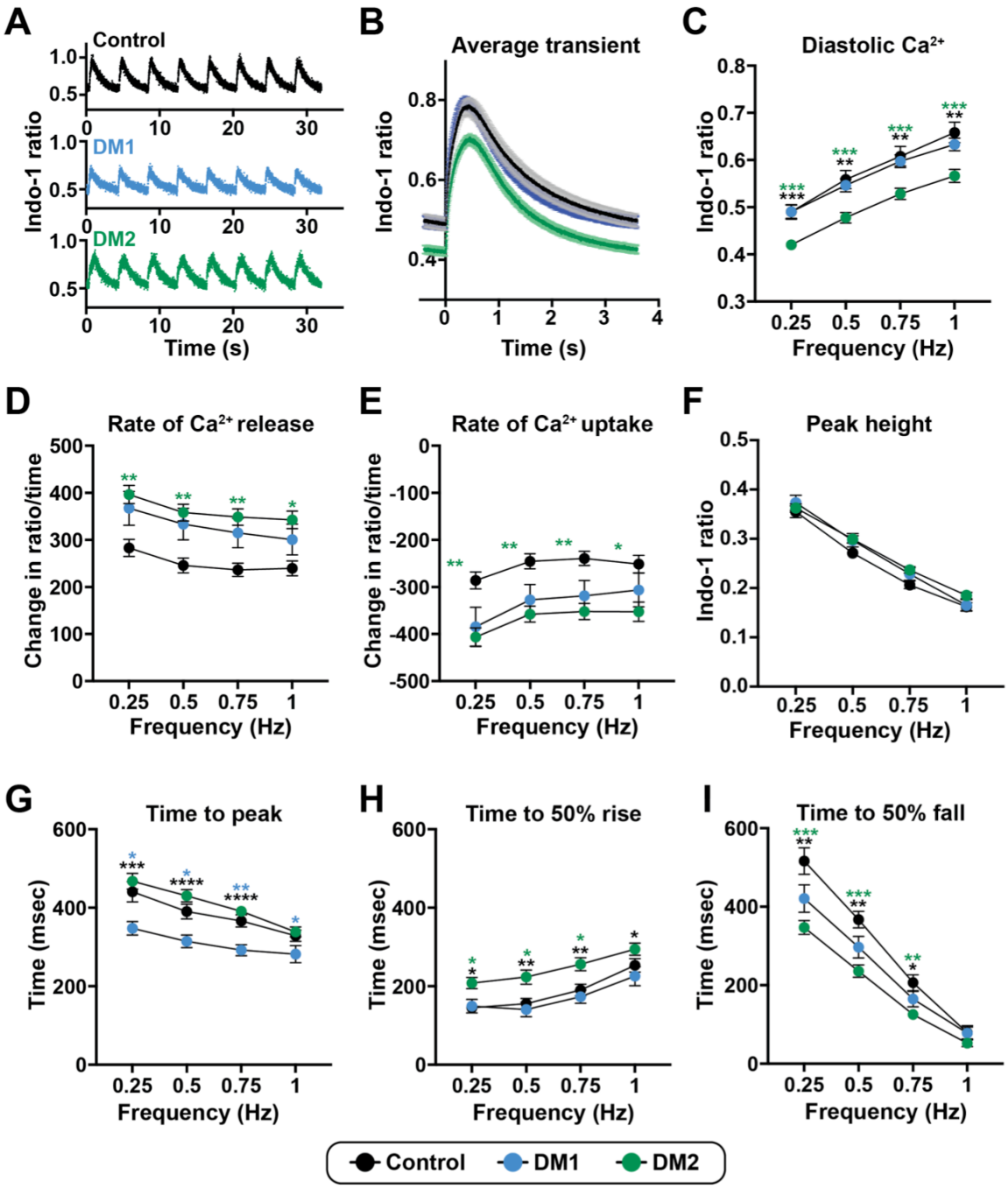

Figure 4.6 Distinct Ca2+ transients between DM1 and DM2 iPSC-CMs

(A) Representative Ca^{2+} transients at 0.25 Hz from control, DM1, and DM2 iPSC-CMs loaded with Indo-1. **(B)** Average Ca^{2+} transients at 0.25 Hz of control, DM1, and DM2 cell lines. **(C)** Diastolic Ca^{2+} is reduced in DM2 iPSC-CMs. **(D)** Peak Ca^{2+} transient amplitude, measured by the difference in peak and diastolic Ca^{2+}, were not different across groups. **(E)** The peak rate of Ca^{2+} release and the **(F)** peak rate of Ca^{2+} reuptake showed DM2 iPSC-CMs to have altered release and reuptake kinetics compared to control lines.

Figure 4.6 continued
Times to **(G)** peak Ca^{2+}, **(H)** 50% Ca^{2+} release, and **(I)** 50% Ca^{2+} reuptake showed different responses between the DM groups and control cell lines. For 0.25, 0.5, and 0.75 Hz: Control include *2* cell lines, 33 cell patches; DM1 include 2 cell lines, 40 cell patches; DM2 include 4 cell lines, 77 cell patches. For 1 Hz: Control include 2 cell lines, 28 cell patches; DM1 include 2 cell lines, 37 cell patches; DM2 include 4 cell lines, 68 cell patches. *p<0.05, **p<0.01, ***p<0.001, ****p<0.0001, one-way ANOVA tested at each frequency. Blue asterisks indicate statistical test between control and DM1, green asterisks indicate statistical test between control and DM2, and black asterisks indicate statistical test between DM1 and DM2.

Transcriptional profiling of DM iPSC-derived cardiomyocytes

To determine if differential expression of particular genes or pathways are driving the calcium handling differences between DM1 and DM2, RNA sequencing was performed on total mRNA isolated from control, DM1, and DM2 iPSC-derived cardiomyocytes (n=2 per genotype). After alignment, gene expression was compared pairwise, creating the following three groups: control versus DM1, control versus DM2, and DM1 versus DM2 to generate a candidate list of genes involved in cardiac function (p<0.15, absolute log fold change >1). GO analysis was performed on misregulated genes for each comparison, and terms relating to cardiac function or development were applied. GO terms from which gene lists were compiled are shown in Table 4.3. Of these candidate genes, there were 44 genes misregulated exclusively in DM1 compared to control, 35 genes misregulated in DM2 compared to control, and 49 genes misregulated in DM2 compared to DM1 (Figure 4.7). This candidate list was further reduced to 61 genes by selecting those implicated in either cardiac or muscle structure, channel formation, ion transport, transcription factors or developmental process genes for further interrogation (Figure 4.6, Table 4.4).

More genes (39 out of 61, 64%) were downregulated in all comparisons, while 23% were upregulated in all comparisons (14 out of 61) and 13% were downregulated in one comparison but upregulated in the other comparison (8 out of 61, 13%). *CASQ2* and *CAMK2N1* both bind Ca^{2+} and their misregulation may contribute to Ca^{2+} handling defects. Notably, multiple potassium channel genes were decreased in expression including *KCNA5, KCND1, KCNE1, KCNF1, KCNJ2, KCNJ3, KCNK1, KCNK3,* and *KCNMA1* (Table 4.4). Potassium channels mediate repolarization of the action potential, and downregulation of these channels could alter Ca^{2+} handling. *KCNN3* and *KCNQ3* were decreased in DM1 but increased in DM2, which may

Table 4.3 GO analysis terms included in candidate gene list generation

GO term	Number of genes	Fold Enrichment
Control vs DM1		
pulmonary valve morphogenesis (GO:0003184)	5	8.96
atrial septum morphogenesis (GO:0060413)	5	6.72
membrane repolarization during cardiac muscle cell action potential (GO:0086013)	5	6.72
cardiac muscle cell action potential (GO:0086001)	9	4.21
action potential (GO:0001508)	17	3.58
regulation of membrane potential (GO:0042391)	38	2.04
heart development (GO:0007507)	43	1.92
Control vs DM2		
cardiac right ventricle morphogenesis (GO:0003215)	6	6.89
positive regulation of blood circulation (GO:1903524)	11	3.48
action potential (GO:0001508)	16	3.42
cardiac chamber development (GO:0003205)	26	2.52
regulation of heart contraction (GO:0008016)	26	2.46
muscle contraction (GO:0006936)	26	2.32
regulation of membrane potential (GO:0042391)	37	2.02
DM1 vs DM2		
regulation of cardiac conduction (GO:1903779)	8	6.97
regulation of anion transport (GO:0044070)	7	5.01
response to calcium ion (GO:0051592)	9	4.47
Notch signaling pathway (GO:0007219)	8	4.22
regulation of ERK1 and ERK2 cascade (GO:0070372)	13	2.92
ion transport (GO:0006811)	41	1.87

help explain the shortened time of peak to 50% fall in DM2 as compared to DM1. *ATP2B2*, which encodes the plasma membrane Ca^{2+} ATPase that transfers Ca^{2+} against its concentration gradient from cells, was upregulated in DM2. This upregulation may lead to an increase of Ca^{2+} flow from cells, contributing to the lower diastolic Ca^{2+} implicated in DM2.

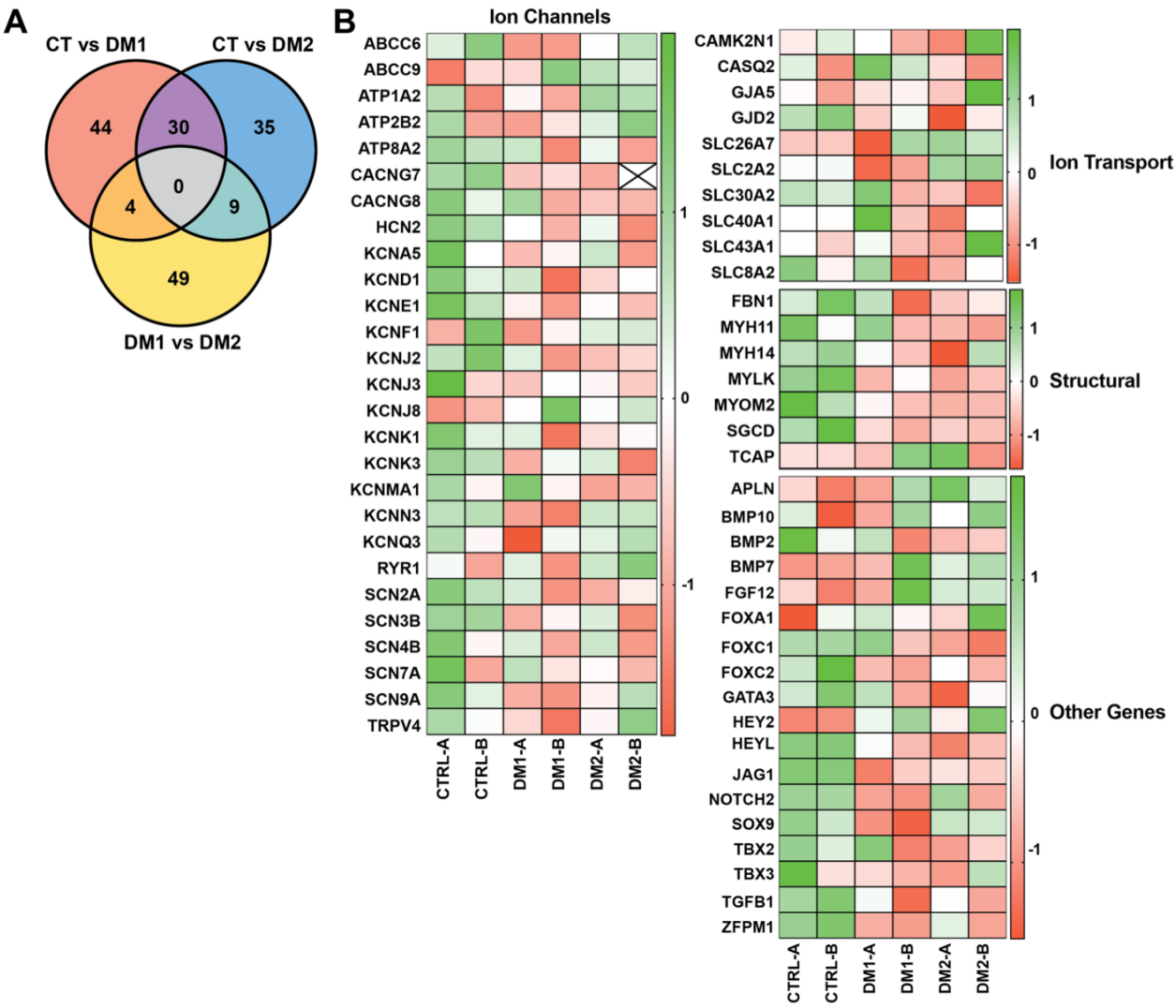

Figure 4.7 Transcriptional profiling of DM1 and DM2 iPSC-cardiomyocytes using RNA-seq

RNA sequencing was performed on total RNA from control, DM1, and DM2 iPSC-CMs (n=2 per genotype). **(A)** Gene expression was compared pairwise in the following three groups: control vs DM1, control vs DM2, and DM1 vs DM2. Genes with *p*-value < 0.15 and absolute log fold change > 1 were included in GO analysis, and genes that fall under categories related to cardiac function, cardiac development, and ion transport were included in the candidate list. From this list, 44 genes were uniquely misregulated in DM1 compared to control, 35 genes were uniquely misregulated in DM2 compared to control, and 49 genes were misregulated in DM2 when compared to DM1. **(B)** Of all the genes in **A**, 61 genes involved in cardiac or muscle structure, channel formation, ion transport, or other processes, such as transcription factors or developmental genes, were selected for further interrogation. Z scores for each patient was calculated and heatmaps of the genes that fall under each category were generated. Green indicates z score greater than 1, while red indicates z score less than 1. Sample that did not have expression of a particular gene was marked with an X.

Table 4.4 Candidate genes in DM

Gene	Fold change		
	CTvDM1	CTvDM2	DM1vDM2
Structural			
FBN1	0.40	0.32	
MYH11		0.14	0.24
MYH14	0.18	0.35	
MYLK	0.17	0.11	
MYOM2	0.37	0.31	
SGCD	0.08	0.09	
TCAP		2.30	
Channels			
ABCC6	0.32		2.39
ABCC9	2.50	2.38	
ATP1A2			2.23
ATP2B2			3.65
ATP8A2	0.43	0.37	
CACNG7	0.25	0.09	
CACNG8		0.45	
HCN2	0.43	0.46	
KCNA5	0.25	0.39	
KCND1	0.48	0.47	
KCNE1	0.15	0.19	
KCNF1	0.27		2.45
KCNJ2	0.42	0.35	
KCNJ3	0.18	0.16	
KCNJ8	2.60		
KCNK1	0.37	0.41	
KCNK3	0.27	0.33	
KCNMA1		0.35	0.28
KCNN3	0.38		2.47
KCNQ3	0.44		2.56
RYR1		2.11	2.11
SCN2A	0.30	0.20	
SCN3B	0.30	0.40	
SCN4B	0.40		
SCN7A		0.33	
SCN9A	0.34		2.13
TRPV4	0.35		3.20

Table 4.4 continued

Gene	Fold change		
	CTvDM1	CTvDM2	DM1vDM2
Ion transport			
CAMK2N1			3.37
CASQ2			0.41
GJA5		2.54	2.29
GJD2	0.44	0.29	
SLC26A7		2.50	
SLC2A2	0.28	2.81	10.13
SLC30A2		0.32	0.29
SLC40A1			0.46
SLC43A1		2.12	2.13
SLC8A2		0.41	
Others			
APLN		7.63	
BMP2	0.41	0.28	
BMP7	2.01		
BMP10		2.21	
FGF12	4.39	2.83	
FOXA1			4.38
FOXC1		0.24	0.32
FOXC2	0.08	0.16	
GATA3	0.39	0.18	
HEY2	3.01	3.20	
HEYL	0.31	0.19	
JAG1	0.35	0.44	
NOTCH2	0.49		
SOX9	0.27		3.06
TBX2		0.36	0.45
TBX3	0.47		
TGFB1	0.49		
ZFPM1	0.36		

DISCUSSION

IPSC-derived cardiomyocytes are immature in nature as they do not express the full complement of adult isoforms nor do they develop normal transverse tubule and sarcoplasmic reticulum, key components of Ca^{2+} handling (Gherghiceanu et al., 2011; Kane, Couch, & Terracciano, 2015; Robertson et al., 2013). Despite these limitations, iPSC-CMs differentiated sufficiently to identify some developmental splicing differences between DM1 and control cells. DM2 cells matured sufficiently to be comparable to control cells and did not display missplicing observed in DM1 cells. Moreover, the presence of clear MBNL1 clusters in DM1 iPSC-CMs but not in DM2 may suggest that cluster formation is an early event in DM1. In addition, as DM1 has earlier onset for disease progression, MBNL1 cluster formation may be reflective of this aspect of the disease. These findings also suggest that DM2 may have additional pathogenic mechanisms that contribute to cardiac dysfunctions. Previously, repeat-associated non-ATG (RAN) translation in DM1 has been described as an additional pathogenic stimulus (Zu et al., 2011). RAN translation occurs in the absence of an ATG-methionine start codon and expresses a polyglutamine protein detectable in the heart of DM1 mouse model as well as myoblasts (Zu et al., 2011). More recently, repeat expansion in DM2 was also shown to create two sequences of RAN translation proteins, each arising from bidirectional transcription of the repeat region, that deposit in brain sections of DM2 patients (Zu et al., 2017). Furthermore, a novel CAGG binding protein, hnRNP A1, has been identified and may contribute to DM pathogenesis (Zu et al., 2017).

Cardiac complications are common in both DM1 and DM2 (Lau et al., 2015; Petri et al., 2012; Sansone et al., 2013). Using iPSC-CMs, we identified abnormal calcium handling in both DM1 and DM2 with each having altered kinetics compared to control cells. In DM2 iPSC-CMs,

calcium mishandling was observed in the absence of MBNL1 sequestration or missplicing of its target genes. These findings suggest that DM2 may have additional mechanisms that underlie alterations to calcium handling. Further, they also suggest that changes to calcium handling may already be occurring earlier on in disease progression. Cardiac molecular mechanisms in DM have been attributed to missplicing of *TNNT2*, which encodes a structural protein, and *SCN5A*, a sodium channel important in the initial upstroke of cardiac action potential (Freyermuth et al., 2016; Philips et al., 1998). Downregulation of miR-1 has been described in human DM, which leads to upregulation of miR-1 targets, *GJA1* and *CACNA1C*, and provides one potential mechanism of calcium mishandling (Rau et al., 2011). *CACNA1C* encodes the major cardiac calcium channel subunit and *GJA1* encodes a critical conductance channel protein. Therefore, upregulation of these proteins could account for abnormal calcium handling in DM cardiomyocytes. Alternatively, RNAseq analysis also supported dysregulation of a large number of potassium channel genes, which were notably downregulated. Given the cellular toxicity from repeat expansions, it is likely that multiple mechanisms contribute to this dysfunction and arrhythmia risk.

CHAPTER 5

DISCUSSION

UTILITY OF CELL-BASED SYSTEMS IN MUSCLE DISEASE MODELING

The muscular dystrophies are a heterogeneous group of disorders that arise from mutations in multiple genes. With advancements and increased availabilities in sequencing technologies, the number of variants being linked to human myopathies is expanding. While animal models have provided valuable platforms upon which to study disease mechanisms, they cannot capture the diverse array of variants that lead to myopathies. In this work, we presented two cell-based models that are both non-invasive and patient-specific. These models can serve as complementary tools to animal models and be used for mechanistic studies as well as therapeutic testing.

Skeletal muscle model in investigation of exon skipping strategies of DMD and LGMD2C

Exon skipping uses antisense oligonucleotides (AONs), which are short DNA or RNA nucleotide sequences complementary to the target pre-mRNA sequence (Nakamura, 2017). Hybridization of AONs with the target sequence modulate alternative splicing of the pre-mRNA either by exon exclusion or inclusion (Kole, Krainer, & Altman, 2012). This modulation of alternative splicing restores the reading frame and leads to production of a transcript that can be translated into a shorter but functional protein (Nakamura, 2017). In Duchenne muscular dystrophy (DMD), exon skipping strategy was effective at restoring dystrophin expression at the sarcolemma with improvements in muscle function (Lu et al., 2003). In 2016, eterplirsen, an exon skipping drug targeting exon 51 of the dystrophin transcript, became the first drug of its kind for DMD to be

approved by the Food and Drug Administration (Lim, Maruyama, & Yokota, 2017). This was followed by approval of nusinersen, which is an AON therapy for spinal muscular atrophy that increases exon 7 inclusion in *SMN2* gene (Singh, Howell, Androphy, & Singh, 2017). Eterplirsen targets exon 51, providing therapy for those with mutation in exons 45-50 and 52-63, which represents about 13-14% of all DMD patients (Bladen et al., 2015; Lim et al., 2017; van Deutekom & van Ommen, 2003). Efforts are ongoing to expand this approach to additional exons and a larger fraction of the DMD population. MyoD-converted myotubes are well positioned to serve as a model to test AON strategies against other exon deletions in DMD. Falzarano *et al* generated MyoD-converted myotubes from urine cells of a DMD patient with an exon 45 deletion. These myotubes showed no dystrophin expression, recapitulating DMD phenotype (Falzarano et al., 2016). Treatment of AON against exon 44 restored dystrophin expression in these DMD myotubes (Falzarano et al., 2016).

The inducible MyoD skeletal model described here has recently been applied to assess the suitability of AON-mediated exon skipping for limb girdle muscular dystrophy 2C (LGMD2C) (Wyatt et al., 2018). LGMD2C is an autosomal recessive caused by a deletion in *SGCG* gene, which encodes γ-sarcoglycan, a dystrophin associated protein (McNally, Duggan, et al., 1996; McNally, Passos-Bueno, et al., 1996; Noguchi et al., 1995). The AON-mediated exon skipping strategy for LGMD2C requires skipping four exons to restore the reading frame of *SGCG* to produce a protein referred to as Mini-Gamma. Expression of a Mini-Gamma as a transgene was shown to improve muscle function in a *Drosophila* model and mouse model of LGMD2C (Gao et al., 2015). In the 2015 study, 2'-*O*-methyl phosphorothioate (2OMePS) AONs were shown to induce exon skipping but did so inefficiently. Recently, MyoD-converted myotubes derived from LGMD2C patients as well as dermal fibroblasts similarly converted by

MyoD were used to test AON-mediated exon skipping from multiple LGMD2C patients. These studies included an LGMD2C patient with a deletion of exon 6 on one allele and a large deletion on the other allele that includes *SGCG*. LGMD2C iMyoD-converted myotubes were then treated with AONs against exons 4, 5, and 7 (Wyatt et al., 2018). AON treatment produced skipped Mini-Gamma transcript, as well as protein localized to the sarcolemma (Wyatt et al., 2018). Notably, these studies tested two different chemistries: 2'-*O*-methyl phosphorothioate (2OMePS) and vivo-phosphorodiamidate morpholino oligomers (vivo-PMOs) (Wyatt et al., 2018). These chemistries aid in effective delivery of the AONs to the target cells by preventing their degradation by nucleases and helping AONs penetrate the cell membranes (Shen & Corey, 2018), In 2OMePS oligomers, nucleotides are linked through phophorothioate bonds and the 2'-hydroxyl group is methylated (Shen & Corey, 2018). Phosphorothioate linkages increase stability of AONs against nucleases and also increases binding to the serum proteins, which allows for AONs to stay in circulation for a longer period of time (Shen & Corey, 2018). Whereas 2OMePS chemistry yields negatively charged backbone, PMO chemistry leads to a neutrally charged backbone through phosphorodiamidate linkages (Saleh, Arzumanov, & Gait, 2012). Vivo-PMOs carry eight guanidinium head groups at the 3' end, which promote an increase in cell permeability to the AONs and thus lead to better penetration of the drug (Morcos, Li, & Jiang, 2008). In LGMD2C patient-derived myotubes, vivo-PMOs exhibited improved efficiency of exon skipping when compared to 2OMePS, displayed by a robust expression Mini-Gamma transcripts (Wyatt et al., 2018).

Loss of SGCG is associated with increased membrane fragility, which leads to an increased in creatine kinase (CK) release from the muscle (Hack et al., 1998). In order to assess functional improvement in AON-mediated exon skipping, the treated myotubes were subjected

to a creatine kinase (CK) release assay. PMO-treated myotubes exhibited decreased CK release when exposed to hypo-osmotic shock, indicating functional improvement in membrane stability (Wyatt et al., 2018). The same study also includes iMyoD-converted myotubes of fibroblasts isolated from two other LGMD2C patients, one with a deletion of a single thymine at nucleotide position 521 (521ΔT) and the other with a deletion of exons 5 and 6 (ex5/6del). Treatments with AONs against exons 4-7 in 521ΔT and exons 4 and 7 in ex5/6del restored SGCG expression at the sarcolemma (Wyatt et al., 2018). These results highlight that cell-based skeletal muscle models can be used to test potential therapies in a patient-specific manner, as well as demonstrating their utility in functional evaluation of the treatments.

IPSC-CMs in investigating cardiac phenotypes of human myopathies

While muscular dystrophies are primarily diseases of skeletal muscles, many forms of muscular dystrophies, including DMD, DM, Emery-Dreifuss MD, and the LGMDs due to sarcoglycan gene mutations, also include cardiomyopathies and cardiac arrhythmias (Mercuri & Muntoni, 2013). IPSC-CMs are useful in elucidating pathogenic mechanisms underlying cardiac diseases and in developing new treatments. Most applications of iPSC-CMs have focused on studying arrhythmias (Itzhaki et al., 2011; Yazawa et al., 2011) or cardiomyopathies (Lan et al., 2013; Sun et al., 2012). In muscular dystrophy, DMD mutations have been modeled extensively in iPSC-CMs (Dick et al., 2013; Guan et al., 2014; Kalra, Montanaro, & Denning, 2016). One group used urine cells isolated from a DMD patient with a deletion in exon 50 to reprogram and differentiate to cardiomyocytes (Guan et al., 2014). Patient iPSC-CMs recapitulated the lack of dystrophin expression, and functional studies with iPSC-CMs demonstrated DMD cells to have altered calcium handling and increased response to hypotonic stress (Guan et al., 2014). Dick *et al*

generated iPSC-CMs using fibroblasts from two DMD patients, one deleted for exons 48-50 and the other deleted for exons 47-50. Using these models, exon skipping with AONs against exon 51 was tested (Dick et al., 2013). Following exon skipping treatments, iPSC-CMs displayed rescue of dystrophin to 30% of control iPSC-CMs (Dick et al., 2013). DMD is associated with dilated cardiomyopathy that can lead to congestive heart failure and increased morbidity and mortality (B. Lin et al., 2015; McNally, 2007). To better understand the mechanism behind cardiac features of DMD patients, Lin *et al* studied molecular phenotypes using DMD iPSC-CMs (B. Lin et al., 2015). DMD iPSC-CMs exhibited an increase in cell death through apoptosis as well as altered calcium handling such as a decreased L-type calcium current and an increased resting cytosolic calcium (B. Lin et al., 2015). Further, treatment of iPSC-CMs with a membrane sealant, poloxamer P188, decreased cytosolic calcium and repressed caspase 3 activity, suggesting that increased cytosolic calcium in DMD iPSC-CMs may be partly driving increased cell death (B. Lin et al., 2015).

Recently, a variant in *MYBPHL* (myosin-binding protein H-like) was identified through whole genome sequencing to be linked to inherited dilated cardiomyopathy (Barefield et al., 2017). *MYBPHL* encodes MyBP-HL protein, a protein with previously unknown role in cardiac physiology that is related to other myosin-binding proteins such as myosin-binding protein C (MyBP-C) (Barefield et al., 2017). A premature stop codon was identified, and iPSC-CMs were generated from the affected patient and an unaffected control. Sequencing of cDNA generated from iPSC-CMs identified expression of only the normal allele, suggesting that the truncated transcript may be degraded through nonsense-mediated decay (Barefield et al., 2017). This disease model can be used to investigate the role of *MYBPHL* truncation mutation in cardiomyocyte structure or function. Together, these findings demonstrate the utility of iPSC-

CMs in disease modeling of muscular dystrophies as well as their potential in drug testing using these functional characteristics as phenotypic readouts.

Limitations of iPSC-CMs

A significant drawback of iPSC-CMs is that they resemble immature, fetal cardiomyocytes in both morphology and physiology, and are not adult cardiomyocytes (Veerman et al., 2015). IPSC-CMs express cardiac-specific genes, such as cardiac troponin, myosin light chain 2a, and α-actinin, and display sarcomeric striations (Lian et al., 2012). However, the cellular morphology of adult cardiomyocytes is strikingly difference from iPSC-CMs with adult CMs having rectangular shape with sarcomeres longitudinally positioned in series. In contrast, iPSC-CMs have round or triangular shapes with sarcomeres running throughout the cell body.

Critically, iPSC-CMs also lack T-tubules, which serve an important function in calcium-induced calcium release during the initiation of an action potential (Gherghiceanu et al., 2011; Veerman et al., 2015). In order to more faithfully recreate adult cardiomyocytes, different methods have been reported to mature iPSC-CMs, include increasing time in culture, electrical stimulation, using extracellular matrix, additional chemical induction, co-culture with other cell types, as well as culture methods in 3D conformation (Veerman et al., 2015). Recently, treatment of iPSC-CMs with a combination of triiodothyronine (T3) and dexamethasone followed by a culture on a bed of Matrigel has been shown to increase the development of T-tubule-like network, which led to improved calcium handling (Parikh et al., 2017). One example of 3D culture methods, where iPSC-CMs were seeded in a hydrogel scaffold held by two silicone posts, improved sarcomeric alignments and displayed action potential parameters similar to human left

ventricular tissue (Lemoine et al., 2017). Continued development of methods to further mature iPSC-CMs would make them a more physiologically relevant model.

POTENTIAL DISTINCTION IN PATHOGENIC MECHANISMS BETWEEN DM1 AND DM2

DM1 and DM2 are thought to share similar pathogenic mechanisms where the transcription of nucleotide repeat expansion either sequester MBNL1 and/or upregulate CUGBP1, leading to a shift in splicing profile from adult to fetal isoforms (Meola & Cardani, 2017). While there are some shared clinical features between DM1 and DM2, such as involvement of the skeletal and cardiac muscles and development of cataracts, there are distinct features between each subtype that may suggest different disease mechanism in DM2 (Meola & Cardani, 2017). One of the prominent differences between the DM1 and DM2 subtypes is the frequent involvement of the central nervous system in DM1, which is uncommon in DM2 (Meola & Cardani, 2015). Another noticeable difference is that the presenting clinical feature in DM1 is commonly myotonia and muscle weakness, while in DM2, myalgia without overt myotonia is more frequently seen (Thornton, 2014). There are a few proposed mechanisms that may account for the difference between DM1 and DM2.

A key first distinction between the two DM subtypes is the normal role and expression of the genes at the disease loci. The exact functions of DMPK and CNBP are not well established, however, insights can be gained from mouse models of DM with either *Dmpk* or *Znf9* (*Cnbp*) deletions. Two mouse models of *Dmpk* deletion ($Dmpk^{-/-}$) have been reported. One model was overtly normal other than very mild myopathic changes seen on histology at 25 weeks of age (Jansen et al., 1996). The other model developed progressive myopathy on histology and electron

microscopy, as well as a decrease in muscle force generation over time (Reddy et al., 1996). Both *Dmpk*$^{-/-}$ models disrupted *Dmpk* expression through replacement of the first 7 exons with antibiotic selection cassettes and were generated on the same background (C57BL/6J) (Jansen et al., 1996; Reddy et al., 1996). However, Jansen *et al* included a nearby gene, *Dmrn9*, in the *Dmpk* deletion allele, whereas Reddy *et al* did not. *Dmrn9* transcript was affected by the insertion of antibiotic selection cassette where the mRNA was shifted to be a larger size without a change to overall *Dmpk* mRNA level (Jansen et al., 1996). Nonetheless, it is possible that alterations in *Dmrn9* transcript processing may have affected phenotypic features of the mouse model. Unlike *Dmpk*, homozygous deletion of *Znf9* (*Znf9*$^{-/-}$) resulted in severe forebrain truncation and embryonic lethality around E10.5 (W. Chen et al., 2007). Heterozygous deletion of *Znf9* (*Znf9*$^{+/-}$) recapitulated some of the features observed in DM2 patients, including cataracts, cardiac arrhythmia, and muscle wasting (W. Chen et al., 2007). Additionally, *Znf9*$^{+/-}$ showed a decrease, but not missplicing, of *Clcn1* transcripts and displayed myotonia, which is not as frequently observed in DM2 (W. Chen et al., 2007). In light of the fact that DM2 patients generally present later in life with milder course of disease when compared to DM1 patients, it is interesting that a haploinsufficiency of *Znf9* leads to a robust disease phenotype that almost resembles DM1. As studies report both a decrease (Huichalaf et al., 2009; Pelletier et al., 2009) and no change (Margolis et al., 2006; Massa et al., 2010) in ZNF9/CNBP levels, the robust disease phenotype from *Znf9*$^{-/-}$ mice could suggest that a decrease in ZNF9/CNBP expression is not the main pathogenic mechanism in human DM2. Interestingly, while DM1 patients exhibit a decreased DMPK expression in the muscle (Fu et al., 1993; Salvatori et al., 2005), homozygous deletion of *Dmpk* leads to progressive muscle weakness and myopathy, but no other phenotypes like DM1. These findings suggest that other mechanisms in addition to a decrease in DMPK

level contribute to DM1 pathogenesis. In both cases, the primary gene only partly explains the phenotypes.

A second potential difference between DM1 and DM2 may relate to RAN-translation. In DM1, nucleotide repeat expansions, when transcribed, can be translated into protein without the ATG start codon (Zu et al., 2011). This process, termed repeat-associated non-ATG (RAN) translation, has been shown to produce polyglutamine protein that deposits in the heart and myoblasts of DM1 mouse model (DMSXL and DM55) (Zu et al., 2011). Recently, the nucleotide repeat expansions in DM2 have been shown to be bidirectionally transcribed and produce two tetrapeptide RAN translation products, Leu-Pro-Ala-Cys (LPAC) and Gln-Ala-Gly-Arg (QAGR) (Zu et al., 2017). Immunostaining for these proteins in brain sections taken from DM2 patients revealed distinct patterns of regional distribution. The first peptide, LPAC, was observed mainly in gray matter, while the second peptide, QAGR, was detected mainly in white matter (Zu et al., 2017). This differential distribution of sense and antisense encoded peptide products may point to different roles of each in pathology. It will be important to test whether sense/antisense products are only seen in the brain or if they are also detected in skeletal and cardiac muscles of DM2 patients.

An third potential difference between DM1 and DM2 may arise from modifiers that differentially affect one but not the other form. For example, studies showed that *CLCN1* mutations co-segregate in DM2 and may serve as a disease modifier (Cardani et al., 2012; Peddareddygari, Grewal, & Grewal, 2016; Suominen et al., 2008). In a study that examined three *CLCN1* variants (R894X, F413C, A531V), Suominen *et al* found that 5% of DM2 cohort (200 patients; 100 from Finland, 100 from Germany) carried one of the three *CLCN1* variants, which was higher than frequencies found in DM1 and control cohorts (1% and 1.6%, respectively). Of

the 10 patients that carried specific *CLCN1* variants, seven patients exhibited clinical myotonia as well as myotonic discharges on EMG. This study suggests that these *CLCN1* variants may be potential modifiers in DM2 specifically with respect to myotonia, which is variably seen in DM2. Another study reported a DM2 patient with an early onset myotonia who also harbored a rare missense variant in *SCN4A* (Bugiardini et al., 2015). No *CLCN1* variants were detected in this individual, suggesting that *SCN4A* may be the modifying variant in this context (Bugiardini et al., 2015). While studies in larger cohorts are needed in order to classify these variants as disease modifiers, the presence of these modifiers may be meaningful in DM2, but perhaps less so in DM1 since the myotonia is already more profound in DM1.

DEVELOPMENT OF THERAPEUTICS IN DM

Currently, there is no cure for DM and treatments involve symptomatic managements for myotonia and cardiorespiratory complications (Meola & Cardani, 2015). Therapy development for DM broadly has centered around the two main mechanisms elucidated for DM1. The first mechanism targets the tandem repeat expansion itself (Thornton, Wang, & Carrell, 2017). The second mechanism aims to correct the relative depletion of splicing regulators either directly, in the case of MBNL (Mankodi et al., 2001), or indirectly through modulation of downstream signaling pathways, in the case of CUGBP1 (Kuyumcu-Martinez et al., 2007). Accordingly, the therapeutic approaches currently reported can be categorized into those that reduce the repeat expansions either on DNA or RNA levels, and those that reduce the interaction of repeat transcripts with splicing regulators (Figure 5.1).

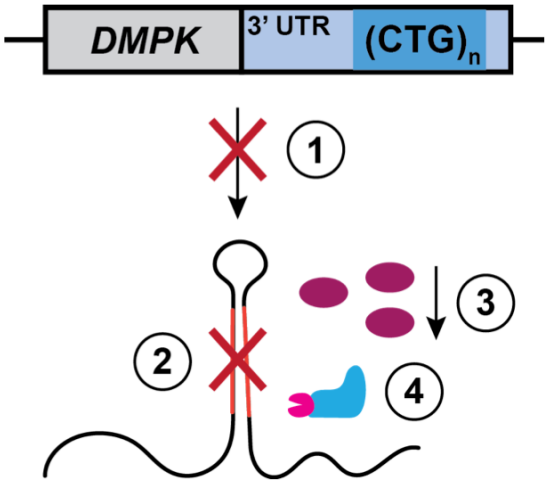

Figure 5.1 Therapeutic strategies in DM1

In order to reduce toxic effects of RNA repeat transcripts, different strategies have been tested in DM1. First method is to reduce *DMPK* transcription level (**1**) and the second method is to disperse the repeat transcripts (**2**). As downstream missplicing events are associated with MBNL sequestration, another strategy is to reduce the interaction between MBNL and repeat transcripts (**3**). A new therapeutic approach using Cas9 targeted against the repeat transcripts has recently been developed (**4**).

Small molecules and AONs have been reported to decrease the expression of RNA repeat transcripts. Identified through a screen for a compound that disrupts the interaction between MBNL1 and $(CUG)_4$ (Warf, Nakamori, Matthys, Thornton, & Berglund, 2009), pentamidine, an FDA-approved drug for the treatment of *Pneumocystis carinii,* was found to improve phenotypes in HSA^{LR} mice by restoring *Clcn1* and *Atp2a1* missplicing events as well as reducing myotonic discharges on electromyography (Coonrod et al., 2013). Siboni *et al* reported the ability of another small molecule, actinomycin D, in binding repeat regions of the DNA and reducing transcription, detected by reduced RNA foci formation in HeLa cells overexpression CUG repeats (Siboni et al., 2015). Intraperitoneal injection of HSA^{LR} mice with actinomycin D partially rescued *Clcn1* and *Atp2a1* missplicing events (Siboni et al., 2015).

As compared to pentamidine and actinomycin D that reduce transcription and thus the production of repeat transcripts (Coonrod et al., 2013; Siboni et al., 2015), AONs are directed against the repeat transcripts directly, with the goal of reducing the double stranded RNA. Injection of $(CAG)_7$ AON into leg muscles of HSA^{LR} mice reduced ribnonuclear foci and partially restored splicing of *Atp2a1*, *Mbnl1*, *Ttn, Clcn1,* and *Tnnt3* (Mulders et al., 2009). Similarly, another group showed treatment with $(CAG)_7$ AONs on myoblasts expressing CTG repeats suppressed *DMPK* transcript level (Gonzalez-Barriga et al., 2013). In 2014, an AON with 2'-*O*-methoxyethyl chemistry was developed and was shown to be effective in restoring normal splicing of *Clcn1* and *Atp2a1,* as well as in reducing repeat expansion transcripts in HSA^{LR} mice (Wheeler et al., 2012). These effects were still detectable one year after the withdrawal of AON injection (Wheeler et al., 2012). A related study used AONs employing different chemical modification (2'-4' constrained ethyl) to improve *in vivo* potency (Seth et al., 2009), and found improved muscle strength and maturation in DMSXL mice (Jauvin et al., 2017). These studies

led a related AON (ISIS 598769/IONIS-DMPKRx) to become the first of its kind to proceed to phase I/IIa clinical for DM1 treatment, which concluded in 2016 (clinicaltrials.gov, NCT02312011). Unfortunately, results from the phase IIa trial did not show sufficient clinical benefit and the clinical trial was stopped.

The small molecules and AONs described above primarily affect the expression of repeats either transcriptionally or post-transcriptionally. Other small molecules exert their effects by interfering with the interaction between the repeat transcripts and splicing regulators such as MBNL1 and CUGBP1. A high-throughput screening for MBNL1-CUG inhibition found a natural antimicrobial lomofungin and its dimer, dilomofungin, to be a potent inhibitor (Hoskins et al., 2014). Treatment with lomofungin partially reduced MBNL1 sequestration and restored some of *Atp2a1* splicing in C2C12 cells expression 800 CTG repeats (Hoskins et al., 2014).

Recently, a method to track RNA in live cells was developed using nuclease-inactive Cas9 (dCas9) tagged with GFP (Nelles et al., 2016). This dCas9 recognizes target RNA sequence under the direction of single guide RNA (sgRNA) against the target sequence and protospacer adjacent motif (PAM)-presenting oligonucleotides (Nelles et al., 2016). Batra *et al* built on this method to develop two lentiviral constructs, one encoding GFP-dCas9 and sgRNA and the other encoding dCas9 fused with PIN endonuclease (PIN-dCas9) and sgRNA (Batra et al., 2017). GFP-dCas9 allowed for visualization of target RNA, which was 105 CTG repeats transfected into COS-M6 cells (Batra et al., 2017). Then, PIN-dCas9 was directed against the RNA repeat expansions in DM1 and DM2 (CUG and CCUG, respectively), where PIN endonuclease was able to degrade RNA expansions and reduce ribonuclear foci in DM1 myoblasts and DM2 fibroblasts (Batra et al., 2017). After correction, DM1 myoblasts correspondingly showed restoration of normal splicing of *ATP2A1, INSR, MBNL2,* and *MBNL1* (Batra et al., 2017).

Alternative splicing analysis revealed that 93% of missplicing in myotubes and 75% in myoblasts have been reversed to normal (Batra et al., 2017). These results speak to the central role RNA repeat transcripts play in missplicing, and hold great promise in development of treatment for DM1 patients that could fundamentally correct the offending transcripts.

The cell-based systems presented in this work can serve as drug screening or testing platforms. Previous reports on DM treatments have identified close to 30 natural compounds and currently marketed drugs that partially rescue DM phenotype (Konieczny et al., 2017). As urine cells are collected in a non-invasive way and are easy to isolate and culture, they can be obtained from a large cohort of DM patients to increase power in these studies. Also, the majority, if not all, of these studies have been conducted for DM1. Skeletal muscle models created from DM2 patients can serve as additional tools to test these compounds and their efficacy, or more likely, to screen for compounds that can be used for DM2. While the heart is similarly affected in DM as skeletal muscle, the scarcity of cardiac models has prevented development and testing of therapeutics in the heart. IPSC-CMs from DM patients presented in this work display observable readouts such as missplicing in DM1, or ribonuclear foci and altered Ca^{2+} in DM1 and DM2. Further, GFP-dCas9 targeted to repeat regions in DM1 and DM2 could serve as a visual phenotype to track tandem repeat dynamics during drug screenings and identify compounds that disperse GFP signal. By monitoring these phenotypes, compounds that have been shown to be effective in skeletal muscles could be tested in iPSC-CMs to alleviate cardiac symptoms in DM patients.

FUTURE DIRECTIONS

In this work, I showed that cell-based models can recapitulate disease phenotypes and serve as disease modeling tools in muscular dystrophies. Further, these models generated from DM patients highlight difference between the two subtypes. A future direction would be to evaluate effects of potassium channel downregulation on the action potential of DM iPSC-CMs. Preliminary analysis of RNA-seq performed on iPSC-CMs found downregulation of potassium channels, such as *KCNN3* in DM1, and *KCNE1* and *KCNJ2* in both subtypes of DM. These potassium channels are involved in repolarizing the cell membrane after an action potential has occurred, and downregulation of these channels may contribute to arrhythmogenesis in DM.

Recently, RAN translation has been shown to produce polyglutamine protein in DM1 and two different proteins, LPAC and QAGR, in DM2. These proteins accumulate in the heart and skeletal muscle in DM1 and in the brain of DM2 patients and exert toxic effects, leading to cell death (Zu et al., 2017; Zu et al., 2011). The mechanism by which these proteins cause cell death has not been elucidated. Inducible MyoD-converted myotubes and iPSC-CMs from DM1 and DM2 patients would first be probed for RAN translation products to evaluate whether they are expressed in these system, and if so, in what distribution. If there are different expression profiles of RAN proteins in DM1 as compared to DM2, this may indicate that RAN translation contributes to distinctive clinical features seen in the two subtypes. Novel interacting partners of RAN proteins could be identified with an immunoprecipitation assay using antibodies against RAN proteins followed by mass spectrometry. As these toxic proteins are thought to induce apoptosis, I would expect proteins involved in apoptotic pathway to be involved. It would also be interesting to study if polyglutamine and LPAC/QAGR polypeptides interact with different

partners depending on tissue type (skeletal muscle versus heart) or disease subtype (DM1 versus DM2).

Most therapy development has focused on DM1, in large part due to DM1 prevalence and severity, and also because DM2 models are generally unavailable. In addition, although cardiac manifestations are common in DM and pose risks for sudden death, cardiac management relies on existing therapies for managing arrhythmias and heart failure rather than mechanism-specific approaches. Here, iPSC-CMs generated from patients can serve as a platform upon which treatments can be tested. Compounds that have previously been shown to improve skeletal muscle phenotypes (Konieczny et al., 2017) can be tested on DM1 and DM2 iPSC-CMs and evaluated for their potential benefits in the heart. After treatment with potential therapeutics, ribonuclear foci formation, MBNL1 sequestration, and missplicing can be examined in DM1 iPSC-CMs. For DM2 iPSC-CMs, responses in calcium handling can be used as a parameter to determine if any treatment can be beneficial in decreasing calcium mishandling phenotypes.

CONCLUDING REMARKS

I present here cell-based models of skeletal and cardiac muscle for patient-specific modeling of human myopathies (Figure 5.2). These models are developed from non-invasive source, making them readily available for any patient, especially for those who have diseases that are difficult to model in animals. Further, the cellular platforms presented herein allow for multiple cell types from one patient to be studied simultaneously, opening up avenues to identify tissue-specific events by comparing findings between the tissues. IPSCs can also be differentiated into other cell types, such as neurons, which adds to the versatility of these models and may be especially relevant for DM1. With drug screening identifying compounds that can be used for gene and

even mutation-specific treatments such as antisense oligonucleotide-mediated exon skipping and other gene-specific avenues, these models will satisfy the need for human disease models that can be used to evaluate such new treatments and potentially aid in their regulatory approvals.

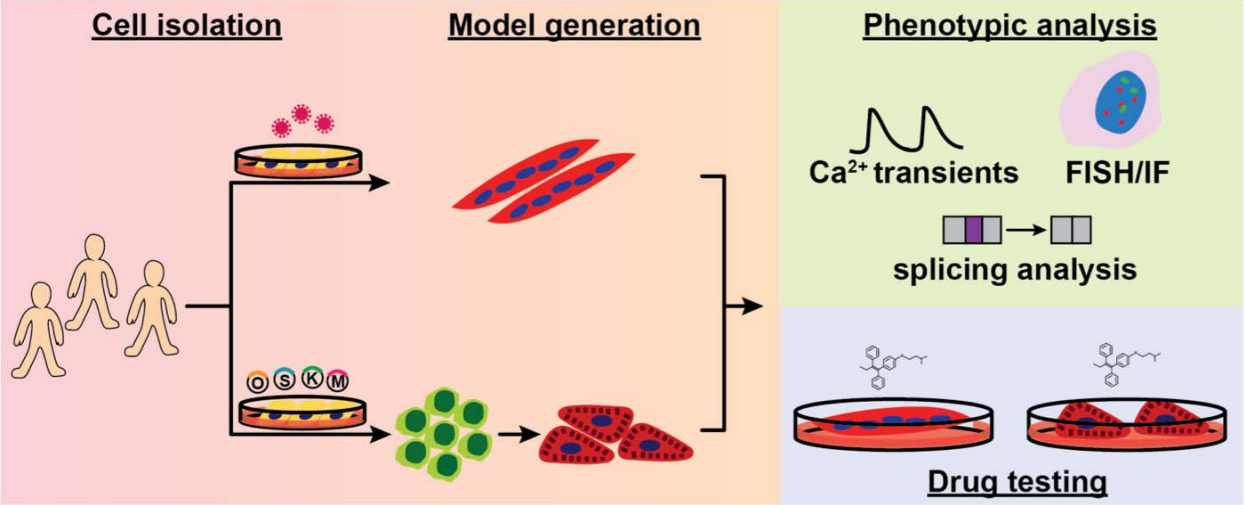

Figure 5.2 Utility of cell-based models

Urine cells are isolated from patients who harbor mutations to be studied. Cells can then be either transduced with inducible MyoD construct and then differentiated to myotubes, or reprogrammed to iPSCs and then differentiated to cardiomyocytes. These models can then be used for phenotypic analysis. In the case of DM, analysis includes FISH, IF, splicing analysis, and calcium transient measurements. Once phenotypes are established, they can then be used as readouts in drug testing.

REFERENCES

Aartsma-Rus, A., Ginjaar, I. B., & Bushby, K. (2016). The importance of genetic diagnosis for Duchenne muscular dystrophy. *J Med Genet, 53*(3), 145-151. doi:10.1136/jmedgenet-2015-103387

Abujarour, R., Bennett, M., Valamehr, B., Lee, T. T., Robinson, M., Robbins, D., . . . Flynn, P. (2014). Myogenic differentiation of muscular dystrophy-specific induced pluripotent stem cells for use in drug discovery. *Stem Cells Transl Med, 3*(2), 149-160. doi:10.5966/sctm.2013-0095

Afzal, M. Z., & Strande, J. L. (2015). Generation of induced pluripotent stem cells from muscular dystrophy patients: efficient integration-free reprogramming of urine derived cells. *J Vis Exp*(95), 52032. doi:10.3791/52032

Amack, J. D., & Mahadevan, M. S. (2004). Myogenic defects in myotonic dystrophy. *Dev Biol, 265*(2), 294-301.

Arandel, L., Polay Espinoza, M., Matloka, M., Bazinet, A., De Dea Diniz, D., Naouar, N., . . . Furling, D. (2017). Immortalized human myotonic dystrophy muscle cell lines to assess therapeutic compounds. *Dis Model Mech, 10*(4), 487-497. doi:10.1242/dmm.027367

Arnold, S. J., & Robertson, E. J. (2009). Making a commitment: cell lineage allocation and axis patterning in the early mouse embryo. *Nat Rev Mol Cell Biol, 10*(2), 91-103. doi:10.1038/nrm2618

Ashizawa, T., Anvret, M., Baiget, M., Barcelo, J. M., Brunner, H., Cobo, A. M., . . . et al. (1994). Characteristics of intergenerational contractions of the CTG repeat in myotonic dystrophy. *Am J Hum Genet, 54*(3), 414-423.

Ashizawa, T., & Baiget, M. (2000). New nomenclature and DNA testing guidelines for myotonic dystrophy type 1 (DM1). The International Myotonic Dystrophy Consortium (IDMC). *Neurology, 54*(6), 1218-1221.

Ashley, E. A. (2016). Towards precision medicine. *Nat Rev Genet, 17*(9), 507-522. doi:10.1038/nrg.2016.86

Bachinski, L. L., Czernuszewicz, T., Ramagli, L. S., Suominen, T., Shriver, M. D., Udd, B., . . . Krahe, R. (2009). Premutation allele pool in myotonic dystrophy type 2. *Neurology, 72*(6), 490-497. doi:10.1212/01.wnl.0000333665.01888.33

Bagshaw, A. T. M. (2017). Functional Mechanisms of Microsatellite DNA in Eukaryotic Genomes. *Genome Biol Evol, 9*(9), 2428-2443. doi:10.1093/gbe/evx164

Barefield, D. Y., Puckelwartz, M. J., Kim, E. Y., Wilsbacher, L. D., Vo, A. H., Waters, E. A., . . . McNally, E. M. (2017). Experimental Modeling Supports a Role for MyBP-HL as a Novel Myofilament Component in Arrhythmia and Dilated Cardiomyopathy. *Circulation, 136*(16), 1477-1491. doi:10.1161/CIRCULATIONAHA.117.028585

Barreau, C., Paillard, L., Mereau, A., & Osborne, H. B. (2006). Mammalian CELF/Bruno-like RNA-binding proteins: molecular characteristics and biological functions. *Biochimie, 88*(5), 515-525. doi:10.1016/j.biochi.2005.10.011

Batra, R., Nelles, D. A., Pirie, E., Blue, S. M., Marina, R. J., Wang, H., . . . Yeo, G. W. (2017). Elimination of Toxic Microsatellite Repeat Expansion RNA by RNA-Targeting Cas9. *Cell, 170*(5), 899-912 e810. doi:10.1016/j.cell.2017.07.010

Bentzinger, C. F., Wang, Y. X., & Rudnicki, M. A. (2012). Building muscle: molecular regulation of myogenesis. *Cold Spring Harb Perspect Biol, 4*(2). doi:10.1101/cshperspect.a008342

Berkes, C. A., & Tapscott, S. J. (2005). MyoD and the transcriptional control of myogenesis. *Semin Cell Dev Biol, 16*(4-5), 585-595. doi:10.1016/j.semcdb.2005.07.006

Bhakta, D., Groh, M. R., Shen, C., Pascuzzi, R. M., & Groh, W. J. (2010). Increased mortality with left ventricular systolic dysfunction and heart failure in adults with myotonic dystrophy type 1. *Am Heart J, 160*(6), 1137-1141, 1141.e1131. doi:10.1016/j.ahj.2010.07.032

Bharadwaj, S., Liu, G., Shi, Y., Markert, C., Andersson, K. E., Atala, A., & Zhang, Y. (2011). Characterization of urine-derived stem cells obtained from upper urinary tract for use in cell-based urological tissue engineering. *Tissue Eng Part A, 17*(15-16), 2123-2132. doi:10.1089/ten.TEA.2010.0637

Bharadwaj, S., Liu, G., Shi, Y., Wu, R., Yang, B., He, T., . . . Zhang, Y. (2013). Multipotential differentiation of human urine-derived stem cells: potential for therapeutic applications in urology. *Stem Cells, 31*(9), 1840-1856. doi:10.1002/stem.1424

Bialk, P., Rivera-Torres, N., Strouse, B., & Kmiec, E. B. (2015). Regulation of Gene Editing Activity Directed by Single-Stranded Oligonucleotides and CRISPR/Cas9 Systems. *PLoS One, 10*(6), e0129308. doi:10.1371/journal.pone.0129308

Bladen, C. L., Salgado, D., Monges, S., Foncuberta, M. E., Kekou, K., Kosma, K., . . . Lochmuller, H. (2015). The TREAT-NMD DMD Global Database: analysis of more than 7,000 Duchenne muscular dystrophy mutations. *Hum Mutat, 36*(4), 395-402. doi:10.1002/humu.22758

Blau, H. M., Pavlath, G. K., Hardeman, E. C., Chiu, C. P., Silberstein, L., Webster, S. G., . . . Webster, C. (1985). Plasticity of the differentiated state. *Science, 230*(4727), 758-766.

Blau, H. M., & Webster, C. (1981). Isolation and characterization of human muscle cells. *Proc Natl Acad Sci U S A, 78*(9), 5623-5627.

Bodin, A., Bharadwaj, S., Wu, S., Gatenholm, P., Atala, A., & Zhang, Y. (2010). Tissue-engineered conduit using urine-derived stem cells seeded bacterial cellulose polymer in urinary reconstruction and diversion. *Biomaterials, 31*(34), 8889-8901. doi:10.1016/j.biomaterials.2010.07.108

Brade, T., Pane, L. S., Moretti, A., Chien, K. R., & Laugwitz, K. L. (2013). Embryonic heart progenitors and cardiogenesis. *Cold Spring Harb Perspect Med, 3*(10), a013847. doi:10.1101/cshperspect.a013847

Brook, J. D., Zemelman, B. V., Hadingham, K., Siciliano, M. J., Crow, S., Harley, H. G., . . . et al. (1992). Radiation-reduced hybrids for the myotonic dystrophy locus. *Genomics, 13*(2), 243-250.

Bugiardini, E., Rivolta, I., Binda, A., Soriano Caminero, A., Cirillo, F., Cinti, A., . . . Meola, G. (2015). SCN4A mutation as modifying factor of myotonic dystrophy type 2 phenotype. *Neuromuscul Disord, 25*(4), 301-307. doi:10.1016/j.nmd.2015.01.006

Burridge, P. W., Holmstrom, A., & Wu, J. C. (2015). Chemically Defined Culture and Cardiomyocyte Differentiation of Human Pluripotent Stem Cells. *Curr Protoc Hum Genet, 87*, 21 23 21-15. doi:10.1002/0471142905.hg2103s87

Burridge, P. W., Keller, G., Gold, J. D., & Wu, J. C. (2012). Production of de novo cardiomyocytes: human pluripotent stem cell differentiation and direct reprogramming. *Cell Stem Cell, 10*(1), 16-28. doi:10.1016/j.stem.2011.12.013

Burridge, P. W., Li, Y. F., Matsa, E., Wu, H., Ong, S. G., Sharma, A., . . . Wu, J. C. (2016). Human induced pluripotent stem cell-derived cardiomyocytes recapitulate the predilection of breast cancer patients to doxorubicin-induced cardiotoxicity. *Nat Med, 22*(5), 547-556. doi:10.1038/nm.4087

Burridge, P. W., Matsa, E., Shukla, P., Lin, Z. C., Churko, J. M., Ebert, A. D., . . . Wu, J. C. (2014). Chemically defined generation of human cardiomyocytes. *Nat Methods, 11*(8), 855-860. doi:10.1038/nmeth.2999

Cardani, R., Bugiardini, E., Renna, L. V., Rossi, G., Colombo, G., Valaperta, R., . . . Meola, G. (2013). Overexpression of CUGBP1 in skeletal muscle from adult classic myotonic dystrophy type 1 but not from myotonic dystrophy type 2. *PLoS One, 8*(12), e83777. doi:10.1371/journal.pone.0083777

Cardani, R., Giagnacovo, M., Botta, A., Rinaldi, F., Morgante, A., Udd, B., . . . Meola, G. (2012). Co-segregation of DM2 with a recessive CLCN1 mutation in juvenile onset of myotonic dystrophy type 2. *J Neurol, 259*(10), 2090-2099. doi:10.1007/s00415-012-6462-1

Cardani, R., Giagnacovo, M., Rossi, G., Renna, L. V., Bugiardini, E., Pizzamiglio, C., . . . Meola, G. (2014). Progression of muscle histopathology but not of spliceopathy in myotonic dystrophy type 2. *Neuromuscul Disord, 24*(12), 1042-1053. doi:10.1016/j.nmd.2014.06.435

Casas-Delucchi, C. S., Brero, A., Rahn, H. P., Solovei, I., Wutz, A., Cremer, T., . . . Cardoso, M. C. (2011). Histone acetylation controls the inactive X chromosome replication dynamics. *Nat Commun, 2*, 222. doi:10.1038/ncomms1218

Chal, J., Al Tanoury, Z., Hestin, M., Gobert, B., Aivio, S., Hick, A., . . . Pourquie, O. (2016). Generation of human muscle fibers and satellite-like cells from human pluripotent stem cells in vitro. *Nat Protoc, 11*(10), 1833-1850. doi:10.1038/nprot.2016.110

Chal, J., Oginuma, M., Al Tanoury, Z., Gobert, B., Sumara, O., Hick, A., . . . Pourquie, O. (2015). Differentiation of pluripotent stem cells to muscle fiber to model Duchenne muscular dystrophy. *Nat Biotechnol, 33*(9), 962-969. doi:10.1038/nbt.3297

Chal, J., & Pourquie, O. (2017). Making muscle: skeletal myogenesis in vivo and in vitro. *Development, 144*(12), 2104-2122. doi:10.1242/dev.151035

Charizanis, K., Lee, K. Y., Batra, R., Goodwin, M., Zhang, C., Yuan, Y., . . . Swanson, M. S. (2012). Muscleblind-like 2-mediated alternative splicing in the developing brain and dysregulation in myotonic dystrophy. *Neuron, 75*(3), 437-450. doi:10.1016/j.neuron.2012.05.029

Chen, F., Pruett-Miller, S. M., Huang, Y., Gjoka, M., Duda, K., Taunton, J., . . . Davis, G. D. (2011). High-frequency genome editing using ssDNA oligonucleotides with zinc-finger nucleases. *Nat Methods, 8*(9), 753-755. doi:10.1038/nmeth.1653

Chen, W., Wang, Y., Abe, Y., Cheney, L., Udd, B., & Li, Y. P. (2007). Haploinsuffciency for Znf9 in Znf9+/- mice is associated with multiorgan abnormalities resembling myotonic dystrophy. *J Mol Biol, 368*(1), 8-17. doi:10.1016/j.jmb.2007.01.088

Chen, W., Xie, M., Yang, B., Bharadwaj, S., Song, L., Liu, G., . . . Zhang, Y. (2014). Skeletal myogenic differentiation of human urine-derived cells as a potential source for skeletal muscle regeneration. *J Tissue Eng Regen Med*. doi:10.1002/term.1914

Cheng, C. S., El-Abd, Y., Bui, K., Hyun, Y. E., Hughes, R. H., Kraus, W. E., & Truskey, G. A. (2014). Conditions that promote primary human skeletal myoblast culture and muscle differentiation in vitro. *Am J Physiol Cell Physiol, 306*(4), C385-395. doi:10.1152/ajpcell.00179.2013

Choi, S. M., Liu, H., Chaudhari, P., Kim, Y., Cheng, L., Feng, J., . . . Jang, Y. Y. (2011). Reprogramming of EBV-immortalized B-lymphocyte cell lines into induced pluripotent stem cells. *Blood, 118*(7), 1801-1805. doi:10.1182/blood-2011-03-340620

Chun, S. Y., Kim, H. T., Lee, J. S., Kim, M. J., Kim, B. S., Kim, B. W., & Kwon, T. G. (2012). Characterization of urine-derived cells from upper urinary tract in patients with bladder cancer. *Urology, 79*(5), 1186 e1181-1187. doi:10.1016/j.urology.2011.12.034

Coonrod, L. A., Nakamori, M., Wang, W., Carrell, S., Hilton, C. L., Bodner, M. J., . . . Berglund, J. A. (2013). Reducing levels of toxic RNA with small molecules. *ACS Chem Biol, 8*(11), 2528-2537. doi:10.1021/cb400431f

Cooper, S. T., Kizana, E., Yates, J. D., Lo, H. P., Yang, N., Wu, Z. H., . . . North, K. N. (2007). Dystrophinopathy carrier determination and detection of protein deficiencies in muscular

dystrophy using lentiviral MyoD-forced myogenesis. *Neuromuscul Disord, 17*(4), 276-284. doi:10.1016/j.nmd.2006.12.010

Darabi, R., Arpke, R. W., Irion, S., Dimos, J. T., Grskovic, M., Kyba, M., & Perlingeiro, R. C. (2012). Human ES- and iPS-derived myogenic progenitors restore DYSTROPHIN and improve contractility upon transplantation in dystrophic mice. *Cell Stem Cell, 10*(5), 610-619. doi:10.1016/j.stem.2012.02.015

Darabi, R., & Perlingeiro, R. C. (2016). Derivation of Skeletal Myogenic Precursors from Human Pluripotent Stem Cells Using Conditional Expression of PAX7. *Methods Mol Biol, 1357*, 423-439. doi:10.1007/7651_2014_134

Darabi, R., & Perlingeiro, R. C. R. (2016). Derivation of Skeletal Myogenic Precursors from Human Pluripotent Stem Cells Using Conditional Expression of PAX7. In K. Turksen & A. Nagy (Eds.), *Induced Pluripotent Stem (iPS) Cells: Methods and Protocols* (pp. 423-439). New York, NY: Springer New York.

Davis, B. M., McCurrach, M. E., Taneja, K. L., Singer, R. H., & Housman, D. E. (1997). Expansion of a CUG trinucleotide repeat in the 3' untranslated region of myotonic dystrophy protein kinase transcripts results in nuclear retention of transcripts. *Proc Natl Acad Sci U S A, 94*(14), 7388-7393.

Davis, R. L., Weintraub, H., & Lassar, A. B. (1987). Expression of a single transfected cDNA converts fibroblasts to myoblasts. *Cell, 51*(6), 987-1000.

Day, J. W., Ricker, K., Jacobsen, J. F., Rasmussen, L. J., Dick, K. A., Kress, W., . . . Ranum, L. P. (2003). Myotonic dystrophy type 2: molecular, diagnostic and clinical spectrum. *Neurology, 60*(4), 657-664.

de Mezer, M., Wojciechowska, M., Napierala, M., Sobczak, K., & Krzyzosiak, W. J. (2011). Mutant CAG repeats of Huntingtin transcript fold into hairpins, form nuclear foci and are targets for RNA interference. *Nucleic Acids Res, 39*(9), 3852-3863. doi:10.1093/nar/gkq1323

Del Alamo, J. C., Lemons, D., Serrano, R., Savchenko, A., Cerignoli, F., Bodmer, R., & Mercola, M. (2016). High throughput physiological screening of iPSC-derived cardiomyocytes for drug development. *Biochim Biophys Acta, 1863*(7 Pt B), 1717-1727. doi:10.1016/j.bbamcr.2016.03.003

Dick, E., Kalra, S., Anderson, D., George, V., Ritso, M., Laval, S. H., . . . Denning, C. (2013). Exon skipping and gene transfer restore dystrophin expression in human induced pluripotent stem cells-cardiomyocytes harboring DMD mutations. *Stem Cells Dev, 22*(20), 2714-2724. doi:10.1089/scd.2013.0135

Dixon, D. M., Choi, J., El-Ghazali, A., Park, S. Y., Roos, K. P., Jordan, M. C., . . . Reddy, S. (2015). Loss of muscleblind-like 1 results in cardiac pathology and persistence of embryonic splice isoforms. *Sci Rep, 5*, 9042. doi:10.1038/srep09042

Dorrenhaus, A., Muller, J. I., Golka, K., Jedrusik, P., Schulze, H., & Follmann, W. (2000). Cultures of exfoliated epithelial cells from different locations of the human urinary tract and the renal tubular system. *Arch Toxicol, 74*(10), 618-626.

Dugre-Brisson, S., Elvira, G., Boulay, K., Chatel-Chaix, L., Mouland, A. J., & DesGroseillers, L. (2005). Interaction of Staufen1 with the 5' end of mRNA facilitates translation of these RNAs. *Nucleic Acids Res, 33*(15), 4797-4812. doi:10.1093/nar/gki794

Duinsbergen, D., Salvatori, D., Eriksson, M., & Mikkers, H. (2009). Tumors originating from induced pluripotent stem cells and methods for their prevention. *Ann N Y Acad Sci, 1176*, 197-204. doi:10.1111/j.1749-6632.2009.04563.x

Echenne, B., & Bassez, G. (2013). Congenital and infantile myotonic dystrophy. *Handb Clin Neurol, 113*, 1387-1393. doi:10.1016/b978-0-444-59565-2.00009-5

England, J., & Loughna, S. (2013). Heavy and light roles: myosin in the morphogenesis of the heart. *Cell Mol Life Sci, 70*(7), 1221-1239. doi:10.1007/s00018-012-1131-1

Falzarano, M. S., D'Amario, D., Siracusano, A., Massetti, M., Amodeo, A., La Neve, F., . . . Ferlini, A. (2016). Duchenne Muscular Dystrophy Myogenic Cells from Urine-Derived Stem Cells Recapitulate the Dystrophin Genotype and Phenotype. *Hum Gene Ther, 27*(10), 772-783. doi:10.1089/hum.2016.079

Fardaei, M., Rogers, M. T., Thorpe, H. M., Larkin, K., Hamshere, M. G., Harper, P. S., & Brook, J. D. (2002). Three proteins, MBNL, MBLL and MBXL, co-localize in vivo with nuclear foci of expanded-repeat transcripts in DM1 and DM2 cells. *Hum Mol Genet, 11*(7), 805-814.

Felix, J. S., Sun, T. T., & Littlefield, J. W. (1980). Human epithelial cells cultured from urine: growth properties and keratin staining. *In Vitro, 16*(10), 866-874.

Freyermuth, F., Rau, F., Kokunai, Y., Linke, T., Sellier, C., Nakamori, M., . . . Charlet-Berguerand, N. (2016). Splicing misregulation of SCN5A contributes to cardiac-conduction delay and heart arrhythmia in myotonic dystrophy. *Nat Commun, 7*, 11067. doi:10.1038/ncomms11067

Fu, Y. H., Friedman, D. L., Richards, S., Pearlman, J. A., Gibbs, R. A., Pizzuti, A., . . . et al. (1993). Decreased expression of myotonin-protein kinase messenger RNA and protein in adult form of myotonic dystrophy. *Science, 260*(5105), 235-238.

Fu, Y. H., Pizzuti, A., Fenwick, R. G., Jr., King, J., Rajnarayan, S., Dunne, P. W., . . . et al. (1992). An unstable triplet repeat in a gene related to myotonic muscular dystrophy. *Science, 255*(5049), 1256-1258.

Gao, Q. Q., & McNally, E. M. (2015). The Dystrophin Complex: Structure, Function, and Implications for Therapy. *Compr Physiol, 5*(3), 1223-1239. doi:10.1002/cphy.c140048

Gao, Q. Q., Wyatt, E., Goldstein, J. A., LoPresti, P., Castillo, L. M., Gazda, A., . . . McNally, E. M. (2015). Reengineering a transmembrane protein to treat muscular dystrophy using exon skipping. *J Clin Invest, 125*(11), 4186-4195. doi:10.1172/JCI82768

Gherghiceanu, M., Barad, L., Novak, A., Reiter, I., Itskovitz-Eldor, J., Binah, O., & Popescu, L. M. (2011). Cardiomyocytes derived from human embryonic and induced pluripotent stem cells: comparative ultrastructure. *J Cell Mol Med, 15*(11), 2539-2551. doi:10.1111/j.1582-4934.2011.01417.x

Gomes-Pereira, M., Cooper, T. A., & Gourdon, G. (2011). Myotonic dystrophy mouse models: towards rational therapy development. *Trends Mol Med, 17*(9), 506-517. doi:10.1016/j.molmed.2011.05.004

Gonzalez-Barriga, A., Mulders, S. A., van de Giessen, J., Hooijer, J. D., Bijl, S., van Kessel, I. D., . . . Wansink, D. G. (2013). Design and analysis of effects of triplet repeat oligonucleotides in cell models for myotonic dystrophy. *Mol Ther Nucleic Acids, 2*, e81. doi:10.1038/mtna.2013.9

Goudenege, S., Lebel, C., Huot, N. B., Dufour, C., Fujii, I., Gekas, J., . . . Tremblay, J. P. (2012). Myoblasts derived from normal hESCs and dystrophic hiPSCs efficiently fuse with existing muscle fibers following transplantation. *Mol Ther, 20*(11), 2153-2167. doi:10.1038/mt.2012.188

Grifone, R., Demignon, J., Houbron, C., Souil, E., Niro, C., Seller, M. J., . . . Maire, P. (2005). Six1 and Six4 homeoproteins are required for Pax3 and Mrf expression during myogenesis in the mouse embryo. *Development, 132*(9), 2235-2249. doi:10.1242/dev.01773

Groh, W. J., Groh, M. R., Saha, C., Kincaid, J. C., Simmons, Z., Ciafaloni, E., . . . Pascuzzi, R. M. (2008). Electrocardiographic abnormalities and sudden death in myotonic dystrophy type 1. *N Engl J Med, 358*(25), 2688-2697. doi:10.1056/NEJMoa062800

Guan, X., Mack, D. L., Moreno, C. M., Strande, J. L., Mathieu, J., Shi, Y., . . . Childers, M. K. (2014). Dystrophin-deficient cardiomyocytes derived from human urine: new biologic reagents for drug discovery. *Stem Cell Res, 12*(2), 467-480. doi:10.1016/j.scr.2013.12.004

Guiraud, S., Aartsma-Rus, A., Vieira, N. M., Davies, K. E., van Ommen, G. J., & Kunkel, L. M. (2015). The Pathogenesis and Therapy of Muscular Dystrophies. *Annu Rev Genomics Hum Genet, 16*, 281-308. doi:10.1146/annurev-genom-090314-025003

Guiraud-Dogan, C., Huguet, A., Gomes-Pereira, M., Brisson, E., Bassez, G., Junien, C., & Gourdon, G. (2007). DM1 CTG expansions affect insulin receptor isoforms expression in various tissues of transgenic mice. *Biochim Biophys Acta, 1772*(11-12), 1183-1191. doi:10.1016/j.bbadis.2007.08.004

Hack, A. A., Ly, C. T., Jiang, F., Clendenin, C. J., Sigrist, K. S., Wollmann, R. L., & McNally, E. M. (1998). Gamma-sarcoglycan deficiency leads to muscle membrane defects and apoptosis independent of dystrophin. *J Cell Biol, 142*(5), 1279-1287.

Hannan, A. J. (2018). Tandem repeats mediating genetic plasticity in health and disease. *Nat Rev Genet, 19*(5), 286-298. doi:10.1038/nrg.2017.115

Hao, M., Akrami, K., Wei, K., De Diego, C., Che, N., Ku, J. H., . . . Chen, F. (2008). Muscleblind-like 2 (Mbnl2) -deficient mice as a model for myotonic dystrophy. *Dev Dyn, 237*(2), 403-410. doi:10.1002/dvdy.21428

Higham, C. F., Morales, F., Cobbold, C. A., Haydon, D. T., & Monckton, D. G. (2012). High levels of somatic DNA diversity at the myotonic dystrophy type 1 locus are driven by ultra-frequent expansion and contraction mutations. *Hum Mol Genet, 21*(11), 2450-2463. doi:10.1093/hmg/dds059

Ho, T. H., Bundman, D., Armstrong, D. L., & Cooper, T. A. (2005). Transgenic mice expressing CUG-BP1 reproduce splicing mis-regulation observed in myotonic dystrophy. *Hum Mol Genet, 14*(11), 1539-1547. doi:10.1093/hmg/ddi162

Hollenberg, S. M., Cheng, P. F., & Weintraub, H. (1993). Use of a conditional MyoD transcription factor in studies of MyoD trans-activation and muscle determination. *Proc Natl Acad Sci U S A, 90*(17), 8028-8032.

Hoskins, J. W., Ofori, L. O., Chen, C. Z., Kumar, A., Sobczak, K., Nakamori, M., . . . Thornton, C. A. (2014). Lomofungin and dilomofungin: inhibitors of MBNL1-CUG RNA binding with distinct cellular effects. *Nucleic Acids Res, 42*(10), 6591-6602. doi:10.1093/nar/gku275

Hudson, J., Titmarsh, D., Hidalgo, A., Wolvetang, E., & Cooper-White, J. (2012). Primitive cardiac cells from human embryonic stem cells. *Stem Cells Dev, 21*(9), 1513-1523. doi:10.1089/scd.2011.0254

Huguet, A., Medja, F., Nicole, A., Vignaud, A., Guiraud-Dogan, C., Ferry, A., . . . Gourdon, G. (2012). Molecular, physiological, and motor performance defects in DMSXL mice carrying >1,000 CTG repeats from the human DM1 locus. *PLoS Genet, 8*(11), e1003043. doi:10.1371/journal.pgen.1003043

Huichalaf, C., Schoser, B., Schneider-Gold, C., Jin, B., Sarkar, P., & Timchenko, L. (2009). Reduction of the rate of protein translation in patients with myotonic dystrophy 2. *J Neurosci, 29*(28), 9042-9049. doi:10.1523/JNEUROSCI.1983-09.2009

Ieda, M., Fu, J. D., Delgado-Olguin, P., Vedantham, V., Hayashi, Y., Bruneau, B. G., & Srivastava, D. (2010). Direct reprogramming of fibroblasts into functional cardiomyocytes by defined factors. *Cell, 142*(3), 375-386. doi:10.1016/j.cell.2010.07.002

Ingelfinger, J. R. (2002). Nephrogenic adenomas as renal tubular outposts. *N Engl J Med, 347*(9), 684-686. doi:10.1056/NEJMe020084

Itzhaki, I., Maizels, L., Huber, I., Zwi-Dantsis, L., Caspi, O., Winterstern, A., . . . Gepstein, L. (2011). Modelling the long QT syndrome with induced pluripotent stem cells. *Nature, 471*(7337), 225-229. doi:10.1038/nature09747

Jansen, G., Groenen, P. J., Bachner, D., Jap, P. H., Coerwinkel, M., Oerlemans, F., . . . Wieringa, B. (1996). Abnormal myotonic dystrophy protein kinase levels produce only mild myopathy in mice. *Nat Genet, 13*(3), 316-324. doi:10.1038/ng0796-316

Jauvin, D., Chretien, J., Pandey, S. K., Martineau, L., Revillod, L., Bassez, G., . . . Puymirat, J. (2017). Targeting DMPK with Antisense Oligonucleotide Improves Muscle Strength in Myotonic Dystrophy Type 1 Mice. *Mol Ther Nucleic Acids, 7*, 465-474. doi:10.1016/j.omtn.2017.05.007

Jones, K., Wei, C., Schoser, B., Meola, G., Timchenko, N., & Timchenko, L. (2015). Reduction of toxic RNAs in myotonic dystrophies type 1 and type 2 by the RNA helicase p68/DDX5. *Proc Natl Acad Sci U S A, 112*(26), 8041-8045. doi:10.1073/pnas.1422273112

Kalra, S., Montanaro, F., & Denning, C. (2016). Can Human Pluripotent Stem Cell-Derived Cardiomyocytes Advance Understanding of Muscular Dystrophies? *J Neuromuscul Dis, 3*(3), 309-332. doi:10.3233/JND-150133

Kamsteeg, E. J., Kress, W., Catalli, C., Hertz, J. M., Witsch-Baumgartner, M., Buckley, M. F., . . . Scheffer, H. (2012). Best practice guidelines and recommendations on the molecular diagnosis of myotonic dystrophy types 1 and 2. *Eur J Hum Genet, 20*(12), 1203-1208. doi:10.1038/ejhg.2012.108

Kanadia, R. N., Johnstone, K. A., Mankodi, A., Lungu, C., Thornton, C. A., Esson, D., . . . Swanson, M. S. (2003). A muscleblind knockout model for myotonic dystrophy. *Science, 302*(5652), 1978-1980. doi:10.1126/science.1088583

Kanadia, R. N., Shin, J., Yuan, Y., Beattie, S. G., Wheeler, T. M., Thornton, C. A., & Swanson, M. S. (2006). Reversal of RNA missplicing and myotonia after muscleblind overexpression in a mouse poly(CUG) model for myotonic dystrophy. *Proc Natl Acad Sci U S A, 103*(31), 11748-11753. doi:10.1073/pnas.0604970103

Kane, C., Couch, L., & Terracciano, C. M. (2015). Excitation-contraction coupling of human induced pluripotent stem cell-derived cardiomyocytes. *Front Cell Dev Biol, 3*, 59. doi:10.3389/fcell.2015.00059

Katagiri, T., Yamaguchi, A., Komaki, M., Abe, E., Takahashi, N., Ikeda, T., . . . Suda, T. (1994). Bone morphogenetic protein-2 converts the differentiation pathway of C2C12 myoblasts into the osteoblast lineage. *J Cell Biol, 127*(6 Pt 1), 1755-1766.

Kawamura, T., Suzuki, J., Wang, Y. V., Menendez, S., Morera, L. B., Raya, A., . . . Izpisua Belmonte, J. C. (2009). Linking the p53 tumour suppressor pathway to somatic cell reprogramming. *Nature, 460*(7259), 1140-1144. doi:10.1038/nature08311

Kendall, G. C., Mokhonova, E. I., Moran, M., Sejbuk, N. E., Wang, D. W., Silva, O., . . . Miceli, M. C. (2012). Dantrolene enhances antisense-mediated exon skipping in human and mouse models of Duchenne muscular dystrophy. *Sci Transl Med, 4*(164), 164ra160. doi:10.1126/scitranslmed.3005054

Kiebler, M. A., Hemraj, I., Verkade, P., Kohrmann, M., Fortes, P., Marion, R. M., . . . Dotti, C. G. (1999). The mammalian staufen protein localizes to the somatodendritic domain of cultured hippocampal neurons: implications for its involvement in mRNA transport. *J Neurosci, 19*(1), 288-297.

Kiehl, T. R., Shibata, H., Vo, T., Huynh, D. P., & Pulst, S. M. (2001). Identification and expression of a mouse ortholog of A2BP1. *Mamm Genome, 12*(8), 595-601.

Kim, E. Y., Page, P., Dellefave-Castillo, L. M., McNally, E. M., & Wyatt, E. J. (2016). Direct reprogramming of urine-derived cells with inducible MyoD for modeling human muscle disease. *Skelet Muscle, 6*, 32. doi:10.1186/s13395-016-0103-9

Kim, Y. K., Furic, L., Desgroseillers, L., & Maquat, L. E. (2005). Mammalian Staufen1 recruits Upf1 to specific mRNA 3'UTRs so as to elicit mRNA decay. *Cell, 120*(2), 195-208. doi:10.1016/j.cell.2004.11.050

Kimura, E., Han, J. J., Li, S., Fall, B., Ra, J., Haraguchi, M., . . . Chamberlain, J. S. (2008). Cell-lineage regulated myogenesis for dystrophin replacement: a novel therapeutic approach for treatment of muscular dystrophy. *Hum Mol Genet, 17*(16), 2507-2517. doi:10.1093/hmg/ddn151

Klesert, T. R., Cho, D. H., Clark, J. I., Maylie, J., Adelman, J., Snider, L., . . . Tapscott, S. J. (2000). Mice deficient in Six5 develop cataracts: implications for myotonic dystrophy. *Nat Genet, 25*(1), 105-109. doi:10.1038/75490

Klesert, T. R., Otten, A. D., Bird, T. D., & Tapscott, S. J. (1997). Trinucleotide repeat expansion at the myotonic dystrophy locus reduces expression of DMAHP. *Nat Genet, 16*(4), 402-406. doi:10.1038/ng0897-402

Klinck, R., Fourrier, A., Thibault, P., Toutant, J., Durand, M., Lapointe, E., . . . Chabot, B. (2014). RBFOX1 cooperates with MBNL1 to control splicing in muscle, including events altered in myotonic dystrophy type 1. *PLoS One, 9*(9), e107324. doi:10.1371/journal.pone.0107324

Kole, R., Krainer, A. R., & Altman, S. (2012). RNA therapeutics: beyond RNA interference and antisense oligonucleotides. *Nat Rev Drug Discov, 11*(2), 125-140. doi:10.1038/nrd3625

Konieczny, P., Selma-Soriano, E., Rapisarda, A. S., Fernandez-Costa, J. M., Perez-Alonso, M., & Artero, R. (2017). Myotonic dystrophy: candidate small molecule therapeutics. *Drug Discov Today, 22*(11), 1740-1748. doi:10.1016/j.drudis.2017.07.011

Konieczny, P., Stepniak-Konieczna, E., & Sobczak, K. (2014). MBNL proteins and their target RNAs, interaction and splicing regulation. *Nucleic Acids Res, 42*(17), 10873-10887. doi:10.1093/nar/gku767

Koshelev, M., Sarma, S., Price, R. E., Wehrens, X. H., & Cooper, T. A. (2010). Heart-specific overexpression of CUGBP1 reproduces functional and molecular abnormalities of myotonic dystrophy type 1. *Hum Mol Genet, 19*(6), 1066-1075. doi:10.1093/hmg/ddp570

Kuyumcu-Martinez, N. M., Wang, G. S., & Cooper, T. A. (2007). Increased steady-state levels of CUGBP1 in myotonic dystrophy 1 are due to PKC-mediated hyperphosphorylation. *Mol Cell, 28*(1), 68-78. doi:10.1016/j.molcel.2007.07.027

La Spada, A. R., & Taylor, J. P. (2010). Repeat expansion disease: progress and puzzles in disease pathogenesis. *Nat Rev Genet, 11*(4), 247-258. doi:10.1038/nrg2748

La Spada, A. R., Wilson, E. M., Lubahn, D. B., Harding, A. E., & Fischbeck, K. H. (1991). Androgen receptor gene mutations in X-linked spinal and bulbar muscular atrophy. *Nature, 352*(6330), 77-79. doi:10.1038/352077a0

Laflamme, M. A., Chen, K. Y., Naumova, A. V., Muskheli, V., Fugate, J. A., Dupras, S. K., . . . Murry, C. E. (2007). Cardiomyocytes derived from human embryonic stem cells in pro-survival factors enhance function of infarcted rat hearts. *Nat Biotechnol, 25*(9), 1015-1024. doi:10.1038/nbt1327

Lambert, N., Robertson, A., Jangi, M., McGeary, S., Sharp, P. A., & Burge, C. B. (2014). RNA Bind-n-Seq: quantitative assessment of the sequence and structural binding specificity of RNA binding proteins. *Mol Cell, 54*(5), 887-900. doi:10.1016/j.molcel.2014.04.016

Lan, F., Lee, A. S., Liang, P., Sanchez-Freire, V., Nguyen, P. K., Wang, L., . . . Wu, J. C. (2013). Abnormal calcium handling properties underlie familial hypertrophic cardiomyopathy pathology in patient-specific induced pluripotent stem cells. *Cell Stem Cell, 12*(1), 101-113. doi:10.1016/j.stem.2012.10.010

Lattanzi, L., Salvatori, G., Coletta, M., Sonnino, C., Cusella De Angelis, M. G., Gioglio, L., . . . Cossu, G. (1998). High efficiency myogenic conversion of human fibroblasts by adenoviral vector-mediated MyoD gene transfer. An alternative strategy for ex vivo gene therapy of primary myopathies. *J Clin Invest, 101*(10), 2119-2128. doi:10.1172/JCI1505

Lau, J. K., Sy, R. W., Corbett, A., & Kritharides, L. (2015). Myotonic dystrophy and the heart: A systematic review of evaluation and management. *Int J Cardiol, 184*, 600-608. doi:10.1016/j.ijcard.2015.03.069

Laurent, F. X., Sureau, A., Klein, A. F., Trouslard, F., Gasnier, E., Furling, D., & Marie, J. (2012). New function for the RNA helicase p68/DDX5 as a modifier of MBNL1 activity on expanded CUG repeats. *Nucleic Acids Res, 40*(7), 3159-3171. doi:10.1093/nar/gkr1228

Lee, K. S., Smith, K., Amieux, P. S., & Wang, E. H. (2008). MBNL3/CHCR prevents myogenic differentiation by inhibiting MyoD-dependent gene transcription. *Differentiation, 76*(3), 299-309. doi:10.1111/j.1432-0436.2007.00209.x

Lee, K. S., Squillace, R. M., & Wang, E. H. (2007). Expression pattern of muscleblind-like proteins differs in differentiating myoblasts. *Biochem Biophys Res Commun, 361*(1), 151-155. doi:10.1016/j.bbrc.2007.06.165

Lemoine, M. D., Mannhardt, I., Breckwoldt, K., Prondzynski, M., Flenner, F., Ulmer, B., . . . Christ, T. (2017). Human iPSC-derived cardiomyocytes cultured in 3D engineered heart tissue show physiological upstroke velocity and sodium current density. *Sci Rep, 7*(1), 5464. doi:10.1038/s41598-017-05600-w

Li, H. L., Fujimoto, N., Sasakawa, N., Shirai, S., Ohkame, T., Sakuma, T., . . . Hotta, A. (2015). Precise correction of the dystrophin gene in duchenne muscular dystrophy patient induced pluripotent stem cells by TALEN and CRISPR-Cas9. *Stem Cell Reports, 4*(1), 143-154. doi:10.1016/j.stemcr.2014.10.013

Lian, X., Hsiao, C., Wilson, G., Zhu, K., Hazeltine, L. B., Azarin, S. M., . . . Palecek, S. P. (2012). Robust cardiomyocyte differentiation from human pluripotent stem cells via temporal modulation of canonical Wnt signaling. *Proc Natl Acad Sci U S A, 109*(27), E1848-1857. doi:10.1073/pnas.1200250109

Lian, X., Zhang, J., Azarin, S. M., Zhu, K., Hazeltine, L. B., Bao, X., . . . Palecek, S. P. (2013). Directed cardiomyocyte differentiation from human pluripotent stem cells by modulating Wnt/beta-catenin signaling under fully defined conditions. *Nat Protoc, 8*(1), 162-175. doi:10.1038/nprot.2012.150

Lim, K. R., Maruyama, R., & Yokota, T. (2017). Eteplirsen in the treatment of Duchenne muscular dystrophy. *Drug Des Devel Ther, 11*, 533-545. doi:10.2147/DDDT.S97635

Lin, B., Li, Y., Han, L., Kaplan, A. D., Ao, Y., Kalra, S., . . . Yang, L. (2015). Modeling and study of the mechanism of dilated cardiomyopathy using induced pluripotent stem cells derived from individuals with Duchenne muscular dystrophy. *Dis Model Mech, 8*(5), 457-466. doi:10.1242/dmm.019505

Lin, X., Miller, J. W., Mankodi, A., Kanadia, R. N., Yuan, Y., Moxley, R. T., . . . Thornton, C. A. (2006). Failure of MBNL1-dependent post-natal splicing transitions in myotonic dystrophy. *Hum Mol Genet, 15*(13), 2087-2097. doi:10.1093/hmg/ddl132

Linkhart, T. A., Clegg, C. H., & Hauschika, S. D. (1981). Myogenic differentiation in permanent clonal mouse myoblast cell lines: regulation by macromolecular growth factors in the culture medium. *Dev Biol, 86*(1), 19-30.

Liquori, C. L., Ikeda, Y., Weatherspoon, M., Ricker, K., Schoser, B. G., Dalton, J. C., . . . Ranum, L. P. (2003). Myotonic dystrophy type 2: human founder haplotype and evolutionary conservation of the repeat tract. *Am J Hum Genet, 73*(4), 849-862. doi:10.1086/378720

Liquori, C. L., Ricker, K., Moseley, M. L., Jacobsen, J. F., Kress, W., Naylor, S. L., . . . Ranum, L. P. (2001). Myotonic dystrophy type 2 caused by a CCTG expansion in intron 1 of ZNF9. *Science, 293*(5531), 864-867. doi:10.1126/science.1062125

Liu, G., Wang, X., Sun, X., Deng, C., Atala, A., & Zhang, Y. (2013). The effect of urine-derived stem cells expressing VEGF loaded in collagen hydrogels on myogenesis and innervation following after subcutaneous implantation in nude mice. *Biomaterials, 34*(34), 8617-8629. doi:10.1016/j.biomaterials.2013.07.077

Long, C., Amoasii, L., Mireault, A. A., McAnally, J. R., Li, H., Sanchez-Ortiz, E., . . . Olson, E. N. (2016). Postnatal genome editing partially restores dystrophin expression in a mouse model of muscular dystrophy. *Science, 351*(6271), 400-403. doi:10.1126/science.aad5725

Long, C., McAnally, J. R., Shelton, J. M., Mireault, A. A., Bassel-Duby, R., & Olson, E. N. (2014). Prevention of muscular dystrophy in mice by CRISPR/Cas9-mediated editing of germline DNA. *Science, 345*(6201), 1184-1188. doi:10.1126/science.1254445

Lu, Q. L., Mann, C. J., Lou, F., Bou-Gharios, G., Morris, G. E., Xue, S. A., . . . Wilton, S. D. (2003). Functional amounts of dystrophin produced by skipping the mutated exon in the mdx dystrophic mouse. *Nat Med, 9*(8), 1009-1014. doi:10.1038/nm897

Lukas, Z., Falk, M., Feit, J., Soucek, O., Falkova, I., Stefancikova, L., . . . Hrabalkova, R. (2012). Sequestration of MBNL1 in tissues of patients with myotonic dystrophy type 2. *Neuromuscul Disord, 22*(7), 604-616. doi:10.1016/j.nmd.2012.03.004

Magli, A., Incitti, T., Kiley, J., Swanson, S. A., Darabi, R., Rinaldi, F., . . . Perlingeiro, R. C. R. (2017). PAX7 Targets, CD54, Integrin alpha9beta1, and SDC2, Allow Isolation of Human ESC/iPSC-Derived Myogenic Progenitors. *Cell Rep, 19*(13), 2867-2877. doi:10.1016/j.celrep.2017.06.005

Mahadevan, M., Tsilfidis, C., Sabourin, L., Shutler, G., Amemiya, C., Jansen, G., . . . et al. (1992). Myotonic dystrophy mutation: an unstable CTG repeat in the 3' untranslated region of the gene. *Science, 255*(5049), 1253-1255.

Mahadevan, M. S., Yadava, R. S., Yu, Q., Balijepalli, S., Frenzel-McCardell, C. D., Bourne, T. D., & Phillips, L. H. (2006). Reversible model of RNA toxicity and cardiac conduction defects in myotonic dystrophy. *Nat Genet, 38*(9), 1066-1070. doi:10.1038/ng1857

Malatesta, M., Giagnacovo, M., Cardani, R., Meola, G., & Pellicciari, C. (2013). Human myoblasts from skeletal muscle biopsies: in vitro culture preparations for morphological and cytochemical analyses at light and electron microscopy. *Methods Mol Biol, 976*, 67-79. doi:10.1007/978-1-62703-317-6_6

Mali, P., Yang, L., Esvelt, K. M., Aach, J., Guell, M., DiCarlo, J. E., . . . Church, G. M. (2013). RNA-guided human genome engineering via Cas9. *Science, 339*(6121), 823-826. doi:10.1126/science.1232033

Malik, N., & Rao, M. S. (2013). A review of the methods for human iPSC derivation. *Methods Mol Biol, 997*, 23-33. doi:10.1007/978-1-62703-348-0_3

Mamchaoui, K., Trollet, C., Bigot, A., Negroni, E., Chaouch, S., Wolff, A., . . . Mouly, V. (2011). Immortalized pathological human myoblasts: towards a universal tool for the study of neuromuscular disorders. *Skelet Muscle, 1*, 34. doi:10.1186/2044-5040-1-34

Mankodi, A., Lin, X., Blaxall, B. C., Swanson, M. S., & Thornton, C. A. (2005). Nuclear RNA foci in the heart in myotonic dystrophy. *Circ Res, 97*(11), 1152-1155. doi:10.1161/01.RES.0000193598.89753.e3

Mankodi, A., Logigian, E., Callahan, L., McClain, C., White, R., Henderson, D., . . . Thornton, C. A. (2000). Myotonic dystrophy in transgenic mice expressing an expanded CUG repeat. *Science, 289*(5485), 1769-1773.

Mankodi, A., Takahashi, M. P., Jiang, H., Beck, C. L., Bowers, W. J., Moxley, R. T., . . . Thornton, C. A. (2002). Expanded CUG repeats trigger aberrant splicing of ClC-1 chloride channel pre-mRNA and hyperexcitability of skeletal muscle in myotonic dystrophy. *Mol Cell, 10*(1), 35-44.

Mankodi, A., Teng-Umnuay, P., Krym, M., Henderson, D., Swanson, M., & Thornton, C. A. (2003). Ribonuclear inclusions in skeletal muscle in myotonic dystrophy types 1 and 2. *Ann Neurol, 54*(6), 760-768. doi:10.1002/ana.10763

Mankodi, A., Urbinati, C. R., Yuan, Q. P., Moxley, R. T., Sansone, V., Krym, M., . . . Thornton, C. A. (2001). Muscleblind localizes to nuclear foci of aberrant RNA in myotonic dystrophy types 1 and 2. *Hum Mol Genet, 10*(19), 2165-2170.

Margolis, J. M., Schoser, B. G., Moseley, M. L., Day, J. W., & Ranum, L. P. (2006). DM2 intronic expansions: evidence for CCUG accumulation without flanking sequence or effects on ZNF9 mRNA processing or protein expression. *Hum Mol Genet, 15*(11), 1808-1815. doi:10.1093/hmg/ddl103

Massa, R., Panico, M. B., Caldarola, S., Fusco, F. R., Sabatelli, P., Terracciano, C., . . . Loreni, F. (2010). The myotonic dystrophy type 2 (DM2) gene product zinc finger protein 9 (ZNF9) is associated with sarcomeres and normally localized in DM2 patients' muscles. *Neuropathol Appl Neurobiol, 36*(4), 275-284. doi:10.1111/j.1365-2990.2010.01068.x

Mathieu, J., Allard, P., Potvin, L., Prevost, C., & Begin, P. (1999). A 10-year study of mortality in a cohort of patients with myotonic dystrophy. *Neurology, 52*(8), 1658-1662.

McMahon, D. K., Anderson, P. A., Nassar, R., Bunting, J. B., Saba, Z., Oakeley, A. E., & Malouf, N. N. (1994). C2C12 cells: biophysical, biochemical, and immunocytochemical properties. *Am J Physiol, 266*(6 Pt 1), C1795-1802. doi:10.1152/ajpcell.1994.266.6.C1795

McNally, E. M. (2007). New approaches in the therapy of cardiomyopathy in muscular dystrophy. *Annu Rev Med, 58*, 75-88. doi:10.1146/annurev.med.58.011706.144703

McNally, E. M., Duggan, D., Gorospe, J. R., Bonnemann, C. G., Fanin, M., Pegoraro, E., . . . Hoffman, E. P. (1996). Mutations that disrupt the carboxyl-terminus of gamma-sarcoglycan cause muscular dystrophy. *Hum Mol Genet, 5*(11), 1841-1847.

McNally, E. M., Passos-Bueno, M. R., Bonnemann, C. G., Vainzof, M., de Sa Moreira, E., Lidov, H. G., . . . Kunkel, L. M. (1996). Mild and severe muscular dystrophy caused by a single gamma-sarcoglycan mutation. *Am J Hum Genet, 59*(5), 1040-1047.

Meola, G., & Cardani, R. (2015). Myotonic dystrophies: An update on clinical aspects, genetic, pathology, and molecular pathomechanisms. *Biochim Biophys Acta, 1852*(4), 594-606. doi:10.1016/j.bbadis.2014.05.019

Meola, G., & Cardani, R. (2017). Myotonic dystrophy type 2 and modifier genes: an update on clinical and pathomolecular aspects. *Neurol Sci, 38*(4), 535-546. doi:10.1007/s10072-016-2805-5

Mercuri, E., & Muntoni, F. (2013). Muscular dystrophies. *Lancet, 381*(9869), 845-860. doi:10.1016/s0140-6736(12)61897-2

Miller, J. W., Urbinati, C. R., Teng-Umnuay, P., Stenberg, M. G., Byrne, B. J., Thornton, C. A., & Swanson, M. S. (2000). Recruitment of human muscleblind proteins to (CUG)(n) expansions associated with myotonic dystrophy. *EMBO J, 19*(17), 4439-4448. doi:10.1093/emboj/19.17.4439

Morales, F., Couto, J. M., Higham, C. F., Hogg, G., Cuenca, P., Braida, C., . . . Monckton, D. G. (2012). Somatic instability of the expanded CTG triplet repeat in myotonic dystrophy type 1 is a heritable quantitative trait and modifier of disease severity. *Hum Mol Genet, 21*(16), 3558-3567. doi:10.1093/hmg/dds185

Morcos, P. A., Li, Y., & Jiang, S. (2008). Vivo-Morpholinos: a non-peptide transporter delivers Morpholinos into a wide array of mouse tissues. *Biotechniques, 45*(6), 613-614, 616, 618 passim.

Moretti, A., Bellin, M., Welling, A., Jung, C. B., Lam, J. T., Bott-Flugel, L., . . . Laugwitz, K. L. (2010). Patient-specific induced pluripotent stem-cell models for long-QT syndrome. *N Engl J Med, 363*(15), 1397-1409. doi:10.1056/NEJMoa0908679

Mulders, S. A., van den Broek, W. J., Wheeler, T. M., Croes, H. J., van Kuik-Romeijn, P., de Kimpe, S. J., . . . Wansink, D. G. (2009). Triplet-repeat oligonucleotide-mediated reversal of RNA toxicity in myotonic dystrophy. *Proc Natl Acad Sci U S A, 106*(33), 13915-13920. doi:10.1073/pnas.0905780106

Nakamura, A. (2017). Moving towards successful exon-skipping therapy for Duchenne muscular dystrophy. *J Hum Genet, 62*(10), 871-876. doi:10.1038/jhg.2017.57

Napierala, M., & Krzyzosiak, W. J. (1997). CUG repeats present in myotonin kinase RNA form metastable "slippery" hairpins. *J Biol Chem, 272*(49), 31079-31085.

Nelles, D. A., Fang, M. Y., O'Connell, M. R., Xu, J. L., Markmiller, S. J., Doudna, J. A., & Yeo, G. W. (2016). Programmable RNA Tracking in Live Cells with CRISPR/Cas9. *Cell, 165*(2), 488-496. doi:10.1016/j.cell.2016.02.054

Nelson, C. E., Hakim, C. H., Ousterout, D. G., Thakore, P. I., Moreb, E. A., Castellanos Rivera, R. M., . . . Gersbach, C. A. (2016). In vivo genome editing improves muscle function in a mouse model of Duchenne muscular dystrophy. *Science, 351*(6271), 403-407. doi:10.1126/science.aad5143

Nerbonne, J. M., Nichols, C. G., Schwarz, T. L., & Escande, D. (2001). Genetic manipulation of cardiac K(+) channel function in mice: what have we learned, and where do we go from here? *Circ Res, 89*(11), 944-956.

Noguchi, S., McNally, E. M., Ben Othmane, K., Hagiwara, Y., Mizuno, Y., Yoshida, M., . . . Ozawa, E. (1995). Mutations in the dystrophin-associated protein gamma-sarcoglycan in chromosome 13 muscular dystrophy. *Science, 270*(5237), 819-822.

Nowak, J. A., Malowitz, J., Girgenrath, M., Kostek, C. A., Kravetz, A. J., Dominov, J. A., & Miller, J. B. (2004). Immortalization of mouse myogenic cells can occur without loss of p16INK4a, p19ARF, or p53 and is accelerated by inactivation of Bax. *BMC Cell Biol, 5*, 1. doi:10.1186/1471-2121-5-1

O'Cochlain, D. F., Perez-Terzic, C., Reyes, S., Kane, G. C., Behfar, A., Hodgson, D. M., . . . Terzic, A. (2004). Transgenic overexpression of human DMPK accumulates into hypertrophic cardiomyopathy, myotonic myopathy and hypotension traits of myotonic dystrophy. *Hum Mol Genet, 13*(20), 2505-2518. doi:10.1093/hmg/ddh266

Okita, K., Matsumura, Y., Sato, Y., Okada, A., Morizane, A., Okamoto, S., . . . Yamanaka, S. (2011). A more efficient method to generate integration-free human iPS cells. *Nat Methods, 8*(5), 409-412. doi:10.1038/nmeth.1591

Orengo, J. P., Chambon, P., Metzger, D., Mosier, D. R., Snipes, G. J., & Cooper, T. A. (2008). Expanded CTG repeats within the DMPK 3' UTR causes severe skeletal muscle wasting in an inducible mouse model for myotonic dystrophy. *Proc Natl Acad Sci U S A, 105*(7), 2646-2651. doi:10.1073/pnas.0708519105

Ousterout, D. G., Kabadi, A. M., Thakore, P. I., Majoros, W. H., Reddy, T. E., & Gersbach, C. A. (2015). Multiplex CRISPR/Cas9-based genome editing for correction of dystrophin mutations that cause Duchenne muscular dystrophy. *Nat Commun, 6*, 6244. doi:10.1038/ncomms7244

Owens, J., Moreira, K., & Bain, G. (2013). Characterization of primary human skeletal muscle cells from multiple commercial sources. *In Vitro Cell Dev Biol Anim, 49*(9), 695-705. doi:10.1007/s11626-013-9655-8

Parikh, S. S., Blackwell, D. J., Gomez-Hurtado, N., Frisk, M., Wang, L., Kim, K., . . . Knollmann, B. C. (2017). Thyroid and Glucocorticoid Hormones Promote Functional T-

Tubule Development in Human-Induced Pluripotent Stem Cell-Derived Cardiomyocytes. *Circ Res, 121*(12), 1323-1330. doi:10.1161/CIRCRESAHA.117.311920

Peddareddygari, L. R., Grewal, A. S., & Grewal, R. P. (2016). Focal seizures in a patient with myotonic disorder type 2 co-segregating with a chloride voltage-gated channel 1 gene mutation: a case report. *J Med Case Rep, 10*, 167. doi:10.1186/s13256-016-0958-8

Pedrotti, S., Giudice, J., Dagnino-Acosta, A., Knoblauch, M., Singh, R. K., Hanna, A., . . . Cooper, T. A. (2015). The RNA-binding protein Rbfox1 regulates splicing required for skeletal muscle structure and function. *Hum Mol Genet, 24*(8), 2360-2374. doi:10.1093/hmg/ddv003

Pelletier, R., Hamel, F., Beaulieu, D., Patry, L., Haineault, C., Tarnopolsky, M., . . . Puymirat, J. (2009). Absence of a differentiation defect in muscle satellite cells from DM2 patients. *Neurobiol Dis, 36*(1), 181-190. doi:10.1016/j.nbd.2009.07.009

Petri, H., Vissing, J., Witting, N., Bundgaard, H., & Kober, L. (2012). Cardiac manifestations of myotonic dystrophy type 1. *Int J Cardiol, 160*(2), 82-88. doi:10.1016/j.ijcard.2011.08.037

Pettersson, O. J., Aagaard, L., Andrejeva, D., Thomsen, R., Jensen, T. G., & Damgaard, C. K. (2014). DDX6 regulates sequestered nuclear CUG-expanded DMPK-mRNA in dystrophia myotonica type 1. *Nucleic Acids Res, 42*(11), 7186-7200. doi:10.1093/nar/gku352

Philips, A. V., Timchenko, L. T., & Cooper, T. A. (1998). Disruption of splicing regulated by a CUG-binding protein in myotonic dystrophy. *Science, 280*(5364), 737-741.

Portier, G. L., Benders, A. G., Oosterhof, A., Veerkamp, J. H., & van Kuppevelt, T. H. (1999). Differentiation markers of mouse C2C12 and rat L6 myogenic cell lines and the effect of the differentiation medium. *In Vitro Cell Dev Biol Anim, 35*(4), 219-227.

Quintana-Bustamante, O., & Segovia, J. C. (2016). Generation of Patient-Specific induced Pluripotent Stem Cell from Peripheral Blood Mononuclear Cells by Sendai Reprogramming Vectors. *Methods Mol Biol, 1353*, 1-11. doi:10.1007/7651_2014_170

Raab, S., Klingenstein, M., Liebau, S., & Linta, L. (2014). A Comparative View on Human Somatic Cell Sources for iPSC Generation. *Stem Cells Int, 2014*, 768391. doi:10.1155/2014/768391

Raheem, O., Olufemi, S. E., Bachinski, L. L., Vihola, A., Sirito, M., Holmlund-Hampf, J., . . . Krahe, R. (2010). Mutant (CCTG)n expansion causes abnormal expression of zinc finger protein 9 (ZNF9) in myotonic dystrophy type 2. *Am J Pathol, 177*(6), 3025-3036. doi:10.2353/ajpath.2010.100179

Rahimov, F., & Kunkel, L. M. (2013). The cell biology of disease: cellular and molecular mechanisms underlying muscular dystrophy. *J Cell Biol, 201*(4), 499-510. doi:10.1083/jcb.201212142

Rahmoune, H., Thompson, P. W., Ward, J. M., Smith, C. D., Hong, G., & Brown, J. (2005). Glucose transporters in human renal proximal tubular cells isolated from the urine of patients with non-insulin-dependent diabetes. *Diabetes, 54*(12), 3427-3434.

Rajesh, D., Dickerson, S. J., Yu, J., Brown, M. E., Thomson, J. A., & Seay, N. J. (2011). Human lymphoblastoid B-cell lines reprogrammed to EBV-free induced pluripotent stem cells. *Blood, 118*(7), 1797-1800. doi:10.1182/blood-2011-01-332064

Ran, F. A., Hsu, P. D., Wright, J., Agarwala, V., Scott, D. A., & Zhang, F. (2013). Genome engineering using the CRISPR-Cas9 system. *Nat Protoc, 8*(11), 2281-2308. doi:10.1038/nprot.2013.143

Rando, T. A., & Blau, H. M. (1994). Primary mouse myoblast purification, characterization, and transplantation for cell-mediated gene therapy. *J Cell Biol, 125*(6), 1275-1287.

Ranum, L. P., Rasmussen, P. F., Benzow, K. A., Koob, M. D., & Day, J. W. (1998). Genetic mapping of a second myotonic dystrophy locus. *Nat Genet, 19*(2), 196-198. doi:10.1038/570

Rau, F., Freyermuth, F., Fugier, C., Villemin, J. P., Fischer, M. C., Jost, B., . . . Charlet-Berguerand, N. (2011). Misregulation of miR-1 processing is associated with heart defects in myotonic dystrophy. *Nat Struct Mol Biol, 18*(7), 840-845. doi:10.1038/nsmb.2067

Ravel-Chapuis, A., Belanger, G., Yadava, R. S., Mahadevan, M. S., DesGroseillers, L., Cote, J., & Jasmin, B. J. (2012). The RNA-binding protein Staufen1 is increased in DM1 skeletal muscle and promotes alternative pre-mRNA splicing. *J Cell Biol, 196*(6), 699-712. doi:10.1083/jcb.201108113

Reddy, S., Smith, D. B., Rich, M. M., Leferovich, J. M., Reilly, P., Davis, B. M., . . . Housman, D. (1996). Mice lacking the myotonic dystrophy protein kinase develop a late onset progressive myopathy. *Nat Genet, 13*(3), 325-335. doi:10.1038/ng0796-325

Robertson, C., Tran, D. D., & George, S. C. (2013). Concise review: maturation phases of human pluripotent stem cell-derived cardiomyocytes. *Stem Cells, 31*(5), 829-837. doi:10.1002/stem.1331

Salama, G., & London, B. (2007). Mouse models of long QT syndrome. *J Physiol, 578*(Pt 1), 43-53. doi:10.1113/jphysiol.2006.118745

Saleh, A. F., Arzumanov, A. A., & Gait, M. J. (2012). Overview of alternative oligonucleotide chemistries for exon skipping. *Methods Mol Biol, 867*, 365-378. doi:10.1007/978-1-61779-767-5_23

Salisbury, E., Schoser, B., Schneider-Gold, C., Wang, G. L., Huichalaf, C., Jin, B., . . . Timchenko, L. T. (2009). Expression of RNA CCUG repeats dysregulates translation and degradation of proteins in myotonic dystrophy 2 patients. *Am J Pathol, 175*(2), 748-762. doi:10.2353/ajpath.2009.090047

Salvatori, S., Fanin, M., Trevisan, C. P., Furlan, S., Reddy, S., Nagy, J. I., & Angelini, C. (2005). Decreased expression of DMPK: correlation with CTG repeat expansion and fibre type composition in myotonic dystrophy type 1. *Neurol Sci, 26*(4), 235-242. doi:10.1007/s10072-005-0466-x

Sansone, V. A., Brigonzi, E., Schoser, B., Villani, S., Gaeta, M., De Ambroggi, G., . . . Meola, G. (2013). The frequency and severity of cardiac involvement in myotonic dystrophy type 2 (DM2): long-term outcomes. *Int J Cardiol, 168*(2), 1147-1153. doi:10.1016/j.ijcard.2012.11.076

Santos-Pereira, J. M., & Aguilera, A. (2015). R loops: new modulators of genome dynamics and function. *Nat Rev Genet, 16*(10), 583-597. doi:10.1038/nrg3961

Sarkar, P. S., Appukuttan, B., Han, J., Ito, Y., Ai, C., Tsai, W., . . . Reddy, S. (2000). Heterozygous loss of Six5 in mice is sufficient to cause ocular cataracts. *Nat Genet, 25*(1), 110-114. doi:10.1038/75500

Savkur, R. S., Philips, A. V., & Cooper, T. A. (2001). Aberrant regulation of insulin receptor alternative splicing is associated with insulin resistance in myotonic dystrophy. *Nat Genet, 29*(1), 40-47. doi:10.1038/ng704

Savkur, R. S., Philips, A. V., Cooper, T. A., Dalton, J. C., Moseley, M. L., Ranum, L. P., & Day, J. W. (2004). Insulin receptor splicing alteration in myotonic dystrophy type 2. *Am J Hum Genet, 74*(6), 1309-1313. doi:10.1086/421528

Schlaeger, T. M., Daheron, L., Brickler, T. R., Entwisle, S., Chan, K., Cianci, A., . . . Daley, G. Q. (2015). A comparison of non-integrating reprogramming methods. *Nat Biotechnol, 33*(1), 58-63. doi:10.1038/nbt.3070

Schmacht, L., Traber, J., Grieben, U., Utz, W., Dieringer, M. A., Kellman, P., . . . Schulz-Menger, J. (2016). Cardiac Involvement in Myotonic Dystrophy Type 2 Patients With Preserved Ejection Fraction: Detection by Cardiovascular Magnetic Resonance. *Circ Cardiovasc Imaging, 9*(7). doi:10.1161/circimaging.115.004615

Schubert, D., Harris, A. J., Devine, C. E., & Heinemann, S. (1974). Characterization of a unique muscle cell line. *J Cell Biol, 61*(2), 398-413.

Seth, P. P., Siwkowski, A., Allerson, C. R., Vasquez, G., Lee, S., Prakash, T. P., . . . Swayze, E. E. (2009). Short antisense oligonucleotides with novel 2'-4' conformationaly restricted nucleoside analogues show improved potency without increased toxicity in animals. *J Med Chem, 52*(1), 10-13. doi:10.1021/jm801294h

Seznec, H., Lia-Baldini, A. S., Duros, C., Fouquet, C., Lacroix, C., Hofmann-Radvanyi, H., . . . Gourdon, G. (2000). Transgenic mice carrying large human genomic sequences with expanded CTG repeat mimic closely the DM CTG repeat intergenerational and somatic instability. *Hum Mol Genet, 9*(8), 1185-1194.

Shao, L., & Wu, W. S. (2010). Gene-delivery systems for iPS cell generation. *Expert Opin Biol Ther, 10*(2), 231-242. doi:10.1517/14712590903455989

Sharma, A., Burridge, P. W., McKeithan, W. L., Serrano, R., Shukla, P., Sayed, N., . . . Wu, J. C. (2017). High-throughput screening of tyrosine kinase inhibitor cardiotoxicity with human induced pluripotent stem cells. *Sci Transl Med, 9*(377). doi:10.1126/scitranslmed.aaf2584

Shelton, M., Metz, J., Liu, J., Carpenedo, R. L., Demers, S. P., Stanford, W. L., & Skerjanc, I. S. (2014). Derivation and expansion of PAX7-positive muscle progenitors from human and mouse embryonic stem cells. *Stem Cell Reports, 3*(3), 516-529. doi:10.1016/j.stemcr.2014.07.001

Shen, X., & Corey, D. R. (2018). Chemistry, mechanism and clinical status of antisense oligonucleotides and duplex RNAs. *Nucleic Acids Res, 46*(4), 1584-1600. doi:10.1093/nar/gkx1239

Shi, Y., Inoue, H., Wu, J. C., & Yamanaka, S. (2017). Induced pluripotent stem cell technology: a decade of progress. *Nat Rev Drug Discov, 16*(2), 115-130. doi:10.1038/nrd.2016.245

Siboni, R. B., Nakamori, M., Wagner, S. D., Struck, A. J., Coonrod, L. A., Harriott, S. A., . . . Berglund, J. A. (2015). Actinomycin D Specifically Reduces Expanded CUG Repeat RNA in Myotonic Dystrophy Models. *Cell Rep, 13*(11), 2386-2394. doi:10.1016/j.celrep.2015.11.028

Singh, N. N., Howell, M. D., Androphy, E. J., & Singh, R. N. (2017). How the discovery of ISS-N1 led to the first medical therapy for spinal muscular atrophy. *Gene Ther, 24*(9), 520-526. doi:10.1038/gt.2017.34

Spater, D., Hansson, E. M., Zangi, L., & Chien, K. R. (2014). How to make a cardiomyocyte. *Development, 141*(23), 4418-4431. doi:10.1242/dev.091538

Spinazzola, J. M., & Gussoni, E. (2017). Isolation of Primary Human Skeletal Muscle Cells. *Bio Protoc, 7*(21). doi:10.21769/BioProtoc.2591

Storbeck, C. J., Drmanic, S., Daniel, K., Waring, J. D., Jirik, F. R., Parry, D. J., . . . Korneluk, R. G. (2004). Inhibition of myogenesis in transgenic mice expressing the human DMPK 3'-UTR. *Hum Mol Genet, 13*(6), 589-600. doi:10.1093/hmg/ddh064

Subramanian, S., Mishra, R. K., & Singh, L. (2003). Genome-wide analysis of microsatellite repeats in humans: their abundance and density in specific genomic regions. *Genome Biol, 4*(2), R13.

Sun, N., Yazawa, M., Liu, J., Han, L., Sanchez-Freire, V., Abilez, O. J., . . . Wu, J. C. (2012). Patient-specific induced pluripotent stem cells as a model for familial dilated cardiomyopathy. *Sci Transl Med, 4*(130), 130ra147. doi:10.1126/scitranslmed.3003552

Suominen, T., Bachinski, L. L., Auvinen, S., Hackman, P., Baggerly, K. A., Angelini, C., . . . Udd, B. (2011). Population frequency of myotonic dystrophy: higher than expected

frequency of myotonic dystrophy type 2 (DM2) mutation in Finland. *Eur J Hum Genet, 19*(7), 776-782. doi:10.1038/ejhg.2011.23

Suominen, T., Schoser, B., Raheem, O., Auvinen, S., Walter, M., Krahe, R., . . . Udd, B. (2008). High frequency of co-segregating CLCN1 mutations among myotonic dystrophy type 2 patients from Finland and Germany. *J Neurol, 255*(11), 1731-1736. doi:10.1007/s00415-008-0010-z

Tabebordbar, M., Zhu, K., Cheng, J. K., Chew, W. L., Widrick, J. J., Yan, W. X., . . . Wagers, A. J. (2016). In vivo gene editing in dystrophic mouse muscle and muscle stem cells. *Science, 351*(6271), 407-411. doi:10.1126/science.aad5177

Takahashi, K., Tanabe, K., Ohnuki, M., Narita, M., Ichisaka, T., Tomoda, K., & Yamanaka, S. (2007). Induction of pluripotent stem cells from adult human fibroblasts by defined factors. *Cell, 131*(5), 861-872. doi:10.1016/j.cell.2007.11.019

Takahashi, K., & Yamanaka, S. (2006). Induction of pluripotent stem cells from mouse embryonic and adult fibroblast cultures by defined factors. *Cell, 126*(4), 663-676. doi:10.1016/j.cell.2006.07.024

Tanaka, A., Woltjen, K., Miyake, K., Hotta, A., Ikeya, M., Yamamoto, T., . . . Sakurai, H. (2013). Efficient and reproducible myogenic differentiation from human iPS cells: prospects for modeling Miyoshi Myopathy in vitro. *PLoS One, 8*(4), e61540. doi:10.1371/journal.pone.0061540

Tanawuttiwat, T., Wagner, K. R., Tomaselli, G., & Nazarian, S. (2017). Left Ventricular Dysfunction and Conduction Disturbances in Patients With Myotonic Muscular Dystrophy Type I and II. *JAMA Cardiol, 2*(2), 225-228. doi:10.1001/jamacardio.2016.4145

Taneja, K. L., McCurrach, M., Schalling, M., Housman, D., & Singer, R. H. (1995). Foci of trinucleotide repeat transcripts in nuclei of myotonic dystrophy cells and tissues. *J Cell Biol, 128*(6), 995-1002.

Tapscott, S. J., Davis, R. L., Thayer, M. J., Cheng, P. F., Weintraub, H., & Lassar, A. B. (1988). MyoD1: a nuclear phosphoprotein requiring a Myc homology region to convert fibroblasts to myoblasts. *Science, 242*(4877), 405-411.

Taubman, M. B., Smith, C. W., Izumo, S., Grant, J. W., Endo, T., Andreadis, A., & Nadal-Ginard, B. (1989). The expression of sarcomeric muscle-specific contractile protein genes in BC3H1 cells: BC3H1 cells resemble skeletal myoblasts that are defective for commitment to terminal differentiation. *J Cell Biol, 108*(5), 1799-1806.

Thornton, C. A. (2014). Myotonic dystrophy. *Neurol Clin, 32*(3), 705-719, viii. doi:10.1016/j.ncl.2014.04.011

Thornton, C. A., Wang, E., & Carrell, E. M. (2017). Myotonic dystrophy: approach to therapy. *Curr Opin Genet Dev, 44*, 135-140. doi:10.1016/j.gde.2017.03.007

Thornton, C. A., Wymer, J. P., Simmons, Z., McClain, C., & Moxley, R. T., 3rd. (1997). Expansion of the myotonic dystrophy CTG repeat reduces expression of the flanking DMAHP gene. *Nat Genet, 16*(4), 407-409. doi:10.1038/ng0897-407

Timchenko, N. A., Cai, Z. J., Welm, A. L., Reddy, S., Ashizawa, T., & Timchenko, L. T. (2001). RNA CUG repeats sequester CUGBP1 and alter protein levels and activity of CUGBP1. *J Biol Chem, 276*(11), 7820-7826. doi:10.1074/jbc.M005960200

Timchenko, N. A., Iakova, P., Cai, Z. J., Smith, J. R., & Timchenko, L. T. (2001). Molecular basis for impaired muscle differentiation in myotonic dystrophy. *Mol Cell Biol, 21*(20), 6927-6938. doi:10.1128/mcb.21.20.6927-6938.2001

Timchenko, N. A., Patel, R., Iakova, P., Cai, Z. J., Quan, L., & Timchenko, L. T. (2004). Overexpression of CUG triplet repeat-binding protein, CUGBP1, in mice inhibits myogenesis. *J Biol Chem, 279*(13), 13129-13139. doi:10.1074/jbc.M312923200

Treangen, T. J., & Salzberg, S. L. (2011). Repetitive DNA and next-generation sequencing: computational challenges and solutions. *Nat Rev Genet, 13*(1), 36-46. doi:10.1038/nrg3117

Turner, C., & Hilton-Jones, D. (2010). The myotonic dystrophies: diagnosis and management. *J Neurol Neurosurg Psychiatry, 81*(4), 358-367. doi:10.1136/jnnp.2008.158261

Turner, C., & Hilton-Jones, D. (2014). Myotonic dystrophy: diagnosis, management and new therapies. *Curr Opin Neurol, 27*(5), 599-606. doi:10.1097/WCO.0000000000000128

Udd, B., & Krahe, R. (2012). The myotonic dystrophies: molecular, clinical, and therapeutic challenges. *Lancet Neurol, 11*(10), 891-905. doi:10.1016/S1474-4422(12)70204-1

Udd, B., Meola, G., Krahe, R., Wansink, D. G., Bassez, G., Kress, W., . . . Moxley, R. (2011). Myotonic dystrophy type 2 (DM2) and related disorders report of the 180th ENMC workshop including guidelines on diagnostics and management 3-5 December 2010, Naarden, The Netherlands. *Neuromuscul Disord, 21*(6), 443-450. doi:10.1016/j.nmd.2011.03.013

Underwood, J. G., Boutz, P. L., Dougherty, J. D., Stoilov, P., & Black, D. L. (2005). Homologues of the Caenorhabditis elegans Fox-1 protein are neuronal splicing regulators in mammals. *Mol Cell Biol, 25*(22), 10005-10016. doi:10.1128/MCB.25.22.10005-10016.2005

van den Berg, C. W., Okawa, S., Chuva de Sousa Lopes, S. M., van Iperen, L., Passier, R., Braam, S. R., . . . Mummery, C. L. (2015). Transcriptome of human foetal heart compared with cardiomyocytes from pluripotent stem cells. *Development, 142*(18), 3231-3238. doi:10.1242/dev.123810

van Deutekom, J. C., & van Ommen, G. J. (2003). Advances in Duchenne muscular dystrophy gene therapy. *Nat Rev Genet, 4*(10), 774-783. doi:10.1038/nrg1180

Veerman, C. C., Kosmidis, G., Mummery, C. L., Casini, S., Verkerk, A. O., & Bellin, M. (2015). Immaturity of human stem-cell-derived cardiomyocytes in culture: fatal flaw or soluble problem? *Stem Cells Dev, 24*(9), 1035-1052. doi:10.1089/scd.2014.0533

Verkerk, A. J., Pieretti, M., Sutcliffe, J. S., Fu, Y. H., Kuhl, D. P., Pizzuti, A., . . . et al. (1991). Identification of a gene (FMR-1) containing a CGG repeat coincident with a breakpoint cluster region exhibiting length variation in fragile X syndrome. *Cell, 65*(5), 905-914.

Vignaud, A., Ferry, A., Huguet, A., Baraibar, M., Trollet, C., Hyzewicz, J., . . . Furling, D. (2010). Progressive skeletal muscle weakness in transgenic mice expressing CTG expansions is associated with the activation of the ubiquitin-proteasome pathway. *Neuromuscul Disord, 20*(5), 319-325. doi:10.1016/j.nmd.2010.03.006

Wahbi, K., Meune, C., Becane, H. M., Laforet, P., Bassez, G., Lazarus, A., . . . Duboc, D. (2009). Left ventricular dysfunction and cardiac arrhythmias are frequent in type 2 myotonic dystrophy: a case control study. *Neuromuscul Disord, 19*(7), 468-472. doi:10.1016/j.nmd.2009.04.012

Wang, G. S., Kearney, D. L., De Biasi, M., Taffet, G., & Cooper, T. A. (2007). Elevation of RNA-binding protein CUGBP1 is an early event in an inducible heart-specific mouse model of myotonic dystrophy. *J Clin Invest, 117*(10), 2802-2811. doi:10.1172/JCI32308

Ward, A. J., Rimer, M., Killian, J. M., Dowling, J. J., & Cooper, T. A. (2010). CUGBP1 overexpression in mouse skeletal muscle reproduces features of myotonic dystrophy type 1. *Hum Mol Genet, 19*(18), 3614-3622. doi:10.1093/hmg/ddq277

Warf, M. B., Nakamori, M., Matthys, C. M., Thornton, C. A., & Berglund, J. A. (2009). Pentamidine reverses the splicing defects associated with myotonic dystrophy. *Proc Natl Acad Sci U S A, 106*(44), 18551-18556. doi:10.1073/pnas.0903234106

Wheeler, T. M., Leger, A. J., Pandey, S. K., MacLeod, A. R., Nakamori, M., Cheng, S. H., . . . Thornton, C. A. (2012). Targeting nuclear RNA for in vivo correction of myotonic dystrophy. *Nature, 488*(7409), 111-115. doi:10.1038/nature11362

Wojtal, D., Kemaladewi, D. U., Malam, Z., Abdullah, S., Wong, T. W., Hyatt, E., . . . Cohn, R. D. (2016). Spell Checking Nature: Versatility of CRISPR/Cas9 for Developing Treatments for Inherited Disorders. *Am J Hum Genet, 98*(1), 90-101. doi:10.1016/j.ajhg.2015.11.012

Wu, S., Liu, Y., Bharadwaj, S., Atala, A., & Zhang, Y. (2011). Human urine-derived stem cells seeded in a modified 3D porous small intestinal submucosa scaffold for urethral tissue engineering. *Biomaterials, 32*(5), 1317-1326. doi:10.1016/j.biomaterials.2010.10.006

Wyatt, E. J., Demonbreun, A. R., Kim, E. Y., Puckelwartz, M. J., Vo, A. H., Dellefave-Castillo, L. M., . . . McNally, E. M. (2018). Efficient exon skipping of SGCG mutations mediated by phosphorodiamidate morpholino oligomers. *JCI Insight, 3*(9). doi:10.1172/jci.insight.99357

Xu, L., Park, K. H., Zhao, L., Xu, J., El Refaey, M., Gao, Y., . . . Han, R. (2016). CRISPR-mediated Genome Editing Restores Dystrophin Expression and Function in mdx Mice. *Mol Ther, 24*(3), 564-569. doi:10.1038/mt.2015.192

Xue, Y., Cai, X., Wang, L., Liao, B., Zhang, H., Shan, Y., . . . Pan, G. (2013). Generating a non-integrating human induced pluripotent stem cell bank from urine-derived cells. *PLoS One, 8*(8), e70573. doi:10.1371/journal.pone.0070573

Yaffe, D. (1968). Retention of differentiation potentialities during prolonged cultivation of myogenic cells. *Proc Natl Acad Sci U S A, 61*(2), 477-483.

Yang, L., Guell, M., Byrne, S., Yang, J. L., De Los Angeles, A., Mali, P., . . . Church, G. (2013). Optimization of scarless human stem cell genome editing. *Nucleic Acids Res, 41*(19), 9049-9061. doi:10.1093/nar/gkt555

Yazawa, M., Hsueh, B., Jia, X., Pasca, A. M., Bernstein, J. A., Hallmayer, J., & Dolmetsch, R. E. (2011). Using induced pluripotent stem cells to investigate cardiac phenotypes in Timothy syndrome. *Nature, 471*(7337), 230-234. doi:10.1038/nature09855

Young, C. S., Hicks, M. R., Ermolova, N. V., Nakano, H., Jan, M., Younesi, S., . . . Pyle, A. D. (2016). A Single CRISPR-Cas9 Deletion Strategy that Targets the Majority of DMD Patients Restores Dystrophin Function in hiPSC-Derived Muscle Cells. *Cell Stem Cell, 18*(4), 533-540. doi:10.1016/j.stem.2016.01.021

Yu, J., Vodyanik, M. A., Smuga-Otto, K., Antosiewicz-Bourget, J., Frane, J. L., Tian, S., . . . Thomson, J. A. (2007). Induced pluripotent stem cell lines derived from human somatic cells. *Science, 318*(5858), 1917-1920. doi:10.1126/science.1151526

Yu, Z., Goodman, L. D., Shieh, S. Y., Min, M., Teng, X., Zhu, Y., & Bonini, N. M. (2015). A fly model for the CCUG-repeat expansion of myotonic dystrophy type 2 reveals a novel interaction with MBNL1. *Hum Mol Genet, 24*(4), 954-962. doi:10.1093/hmg/ddu507

Zhang, C., Zhang, Z., Castle, J., Sun, S., Johnson, J., Krainer, A. R., & Zhang, M. Q. (2008). Defining the regulatory network of the tissue-specific splicing factors Fox-1 and Fox-2. *Genes Dev, 22*(18), 2550-2563. doi:10.1101/gad.1703108

Zhang, Y., McNeill, E., Tian, H., Soker, S., Andersson, K. E., Yoo, J. J., & Atala, A. (2008). Urine derived cells are a potential source for urological tissue reconstruction. *J Urol, 180*(5), 2226-2233. doi:10.1016/j.juro.2008.07.023

Zhou, T., Benda, C., Dunzinger, S., Huang, Y., Ho, J. C., Yang, J., . . . Esteban, M. A. (2012). Generation of human induced pluripotent stem cells from urine samples. *Nat Protoc, 7*(12), 2080-2089. doi:10.1038/nprot.2012.115

Zhou, T., Benda, C., Duzinger, S., Huang, Y., Li, X., Li, Y., . . . Esteban, M. A. (2011). Generation of induced pluripotent stem cells from urine. *J Am Soc Nephrol, 22*(7), 1221-1228. doi:10.1681/ASN.2011010106

Zhou, W., & Freed, C. R. (2009). Adenoviral gene delivery can reprogram human fibroblasts to induced pluripotent stem cells. *Stem Cells, 27*(11), 2667-2674. doi:10.1002/stem.201

Zu, T., Cleary, J. D., Liu, Y., Banez-Coronel, M., Bubenik, J. L., Ayhan, F., . . . Ranum, L. P. W. (2017). RAN Translation Regulated by Muscleblind Proteins in Myotonic Dystrophy Type 2. *Neuron, 95*(6), 1292-1305 e1295. doi:10.1016/j.neuron.2017.08.039

Zu, T., Gibbens, B., Doty, N. S., Gomes-Pereira, M., Huguet, A., Stone, M. D., . . . Ranum, L. P. (2011). Non-ATG-initiated translation directed by microsatellite expansions. *Proc Natl Acad Sci U S A, 108*(1), 260-265. doi:10.1073/pnas.1013343108

Zuk, P. A., Zhu, M., Ashjian, P., De Ugarte, D. A., Huang, J. I., Mizuno, H., . . . Hedrick, M. H. (2002). Human adipose tissue is a source of multipotent stem cells. *Mol Biol Cell, 13*(12), 4279-4295. doi:10.1091/mbc.E02-02-0105